XXXII CYCLE PhD COURSE IN SCIENCE AND TECHNOLOGIES OF CHEMISTRY AND MATERIALS

Curriculum: Drug discovery and Nanobiotechnologies

NANOBIOINTERACTIONS: CHEMOKINE MEDIATED SELECTIVE TARGETING OF NANOPARTICLES

PI

Pier Paolo Pompa

Candidate

Roberta Cagliani

Supervisor

Giuseppe Bardi

Co-Supervisor

Sara Baldassari

Academic years 2016-2019

Table of contents

List of acronyms

ADC	Analog-to-digital conversion
ALG	Alginate
Ag NPs	Silver nanoparticles
AnnV/PI	Annexin V/Propidium iodide
AOTFs	Acousto-optic tunable filters
ATRA	All-trans retinoic acid
BBB	Blood brain barrier
BNNT	Boron nitride nanotubes
BSA	Bovine serum albumin
CD	Circular dichroism
CLSM	Confocal laser-scanning microscope
CNT	Carbon nanotubes
CPP	Cell penetrating peptides
CS	Chitosane
DLS	Dynamic light scattering
DMSO	Dimethyl sulfoxide
DMTMM	4-(4,6-dimethoxy-1,3,5-triazin-2-yl)-4-methyl-morpholinium chloride
EDAC	1-etil-3-(3 dimethylaminopropil) carbodiimide
EDC	1-ethyl-3-(3-dimethylaminopropyl) carbodiimide
EDS	Energy-dispersive X-ray spectroscopy
EGFR	Epidermal growth factor receptor
EPR	Enhanced vascular permeability and retention
FACS	Fluorescence-activated cell sorting
FBS	Fetal bovine serum
FDA	Food and drug administration
FGFR	Fibroblast growth factor receptor
FITC	Fluorescein isothiocyanate
FSC	Forward scattering
GNPs	Gold nanoparticles

GPCR	G coupled protein receptor
HS	Human serum
MES	2-(N-morpholino)ethanesulfonic acid
MFI	Median fluorescence intensity
MRI	Magnetic resonance imaging
NHS	N-Hydroxysuccinimide
NM	Nanomaterial
NPs	Nanoparticles
PDI	Polydispersity index
PEG	Polyehylene glycol
PEM	Photo Elastic Modulator
PI	Propidium iodide
PLGA	Poly(lactic-co-glycolic acid)
PMT	Photomultiplier tube
Pt NPs	Platinum nanoparticles
PVP	Polyvinylpyrrolidone
QDs	Quantum dots
RES	Reticuloendothelial system
RMFI	Relative median fluorescence intensity
ROS	Reactive Oxygen Species
SEM	Standard error mean
SiO_2	Silica
SD	Standard deviation
SOP	Standard operating procedure
SSC	Side scattering
TEM	Transmission electron microscopy
TEOS	Tetraethylorthosilicate
TLC	Thin layer chromatography
VCAM	Vascular cell adhesion molecule protein

Abstract

A major challenge in nanomedicine is the preparation of nano-tools with the ability to selectively targeting diseased tissues. Functionalization of nanoparticles (NPs) by conjugation with specific ligands possessing the inherent ability to bind only cell subsets confer "smartness" to NPs. Due to their small sizes, nanostructures exhibit unique physicochemical and biological properties, such as enhanced reactive area and the ability to cross tissue barriers, making them a favorable material for biomedical applications. NPs vary in size ranging from 5 to 500 nm. Through the manipulation of size, surface chemistry and material structure, NPs can be tailored to carry therapeutic or imaging agents for delivery to specific tissues. In particular, surface functionalization can modify NP interaction with the immune system cells and the acquisition of stealth or specific-targeting properties. NP surface decoration with peptide moieties is one of the most efficacious cell-targeting strategies. In the first part of my PhD project, I focused on NP surface functionalization with stable proteins that interact with different immune cells in a selective manner. I used chemokines (chemo-attractant cyto-kines) due to their role in physiological and pathological binding and regulation of immune cells, as well as their structural stability in biological media. I modified a prototype SiO_2-NP surface with the chemokine CXCL5, adsorbed or covalently bound, to precisely targeting CXCR2+ immune cells. The development of CXCL5-NPs and the discovery of their targeting properties provide novel results. Specifically, these protein-decorated nano-tools showed enhanced uptake and precise receptor-mediated cell subset localization. Moreover, given the crucial role of CXCR2 in inflammatory responses and cancer biology, CXCL5-NPs pave the way to prepare new delivery systems with increased capabilities and potential modulation of immune responses.

In the second part of my PhD project, I evaluated the effects of PtNPs on HL60 (Human promyelocytic leukemia cells) and differentiated HL60 (Neutophils-like cells) cells in immune responses and inflammatory diseases. Reactive Oxygen Species (ROS) removing activity within cells is often achieved with different catalytic nanomaterials. Among them, PtNPs attract great attention due to their efficient catalysis and good degree of cyto-compatibility, but information about their effects on the human immune system is still missing. Further investigation using undifferentiated and differentiated neutrophil-like HL60 confirmed the harmlessness and non-cytotoxicity of PtNPs with non-adherent

innate immune cells, contributing to the knowledge of PtNP interaction with immune cells in view of their potential applications in nanomedicine.

Chemokine mediated selective targeting of nanoparticles

1. Introduction

1.1 Nanoparticles definition and characteristics

NPs are solid, colloidal particles with size range from 10 nm to <1000 nm [1]. Due to their small size and large surface area, NPs are used to increase drug solubility and enhanced bioavailability. Depending on physical-chemical characteristics some of them have the ability to cross the blood brain barrier (BBB), enter the pulmonary system and be absorbed through the tight junctions of endothelial cells of the skin [2]. In particular NPs made from natural and synthetic biodegradable polymers have received more attention because polymers undergo hydrolysis in the body, producing biodegradable metabolite monomers, such as lactic acid and glycolic acid [3]. NPs can be released through direct injection, inhalation and oral intake. Once, they enter systemic circulation, particle-protein interaction happens immediately before their distribution into the various organs. Shape, size and surface chemistry of NPs affects how cells ‘‘see” them and dictate their distribution, toxicity, and targeting ability. To create efficient nano-drug delivery systems, the functionalization with targeting ligands, surface curvature and reactivity are crucial features to consider, in order to avoid NP aggregation, improving their stability and guarantee the pharmacological effects of the drug [4]. The more hydrophobic NPs are, the more likely will be cleared because of the higher binding affinity to blood components [5]. As hydrophobic NPs are cleared easily, making their surface hydrophilic would increase their time in circulation. In particular polyethylene glycol (PEG) is a hydrophilic and relatively inert polymer that when linked onto the NP surface, hinders the binding of plasma avoiding phagocytosis of the particle by tissue macrophages (opsonization), preventing the particles degradation. PEGylated NPs are considered as ‘‘stealth” NPs, because they escape the surveillance of reticuloendothelial system (RES) better than other NPs [6]. RES consists of cells descending from monocytes which are able to perform phagocytosis of foreign materials and particles. The most important function of the RES is phagocytosis, but it also takes part in cytotoxicity against tumor cells and has a function in the regulation of the immune system [7]. RES is able to

recognize the circulating nanoparticles, causing a major loss of the injected dose (>50%) within a few hours after intra venous injection. Theoretically, a perfectly stealth NP should not be opsonized at all and should stay in the circulation until it encounters and penetrates a leaky vasculature [6].

Figure 1.

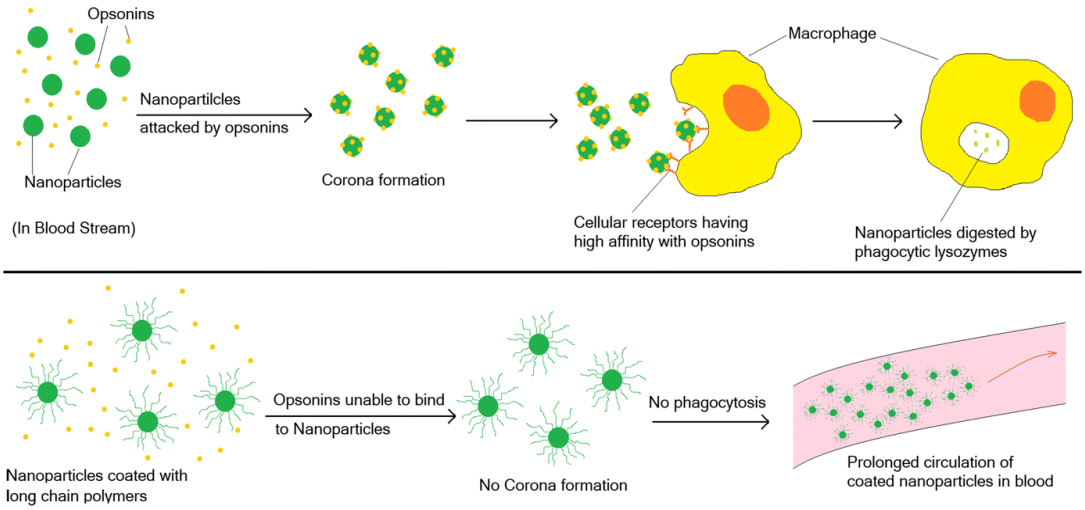

Representation of opsonization process by macrophages. Opsonins are unable to bind nanoparticles coated with polymers that don't undergo phagocytosis [8].

1.2 Classification of different types of nanoparticles

According to the different characteristics and functionality of the materials, NPs could be divided in different classes. The most important are inorganic, organic and carbon based NPs [9].

1.2.1 Inorganic nanoparticles.

Inorganic NPs are particles that are not made up of carbon. Metal and metal oxide based nanoparticles are the most important classes. Some of inorganic NPs have optical, electronic, magnetic and catalytic properties. The most used NPs are iron oxides, gold, silver, quantum dots, silica and carbon-based [10].

- **Metal based Nanoparticles.** They are synthesized from metals to nanometric sizes and the commonly used metals for nanoparticle synthesis are aluminum, cadmium, cobalt, copper, gold, iron, lead, silver and zinc. NPs have distinctive properties such sizes as low as 10 to 100 nm, high surface area to volume ratio, pore size, surface charge and surface charge density, crystalline and amorphous structures, shapes like spherical and cylindrical [11].They have been used in different medical applications, such as bioimaging, biosensor, hyperthermia, sustained drug deliver [12][13].

- **Metal oxides based**. The metal oxide based NPs are synthesized to modify the properties of their respective metal based NPs, for example NPs of iron instantly oxidizes to iron oxide in the presence of oxygen at room temperature that increases its reactivity compared to iron NPs**.** The commonly synthesized are Aluminum oxide, Cerium oxide, Iron oxide, Silicon dioxide, Titanium oxide, Zinc oxide [14].

- **Silica nanoparticles.** Silica NPs (SiO_2) have obtained great interest to be used for biomedical applications and they can be categorized as mesoporous or non-porous (solid) NPs. Mesoporous SiO_2 NPs are characterized by the mesopores (2-50 nm pore size) and are used for delivery of pharmacological compounds based on physical or chemical adsorption [15][16]. They are also promising candidates for improved drug delivery systems. Drug molecules have been loaded into SiO_2 NPs and surface modification of the NPs with bio recognition entities can allow specific cells or receptors in the body to be located [17]. There are various methods of NPs preparation such as Stöber method, reverse micro emulsion, sol-gel method, spray drying, template method, heating degradation etc. [18][19]. The synthesis of mesoporous silica is accomplished using sol–gel chemistry in the presence of surfactants. Furthermore, thermal crosslinking rigidifies the preceramic material, and then, the surfactant is removed to expose the pore structure [20]. SiO_2 NPs can be used for stimuli-responsive drug delivery, photodynamic therapy, gene delivery, protein delivery, imaging and diagnosis, DNA and microarray detection.

Carbon based

NPs made completely of carbon are knows as carbon based. They can be classified into fullerenes, graphene, carbon nanotubes (CNT), carbon nanofibers and carbon black

- **Fullerenes.** Fullerenes is a carbon molecule that is spherical in shape and made up of carbon atoms held together by sp2 hybridization. About 28 to 1500 carbon atoms forms the spherical structure with diameters up to 8.2 nm for a single layer and 4 to 36 nm for multi-layered fullerenes.
- **Graphene.** Graphene is an allotrope of carbon and it is a hexagonal network of honeycomb lattice made up of carbon atoms in a two dimensional planar surface. Generally the thickness of the graphene sheet is around 1 nm [14].
- **Nanotubes** are self-assembling sheets of atoms arranged in tubes with single- or multiwalled structures, with large internal volume. The external surface of nanotubes can be easily functionalized [21]. One of the most popular nanotubes is CNT. They are graphene sheets rolled up into tubular form, wherein each layer consists of hexagonal networks of carbon atoms. Nanotubes are divided in single-walled nanotubes (SWNTs) and multi-walled nanotubes layers of graphite characterized by a large surface area and an excellent electronic and thermal conductivity [22]. Boron nitride nanotube (BNNT) has similar tubular nanostructure as carbon nanotube (CNT) in which boron and nitrogen atoms arranged in a hexagonal network. Owing to the unique atomic structure, BNNT has numerous excellent intrinsic properties such as superior mechanical strength , high thermal conductivity, electrically insulating behavior, piezoelectric property, neutron shielding capability, and oxidation resistance [23].
- **Carbon Nanofiber**. The same graphene nanofoils are used to produce carbon nanofiber as CNT but wound into a cone or cup shape instead of a regular cylindrical tubes.
- **Carbon black.** An amorphous material made up of carbon, generally spherical in shape with diameters from 20 to 70 nm. The interaction between the particles are so high that they bound in aggregates and around 500 nm agglomerates are formed [14].

Nanocrystals

Usually a nanocrystals have a size smaller than 100 nm and they are aggregates of around hundreds or thousands of molecules that combine in a crystalline form, composed of drug surrounded by a thin coating comprised of surfactant [22]. There is no carrier material in nanocrystals and are composed of 100% of drug [24]. The traditional method involves molecular precursors, which can include typical metal salts and a source of the anion like chalcogenides (SS−, SeS−, TeS−) and pnictides (P3−, As3−, Sb3−).

Quantum dots

Quantum dots (QDs) are known as semiconductor nanocrystals with diameter range from 2 to 10 nm and their optical properties, such as absorbance and photoluminescence are size-dependent [25]. QDs have obtained great attention in the field of nanomedicine because they presents emission in the near-infrared region (< 650 nm), a very desirable characteristic in the field of biomedical images, due to the low absorption by the tissues. In this sense, QDs are very appealing for multiplex imaging, as targeted drug delivery, sensors and bioimaging [22].

Magnetic nanoparticles

Magnetic NPs can be composed of cobalt, nickel, manganese, and iron and exhibit a wide variety of properties which make them highly promising carriers for drug delivery. In particular, with the aid of an external magnetic field they could be used for passive and active drug delivery strategies [26].

1.2.2 Organic nanoparticles

Organic NPs can be explained as solid particles composed of organic compounds (mainly lipids or polymeric) ranging in diameter from 10 nm to 1 µm. Most important classes are dendrimers, micelles and liposomes. Organic NPs usually are biodegradable and non-toxic. They can load molecules either by conjugation on the surface or in the core, or by physical encapsulation, which makes them appealing systems for drug delivery and biomedical applications [22].

- **Liposome.** They are vesicles of spherical form composed of phospholipids and steroids, their membrane structure is similar to the cell membranes and they are also biocompatible and biodegradable [27][22]. Liposomes reveal several exclusive properties such as long systemic circulation half-life, surface modifications and safety profiles for both hydrophilic and lipophilic drugs. Most of the liposomes are PEG coated because PEGylated liposomes decrease the monocyte system uptake, increase circulation time and reduce immune recognition [28]. These kinds of liposomes are called stealth liposome or sterically stabilized liposomes [29]. Liposomes have been used to improve the therapeutic index of new or established drugs by modifying drug absorption, reducing metabolism, prolonging biological half-life or reducing toxicity. Lipids forming liposomes may be natural or synthetic, and liposome constituents are not exclusive of lipids, new generation liposomes can also be formed from polymers (sometimes referred to as polymersomes) [29]. Liposomes used for gene delivery into cells are called genosomes. For the production of genosomes, cationic phospholipids were found to be more suitable because they possess high biodegradability and stability in the blood stream [29].
- **Polymeric nanoparticles.** Polymeric NPs are colloidal particles of size range 10 nm–1 μm and solid in nature. They include conjugates, dendrimers, micelles, nanoparticles, nanogels and polymerosomes. Depending on preparation method, polymeric nanoparticles can form two types of structures: nanosphere and nanocapsule. Nanospheres consist of matrix system in which the drug is uniformly dispersed whereas in nanocapsules the drug is embedded in a cavity and the cavity is surrounded by a polymeric membrane. Polymeric nanoparticles have immense potential as drug carriers as they can deliver drugs in various organ systems. They can be made from synthetic and natural polymers. The most widely used synthetic polymers are polylactide, polylactide–polyglycolide copolymers, polycaprolactones, and polyacrylates. Among the various natural polymers, alginate, albumin, or chitosan have been widely explored [30]. Alginate (ALG) is a water soluble linear polysaccharide extracted from brown sea weed and is composed of alternating blocks of 1-4 linked α-L-guluronic and β-Dmannuronic acid residues. ALG has been reported to be muco-adhesive, biodegradable, and

biocompatible [31][32]. Alginate micro and nanoparticles can be obtained easily by inducing gelation with calcium ions [33][34]. Chitosan (CS) a linear polysaccharide consisting of glucosamine and N-acetylglucosamine units, is biocompatible, biodegradable, and nontoxic. The addition of CS can not only endow nanoparticles positive surface charge, but also prolong the time that the active ingredients contact with the epithelium and enhance absorption via the para-cellular transport pathway through the tight junctions [35][36]. Synthetic polymers undergo hydrolysis in the body, producing biodegradable monomers. The drug can be entrapped or encapsulated within the carrier, physically adsorbed on the surface of the carrier, or chemically linked to the surface. These nanocarriers are known by their attractive characteristics, such as small size, biodegradability, water solubility, nontoxicity, long shelf life, and stability during storage. These characteristics make them a point of interest for the delivery of drugs, proteins, and DNA or genes to specific targeted tissues or organs [37].

- **Dendrimers.** Dendrimers are nano-sized, radially symmetric molecules with well-defined, homogeneous and monodisperse structure consisting of tree-like arms or branches. Manipulating these structural features of dendrimers allows controlled synthesis of a whole series of highly branched end-functionalized macromolecules that are drawing increased attention for many potential applications [38]. They could be made of globular, monodisperse, three dimensional nanoscales synthetic polymers [22]. The drug may be encapsulated in the internal structure of dendrimers or it can be chemically attached or physically adsorbed on dendrimers surface. Usually encapsulation is used for toxic or poorly soluble drugs. Instead covalent coupling provides the possibility to control quantity of drugs on dendrimers surface [39].

Figure 2.

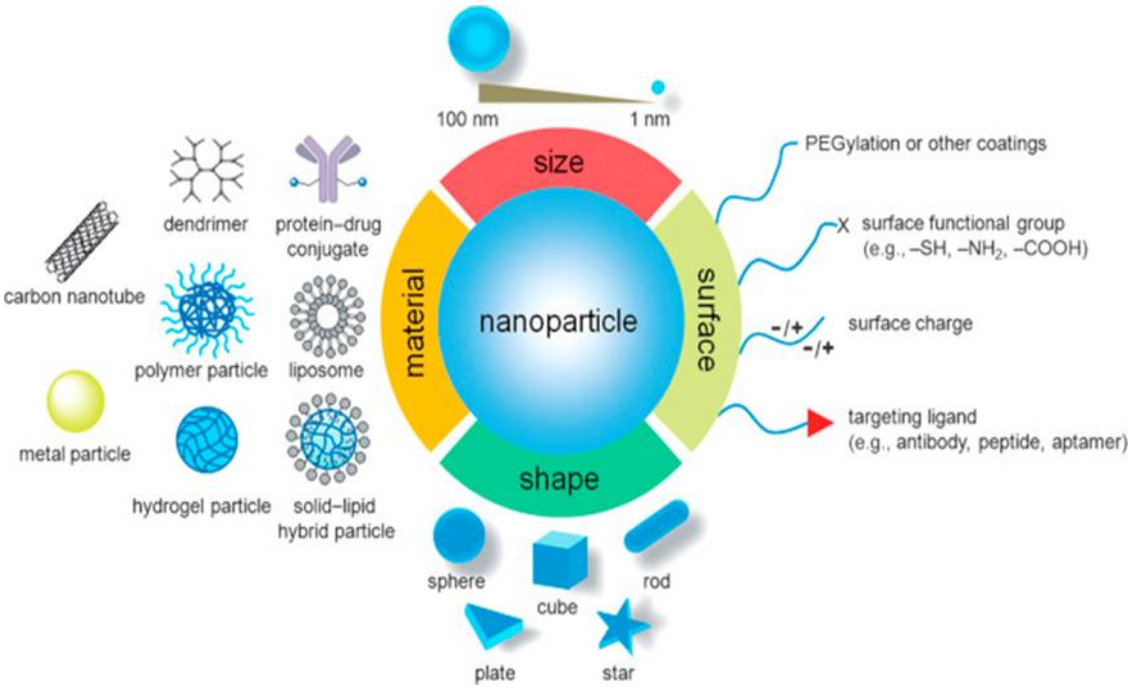

Examples of NPs that could be used as carriers for drug delivery and selective targeting. Representation of different types of organic and inorganic NPs [40].

1.3 Nanoparticles for targeting pathological tissues.

One major challenge in nanomedicine is to create a nano-tool that can selectively target diseased tissues. The penetration of NPs in tissues can occur passively or actively. Active targeting occurs when the drug carrier system is conjugated to a cell-specific ligand or absorbed on NPs surface. The passive targeting is achieved by incorporating the therapeutic agent into a NP that reaches the target organ without modification of its surface. In this strategy, the leaky nature of vessels in cancer tissue and lack of well-defined lymphatic system can enhance the permeation and retention of NPs, which is called the enhanced permeation and retention (EPR) effect [41].

Figure 3.

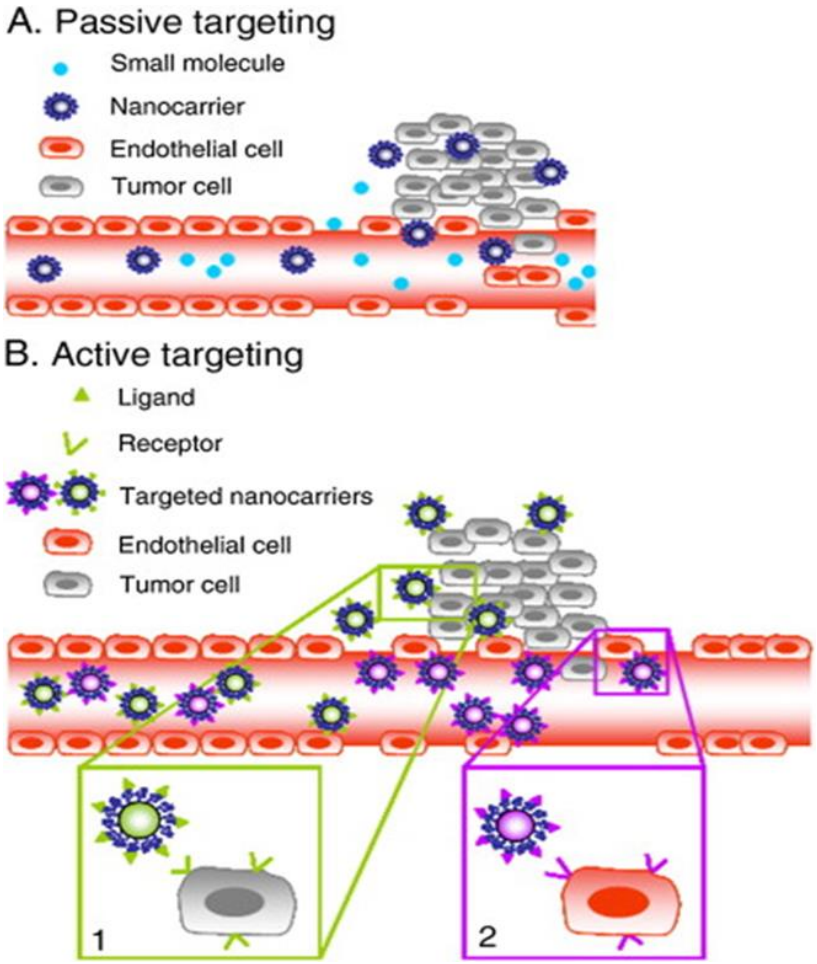

Schematic representation of passive (A) and active (B) targeting. Examples of different molecules involved in active and passive targeting [42].

An ideal drug delivery system should be able to bind and deliver its load to specific pathologic tissues, and minimize or avoids drug-induced collateral damage to the healthy tissues. Coating the NP surface with specific ligands is a fruitful strategy. These ligands could be small molecules, peptides, antibodies, designed proteins, nucleic acid and aptamers [43]. Commonly used ligands are Biotin (vitamin H), due to its very high affinity for streptavidin, and folic acid (vitamin B9), because of its binding for endogenous folate receptor that is, for example, overexpressed in many types of cancers [44]. The most common peptide used for targeting is RGD that binds integrins on the cell surface involved in cell migration, growth, differentiation and apoptosis in addition to cell–cell integrations. Integrin αvβ3 that bind to RGD peptides with high affinity is

involved in intracellular signaling and direct roles in tumor angiogenesis. Recent uses of RGD peptides for treating cancer include conjugation of PEGylated RGD peptides to gold nanoshells that are able to target U87 glioblastoma cells [45]. Carbohydrates, which interact weakly with some cell surface receptors, can also serve as NPs small molecule targeting ligands. In particular, carbohydrates permit NPs glyco-targeting, which is based on endogenous lectin interactions with carbohydrates. A disadvantage of this targeting method is that glycol-targeting often requires multiple interacting carbohydrates to achieve strong enough binding strength [43]. Moreover, AuNPs with diameter $\leq$ 50 nm can cross the BBB (ref). Gold nanorod–DARPP–32 siRNA complexes have been developed to target and diminish expression of the key proteins (DARPP-32), extracellular signal-regulated kinase (ERK), and protein phosphatase 1 (PP-1) in the brain cell dopaminergic signaling pathway for ailment of drug addiction [46]. Magnetic NPs are able to target a specific site in the human body due to applied magnetic field. Usually these particles contain magnetic cores encapsulated by polymer or metal coating, or may consist of porous polymers containing magnetic NP precipitate within the pores [47]. Recently a group of researchers used therapeutic ceria (CeO_2) NPs to remove ROS in mice genetically modified to show the symptoms of Alzheimer disease. $CeCO_2$ NPs worked as strong and recyclable ROS scavengers shuttling between Ce^{3+} and Ce^{4+} oxidation states [48]. Recently, Aouadi et al. investigated the efficacy of β-glucan-encapsulated siRNA particles as oral delivery vehicles to targeting macrophages. These NPs can silence the Map4k4 gene and protect animals from lipopolysaccharide-induced lethality [49]. Aptamer-conjugated nanoparticles have immense application including early diagnosis and drug delivery. For instance, the 20-fluorinated A10 RNA aptamer-conjugated on Poly(lactic-co-glycolic acid)-polyethylene glycol (PLGA-PEG) NPs shall be adopted in targeted prostate-specific membrane antigen in case of prostate cancer model [50].

1.4 Covalent coupling

Significant research effort has been devoted to decorating NP surfaces with a range of biological moieties to target specific cellular receptors, using a range of methods including adsorption, covalent coupling and specific interactions, resulting in biologically active composite NPs [51]. Covalent conjugation is attractive as it can provide a route to irreversibly bound biofunctional layer, which would be expected to be stable across the

biological conditions. The most common procedures utilize carbodiimide chemistry, whereby the amine of the biomolecule forms an amide bond to a carboxylated nanoparticle. This so-called "EDAC" chemistry is a biocompatible coupling procedure which can be performed in one step with 1-etil-3-(3 dimethylaminopropil) carbodiimide (EDAC) forming an active intermediate with carboxylic acids susceptible to amine substitution. This chemistry has been applied to functionalization of a range of nanoparticle types including silica [52] polystyrene [53] and gold [54]. N-hydroxysuccinimide or sulfo-N-hydroxysuccinimide can also be used in parallel to form an activated ester and avoid NPs aggregation. For amino functionalized particles a common functionalization approach is to use the bifunctional glutaraldehyde as a cross-linking agent between the particle and protein amino groups with the formation of a reversible imine groups. This method has been commonly applied to the amino expressing silica or silica shell nanoparticles, which result from aminopropylsilane functionalization.

Figure 4.

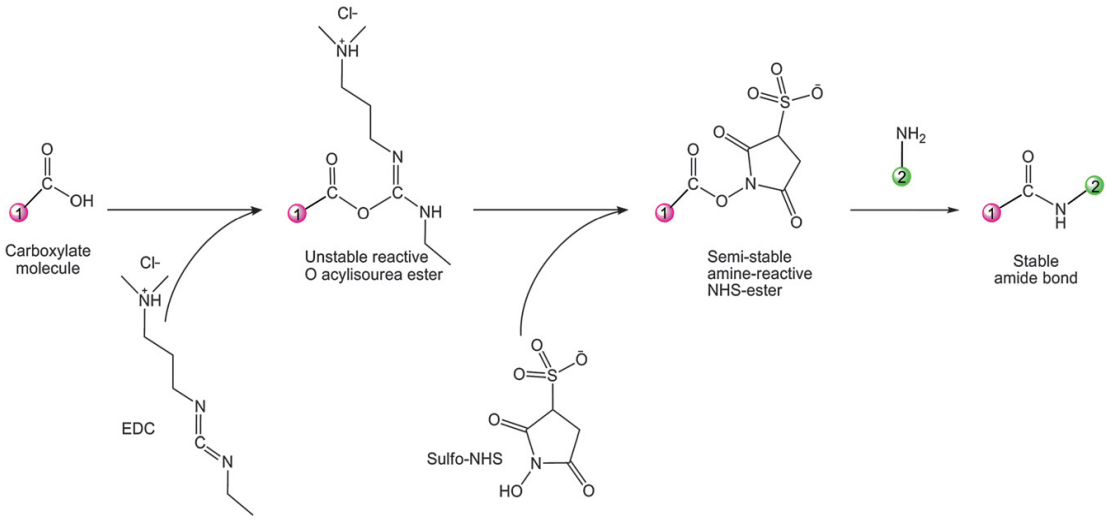

Representation of EDC–NHS chemistry: EDC reacts with a carboxylic-acid group, forming an amine-reactive O-acyl isourea intermediate. This intermediate may reacts with an amine, yielding a conjugate of the two molecules joined by a stable amide bond. The addition of sulfo-NHS stabilizes the amine-reactive intermediate by converting it to an amine reactive sulfo-NHS ester, thus increasing the efficiency of EDC-mediated coupling reactions [55].

Nevertheless, the direct attachment of a protein to a surface without a spacer can cause steric constraint modifying the protein reactivity compared to the protein in solution. In addition, without a spacer, multiple contacts between protein and nanoparticle surface are more probable favoring total or partial protein denaturation and thus decreasing protein activity. The Huisgen cycloaddition "Click" reaction is considered especially attractive given its chemoselectivity and stability [56][57]. Gold readily forms Au\S and Au\N bonds, thus gold NPs have been used for direct coupling of proteins on their surface through binding with free amino and cysteine presenting residues which may be present on the targeting moiety. Adsorption effects due to physical interaction between bio-macromolecule and a range of materials are known to cause significant structural changes [58]. For example NPs surface have been shown to induce size dependent effects on protein conformation upon adsorption [59][60]. Besides size, as one would expect, hydrophobicity and electrostatics play important roles which may be controlled through surface chemistry modifications [61][62]. Interestingly in some cases NP conjugation has been cited as beneficial to protein activity and stability. Besides the physical effects on the protein structure that may result from binding to NP surfaces, the actual directionality of the protein components becomes vital as regards biological efficacy because it is necessary to ensure the correct epitope presentation in order to engage with the target receptor. Greater control of the protein orientation at the NP surface can be accomplished through careful attention to surface topography and chemistry properties on one hand, and protein structural details on the other. Controlled directionality can be attained through advanced protein modification/synthesis techniques to control the point of attachment and the consequent interface biological activity. So covalently conjugating proteins to NP surface also provides control over protein reactivity and NP aggregation.

Figure 5.

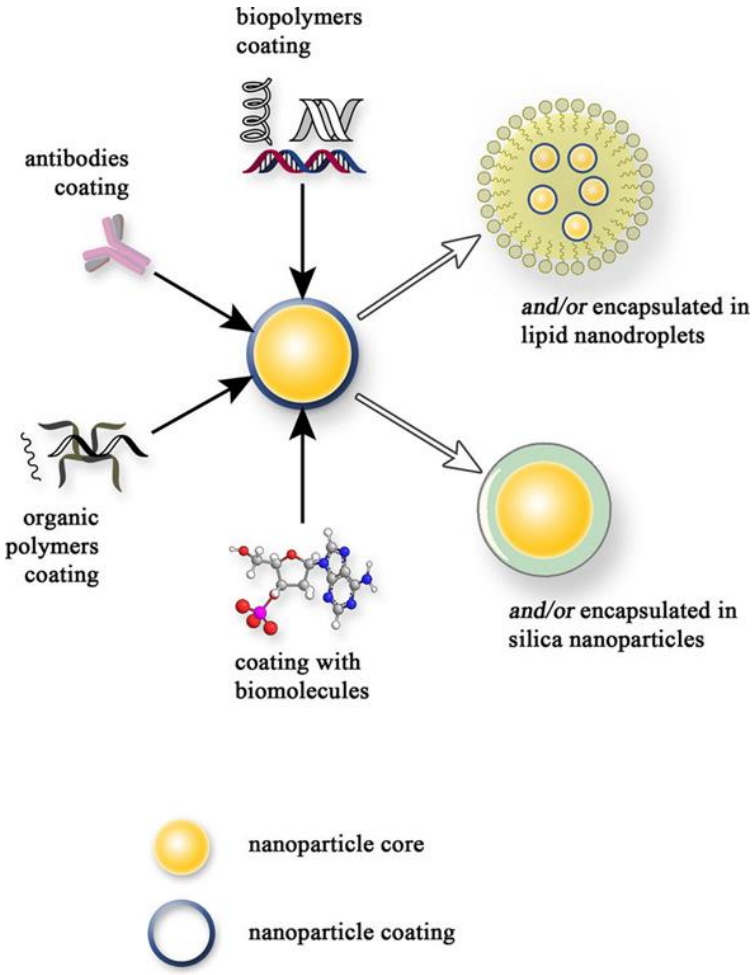

Several coating agents or ligands for NPs surface functionalization. Representation of different molecules used as ligand for selective targeting [63].

1.5 The role of protein corona

An evolution from a loosely bound to irreversibly attached protein "corona" around the NPs over time has been observed in cell culture media containing serum, a process that potentially correlates the cellular uptake and other biological processes with NP-protein complexes. Numerous NMs show the intrinsic property to adsorb specific proteins present in biological fluids that can be used as targeting molecule to drive cell localization [64]. Although the formation of a selective protein corona is attractive it cannot exclude some concerns regarding the non-advantageous peptide orientation or the presence of conformational changes due to the chemical and physical interactions with the particle

surface [65]. In particular, drug delivery systems often require the release of NPs into the bloodstream, which is populated by blood cells and small peptides, proteins, sugars, lipids, and complexes of all these molecules. Generally, in biological fluids, a NPs surface is covered by different biomolecules, which influence their interactions with tissues and cells. The adsorption of molecules onto the nanomaterial is defined as "corona" formation. Every blood particulate component, in particular proteins and extracellular matrix components can contribute to the creation of the corona. Many different physical events contribute to a corona's formation, such as temperature, pH, and the time of interaction between the NPs and the medium's components. The protein corona can be distinguished in "hard corona" and "soft corona" [66]. The hard corona contains proteins with a higher affinity for the NP surface that may irreversibly bind the chemical moieties on the particle. In contrast, the soft corona layer harbors proteins that have a lower affinity for the NP external chemistry [67].

Figure 6.

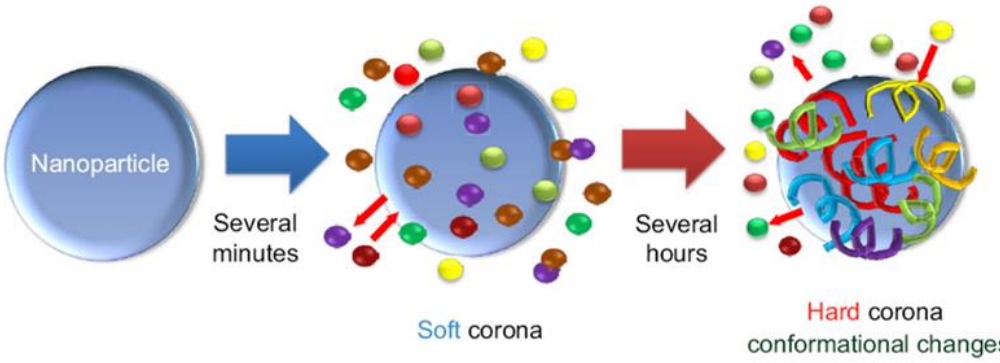

Schematic illustration and characteristics of a hard and a soft corona [67].

Hard coronas are characterized by slow exchange (ie, several hours) and lower abundance, with a high affinity of proteins, whereas soft coronas are characterized by rapid exchange (ie, several minutes) and lower affinity of proteins with weakly bound outer layers on NPs [67]. Many of these proteins increase NP internalization into cells by specific binding with their cognate receptors expressed on cell membranes, whereas others are reported to avoid NP internalization, such as CD47 or clusterin [68][69]. These

observations have encouraged some researchers to use this strategy to evaluate the effect protein corona for NP surface functionalization aimed at type-specific cell delivery [64]. Protein denaturation, steric hindrance (crowding), an unfavorable orientation due to the rearrangement of their spatial configurations to adapt to the NM could influence the fate and the functionality of NPs in cellular uptake [70]. Changes in protein conformation may create new epitopes towards the cellular interaction leading to inappropriate signaling. On the contrary, proteins could not modify their tertiary structure if the NM has high curvature not promoting major conformational variations [70].

Figure 7.

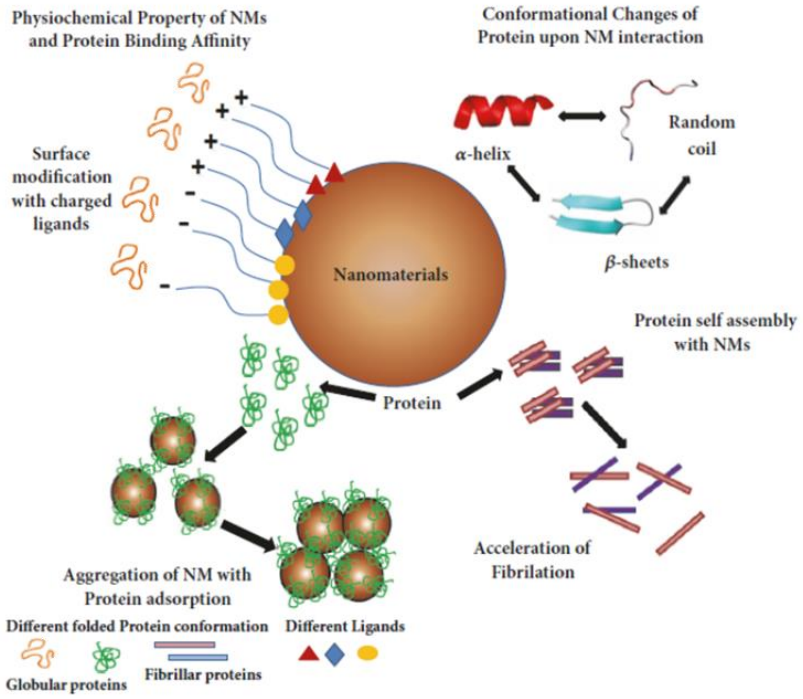

Overview of NM-protein interaction: cause and effect of nanobiointerface. Protein adsorption on NMs depends on physiochemical properties of NMs, such as size, shape, and charges on the NMs surface. Proteins often are affected by conformational changes upon NM interaction. The secondary structure (α-helices, β-sheets, and random coils) gets perturbed due to interaction with NMs. The binding of proteins onto NMs can lead to NM aggregation associated with protein aggregation [71].

Figure 8.

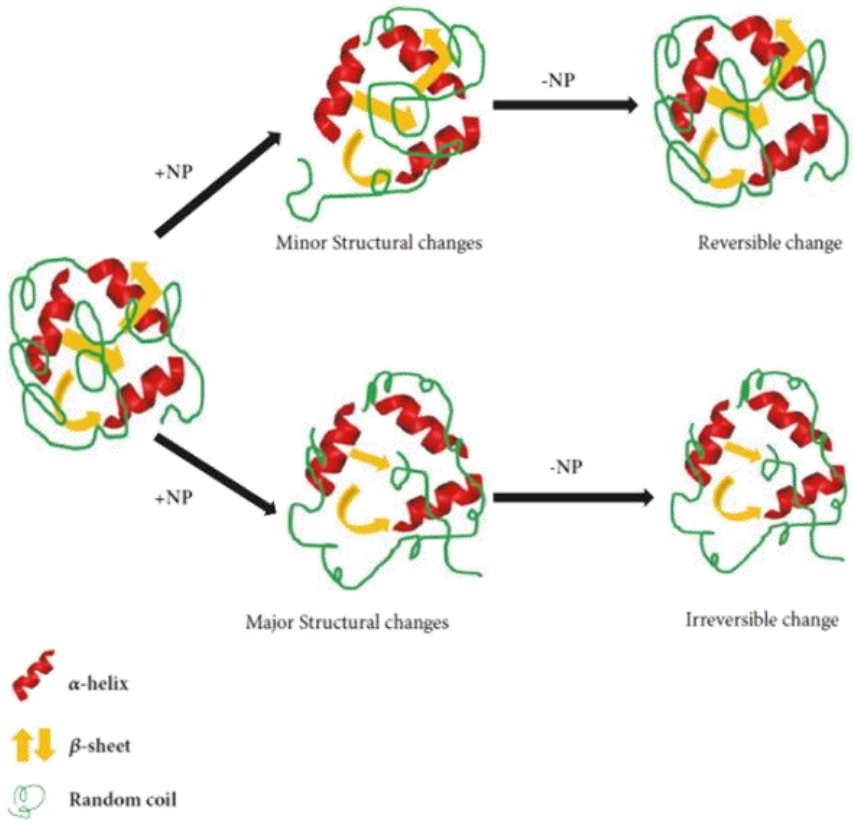

Reversible and irreversible changes of protein by NP interaction. Minute structural changes of protein by NPs, which would be regained by removal of NPs, can be considered as reversible mechanism. Significant NP-induced changes of protein structure (loss of β-sheets, α-helix), which will never be restored by removing NPs, may produce irreversible changes [71].

Tonigold et al. demonstrated that the pre-adsorption of antibodies against the CD63 antigen of monocyte-derived dendritic cells or the T lymphocyte CD3 antigen exerts remarkable targeting properties, proving that pre-coating with particular antibodies could be a promising approach to targeted NP-mediated delivery [72]. The precise detection of structural modifications occurring in adsorbed proteins is very challenging and requires the coordinated employment of several techniques, including Dynamic Light Scattering (DLS), electron microscopy, electrophoresis, Circular Dichroism (CD), Fourier Transform Infrared Spectroscopy (FTIR), Mass Spectroscopy (MS), and Nuclear

Magnetic Resonance (NMR) [73]. The ratio between NP and protein size is an important factor determining the amount of adsorbed proteins and alterations in their structure. It is realistic to presume that if the NP is much bigger than a single protein, more peptides can be harbored on the NP surface. On the other hand, smaller NPs of the same material have less contact with protein domains and a lower chance to induce structural changes. In agreement with this hypothesis, 110 nm citrate and Polyvinylpyrrolidone (PVP)-stabilized Ag NPs were found to bind a higher number of proteins compared to 20 nm citrate and PVP-stabilized Ag NPs, suggesting a different corona formation due to size and surface curvature of the NPs [74]. Actually, it has been shown that the adsorption of certain proteins on 100 nm NPs induces increased protein modification compared to particles of the same material smaller than 5 nm. In addition, the surface charge and hydrophilicity of NPs can affect proteins conformation. In particular, neutral part of protein does not attach to the NPs surface whereas charged portion majorly affect their orientation and folding on the surface of NPs [70]. Studies on polystyrene NPs demonstrated that proteins with an isoelectric point of less than 5.5 (e.g., albumin) mainly adsorbed on positively charged particles, whereas proteins with higher values (e.g., IgG) prefer negatively charged NPs. Therefore, NP functionalization with negative (e.g., COOH) or positive (e.g., NH_2) chemical groups may represent a way to select the protein coating. Hydrophilic NPs induce very less structural changes to proteins, in contrast to hydrophobic NPs. According to Keselowsky et al. [75], attachment of fibronectin on NPs surface alters its conformation/structure that affect its cell adhesion capability. The avoidance of complement-mediated phagocyte sequestration of NPs remains one of the major issues in nanotechnology applications to drug delivery [76]. Poly(ethylene glycol) (PEG) covering of NM surfaces is a method to delay phagocyte sequestration and allow NM presence in the blood circulation by retarding protein adsorption [77]. PEG interaction with specific plasma proteins, such as clusterin, has been shown to be an essential event to avoid cellular uptake [78]. Some of the presented properties of protein corona have been investigated in my PhD project to explore adsorbed-CXCL5 mediated targeting efficiency.

1.6 Silica Nanoparticles synthesis

During my PhD fellowship, I focused my attention on SiO_2 NPs synthesis and characterization exploiting their application as targeting tool. SiO_2 NPs demonstrated a

good degree of biocompatibility and they have the ability to enter the cell without affecting cell survival [79]. In vitro studies of SiO_2 NPs indicate that the particle surface area as well as the particle size or shape may play a crucial role in the toxicity of nanosilica. The absence of detectable toxic effects in vitro makes SiO_2 NPs a promising material for biomedical applications [79]. The sol-gel process is widely used to produce silica particles due to its ability to control the particle size, size distribution and morphology monitoring the reaction parameters. The process involves hydrolysis and condensation of metal alkoxides ($Si(OR)_4$) such as tetraethylorthosilicate (TEOS, $Si(OC_2H_5)_4$) or inorganic salts such as sodium silicate (Na_2SiO_3) in the presence of mineral acid (e.g., HCl) or base (e.g., NH_3) as catalyst [80][81]. The condensation/polymerization between the silanol groups or between silanol groups and ethoxy groups creates siloxane bridges (Si–O–Si) that are able to create silica structure. I decided to use the Stöber method to produce spheroidal and monodispersed silica NPs by using aqueous alcohol solutions of silica alkoxides in the presence of ammonia as catalyst (basic condition) [82].

Figure 9.

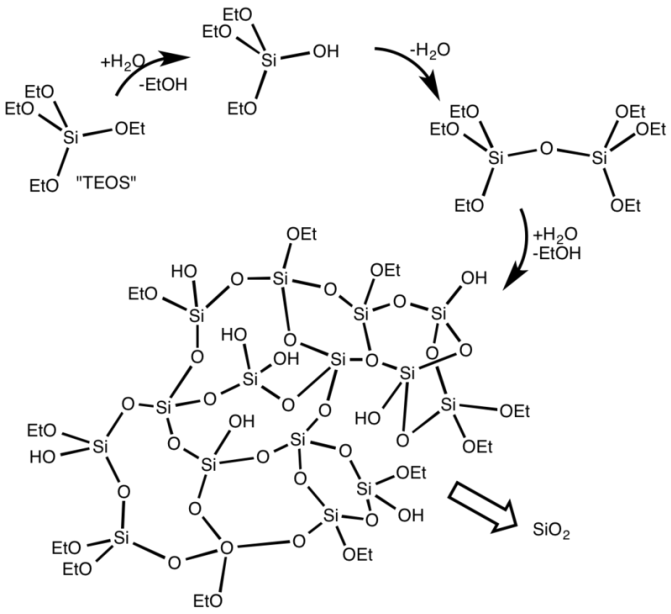

Simplified representation of the hydrolysis and condensation of TEOS in the Stöber process. Chemical reaction steps involved in the formation of siloxanes bridges.

1.7 Chemical Modification of Silica nanoparticles surface

The chemical modification of silica surface with organo functional groups is an important step towards the preparation of silica-polymer nanocomposites. Modification of silica surface with silane coupling agents is one of the most effective techniques available. In aqueous system, the silanes undergo hydrolysis and condensation before deposition on the surface and the alkoxy molecules are hydrolyzed in contact with water. Then, the silane molecules are deposited on the silica surface through formation of siloxane bonds between the silanol groups and hydrolyzed silanes with the release of water molecules [83]. Surface modification of silica nanoparticles can occur by using various types of silane coupling agents such as aminopropyltrimethoxysilane and methacryloxypropyltriethoxysilane [84]. Surface modification makes possible the conjugation of the silica NP surface with polymers or proteins [82]. SiO_2 NPs have the advantageous ability to encapsulate fluorescent dyes inside their "core", overcoming some limitations presented by free organic dyes, such as high photobleaching rates. Fluorescent SiO_2 NPs are very useful to study the interaction between NPs and biological system by confocal microscopy, flow cytometry and other optical techniques. Depending on the chemical properties of the fluorophore, it is possible to entrap more than one fluorophore into the particle [85]. SiO_2 NPs negative surface charge can be modified either via covalent coupling using silane chemistry, or via physical adsorption and electrostatic interactions [86][18]. SiO_2 NP surface can be functionalized with different molecules, including antibodies, folic acid, aptamers, PEG, carbohydrates, lipids [87][88]. Covalent functionalization on the silica surface is possible by using silane chemistry. The use of halosilanes and alkoxysilanes allow the introduction of functional groups like amines, carboxylates, epoxides and thiols. In my project 3-aminopropyltrimetoxysilane (APTMS) has been used as coupling agent. APTMS promotes strong covalent linkages onto the SiO_2 NPs surface creating protonated amine groups that allow electrostatic interaction with negatively charged species, such as DNA or proteins. Surface functionalization with PEG has been used to modify SiO_2 NPs surface to enhance the stealth effect of PEG and to avoid the opsonization by macrophages, hiding the silanol groups and stabilizing the colloidal particles. Several studies have demonstrated that ligand nature affects the interaction with serum proteins and cell membrane receptors, and consequently, the pathway by which cells internalize nanoparticles determining intracellular localization [89][90]. So the presence of

functional ligands (proteins) on NP surface is used to enhance the binding to specific target receptors present in the cellular membrane [91].

Figure 10.

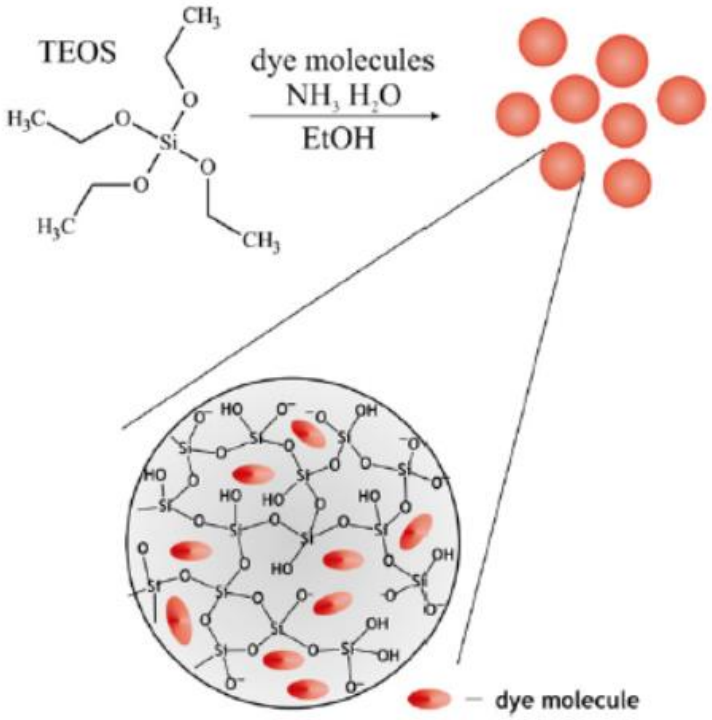

Schematic representation of Stöber method with the encapsulation of a dye in SiO_2 NPs [92]**.**

1.8 Chemokines

Chemokines are small proteins consisting of 70-100 amino acids secreted by almost all the cell types. They are chemotactic cytokines able to bind cognate receptors on cell membrane. They are involved in the homeostatic movement of cells, as well as leukocyte recruitment during immune responses. Some of them can also function as growth and angiogenic factor and chemoattractant for cancer cells. Chemokines are characterized by the presence of cysteine residues that define four families depending on the number of cysteines and the presence or not of amino acids in between them (i.e. CXC, CC, C, and CX3C) [93]. They also show a highly conserved tertiary structural fold consisting of

three-stranded β-sheet and a α-helix, though their quaternary structures may significantly vary with the sub-families [94].

1.8.1 CXCL5

Among the different chemokines that bind the receptor CXCR2 like GROα(CXCL1), ENA-78 (CXCL5), and interleukin-8 (IL-8; CXCL8) [95], I have chosen for my project the chemokine CXCL5.Structure of CXCL5 also called Epithelial neutrophil- activating protein (ENA-78) was initially identified in stimulated epithelial cells A549 since 1990s [96]. CXCL5 is composed of a tripeptide motif Glu-Leu-Arg at the NH_2 terminus relate to neutrophil-activating peptide 2 and growth-related oncogene-a. CXCL5 shares structural homological qualities with IL-8 and plays the similar role in processes of proliferation, metastasis, angiogenesis and neutrophils infiltration in different types of cancers. The monomer structure consists of an extended N-terminal loop (N-loop) followed by three β-strands and a terminal α-helix. The core structure is defined by hydrophobic contacts between residues of the α-helices and β-strands. CXCL5 is considered as a pro-inflammatory and angiogenic factor and it is involved in proliferation, invasion, metastasis, angiogenesis in cancer. Targeting CXCL5 may provide therapeutic benefits in several pathogenic conditions involving inflammatory processes [97].

Figure 11.

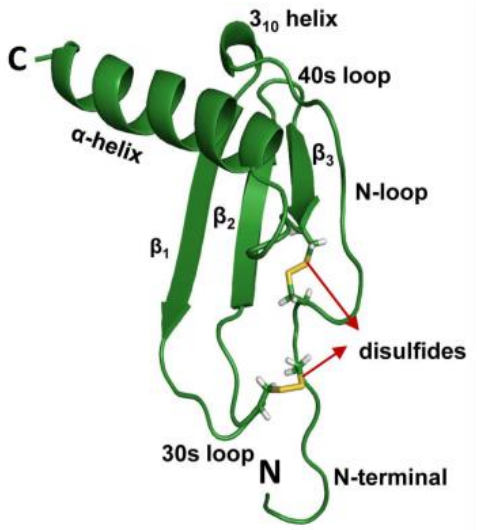

Structure of CXCL5 chemokine. The monomer consists of three antiparallel beta strands and an alpha helix; the disulfide bonds are shown in yellow [98].

CXCLs/CXCR2 axis produces multiple signaling pathways, like the PI3K, p38/ERK, and JAK involved in cell survival and migration. In particular, extensive infiltration of neutrophils during chronic inflammation is one of the most important pathogenic factors in various inflammatory diseases. Current therapeutic development of CXCLs/CXCR2 axis aims at target the receptor, inhibiting CXCR2 ligands through the blockade of signaling pathway, by transfecting microRNA (miRNA) in cells and using neutralizing antibodies [99]. Based on the knowledge of chemokine ability to bind its cognate receptor expressed on immune cells [100][101][102] as well as SiO_2 NPs cytocompatibility [103] [104][79], The starting hypothesis was that the chemokine-receptor binding could improve NPs localization on CXCR2 expressing leukocytes. The formulation of NPs functionalized with CXCL5 can be considered an innovative tool to prepare precise-targeting NPs for several applications to immune system.

Figure 12.

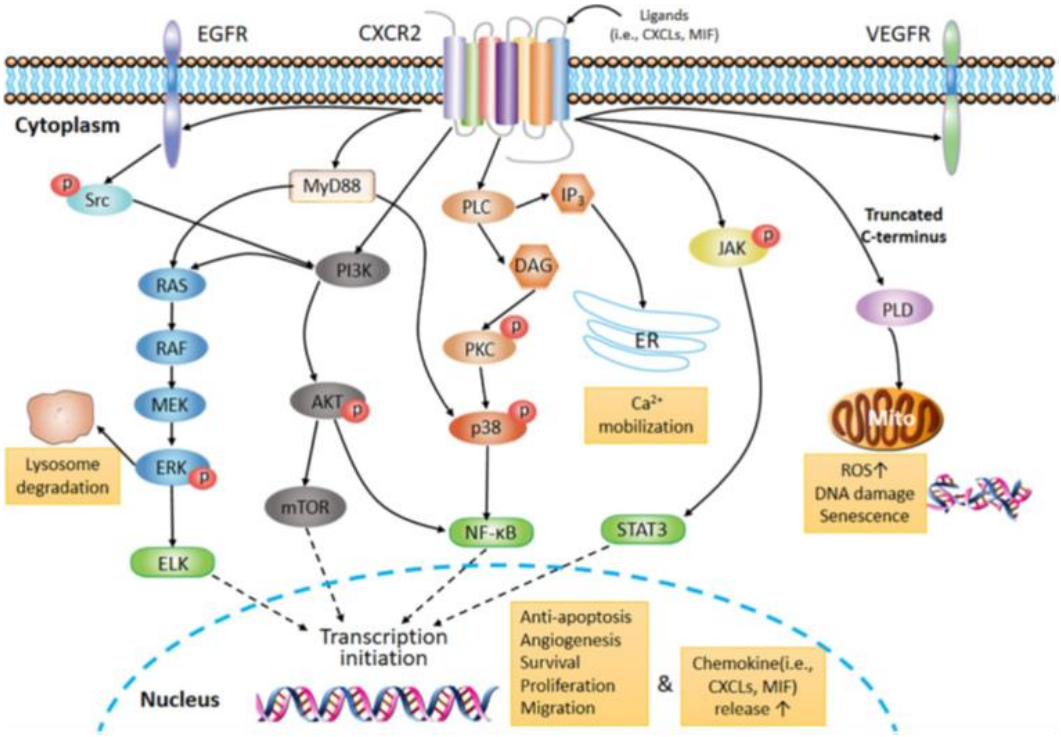

CXCLs/CXCR2 signal transduction pathway. CXCR2 is a typical GPCR. Its activation leads to transcription of various genes, such as ERK, p38, AKT, JAK2, and

modulates cell survival, angiogenesis, proliferation and senescence. Activation of CXCR2 also leads to Ca2+ mobilization Endoplasmic Reticulum and affects cell contraction and morphology [99].

1.9 Chemokine receptors and immune system

Chemokine and chemokine receptors have an important role in innate immune system. In particular, CXCL12/CXCR4 interactions remain essential for bone marrow retention and normal development of multiple immune lineages, including B cells, monocytes, macrophages, neutrophils, natural killer (NK) cells, and plasmacytoid dendritic cells [105]. CXCL14 is homeostatically produced by human fibroblasts in the skin and lamina propria, and tissue macrophages can be found in close association with CXCL14-producing cells [106]. Basophils express CXCR4 and so it is possible that they are released into the peripheral blood by CXCR4-mediated mechanisms, where they remain in the absence of inflammatory stimuli. Human basophils constitutively express CXCR1, CXCR4, CCR1, CCR2, and a majority express CCR3 [107][108]. Mast cells (MCs) are found throughout all vascularized tissues, where they act as innate immune sentinels and effector cells. Immature, resident DCs express various chemokine receptors (e.g., CCR1, CCR2, CCR5, CCR6, CXCR1, CXCR2, and CXCR4) that allow DCs to migrate to sites of inflammation, but they may also actively promote their maintenance in the periphery [109]. Although resident innate immune cells are the initial responders to inflammatory cues, circulating innate cells such as neutrophils, monocytes, and eosinophils quickly become the major immune cells during acute inflammation. Neutrophils are cells of acute inflammation; they express many chemokine receptors, including CXCR2 and CCR1 in mice and CXCR1 and CXCR2 in humans, which respond to early chemokines released by MCs and macrophages. Monocytes are defined by their expression of CCR2, they also express CXCR2, which may play an important role in initial activation and transmigration. In an atheroma model, CXCL8/CXCR2 interactions were necessary for firm adhesion of monocytes to vascular endothelium [110]. So, evaluated the important role of chemokine receptors in immune system, the use of chemokine to selectively target chemokine receptor is an important tool to be investigated for different biomedical applications.

Figure 13.

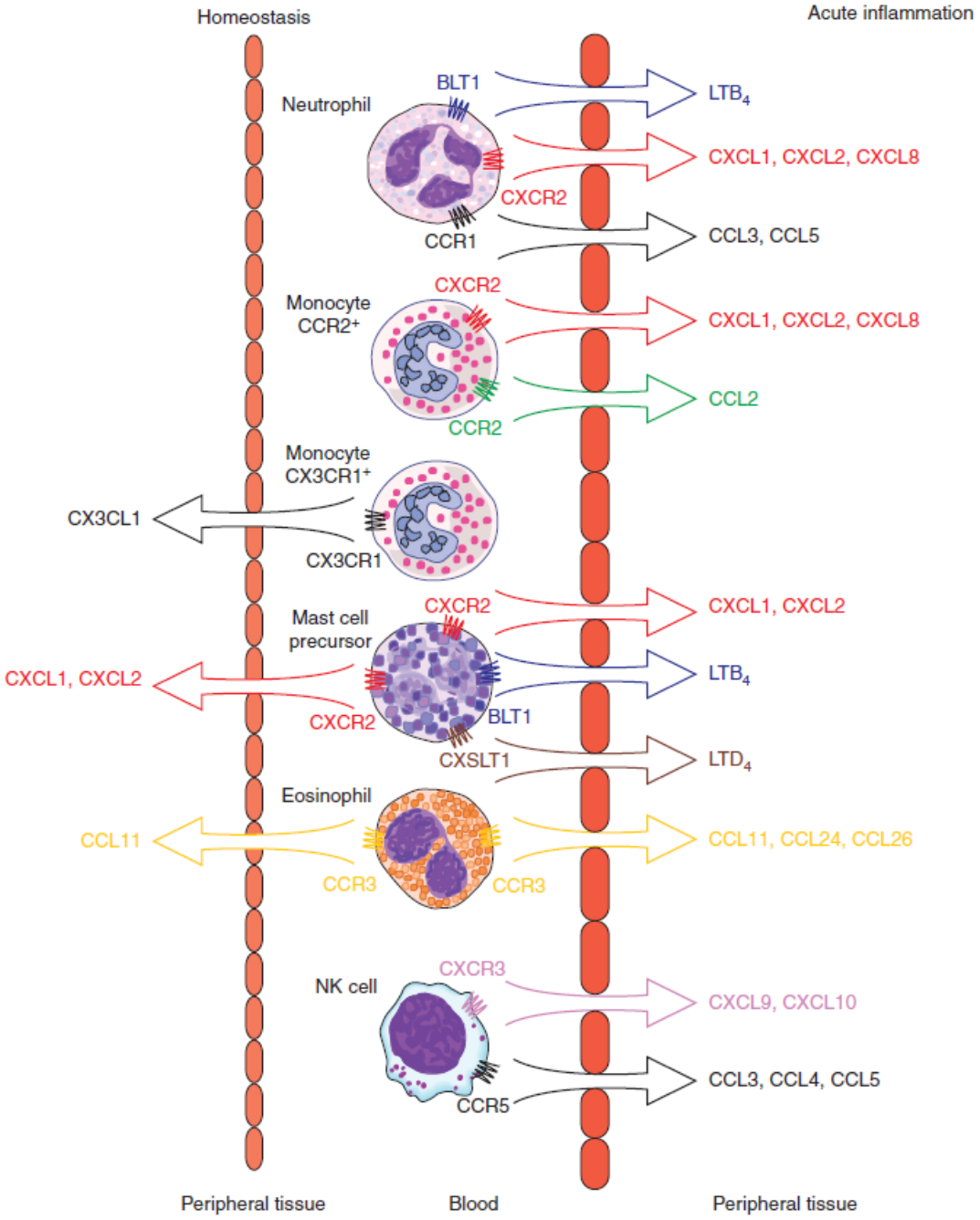

Chemokine control of innate immune cell migration in homeostasis and inflammation. Expression of different receptor on immune system cells [111].

1.10 CXCR2 receptor

Currently, 19 different chemokine receptors have been discovered, separated into four different subfamilies: C, CC, CXC and CX3C. In humans, the CXC subfamily contains seven chemokine receptors and 15 ligands. The CXC chemokine subfamily can be divided in a group of chemokines containing a glutamic acid leucine- arginine (ELR) motif, and a group in which the ELR motif is absent [93][112]. Seven of the 15 CXC ligands (CXCL1-3 and CXCL5-8) contain an ELR motif, all having high binding affinity for chemokine receptor CXCR2. The receptor belongs to the G coupled protein receptor family (GPCR) and it is composed of seven transmembrane segments, three extracellular and three intracellular loops, an extracellular N-terminal domain, and a cytosolic C-terminal segment. The amino acid aspartate in the second extracellular loop and a LLKIL motif in the C-terminus are both required for rapid receptor internalization, while the second intracellular loop contains a DRY (Asp – Arg – Tyr) motif as the G protein docking site, giving the chemokine receptor the ability to signal after ligand binding [113]. Chemokine receptors are activated through two-site interaction between the chemokine and its receptor. The first step in the receptor binding is the interaction of the chemokine's N terminal residues with the N-terminal domain of the receptor (site 1). After receptor activation, the heterotrimeric G protein, Gαβγ, separates into the subunits Gα and Gβγ, through the exchange of GDP for GTP on the Gα subunit. The Gβγ subunit then activates phospholipase C, which cleaves phosphatidylinositol (4,5)-biphosphate into inositol triphosphate and diacylglycerol that promote the rise of intracellular calcium causing chemotaxis and degranulation. Among the resulting effects of the chemokine-receptor binding, internalization of receptor represents the major mechanism for receptor-recycle and chemokine degradation. Internalization depends on the interactions between the chemokine N-terminus and the N-domain of the receptor [114]. In case of the recycling pathway, CXCR2 returns back to the cell surface after dephosphorylation, while, in the case of the lysosomal sorting pathway, the receptor will be also degraded by proteolytic enzymes [115]. The mechanism of receptor internalization is a clathrin-mediated endocytosis [116]. In particular the process starts with receptor activation by the ligand and phosphorylation (mediated by G protein receptor kinases, GRKs) of serine or threonine residues near the C-terminus of the receptor, leading to receptor desensitization. The phosphorylated receptors favors the recruitment of molecules like adaptin 2 and β-arrestin [115].The complex of the receptor with adaptin 2 and β-arrestin attracts clathrin, leading to internalization of the receptor from the plasma membrane to

form clathrin-coated vesicles. The receptor and the ligand are then transported to endosomes in which the chemokine and receptor can dissociate because of the acidic endosomal environment allowing the receptor to be recycled back to the cell membrane [115]. Given the crucial role of CXCR2 in inflammatory responses and immune diseases, I decided to exploit the interaction between CXCL5 and CXCR2 to create a new tool to selectively target CXCR2+ immune cells. In this way using CXCL5 decorated NPs it's possible to target only a particular immune system cell line that express the interested receptor.

Figure 14.

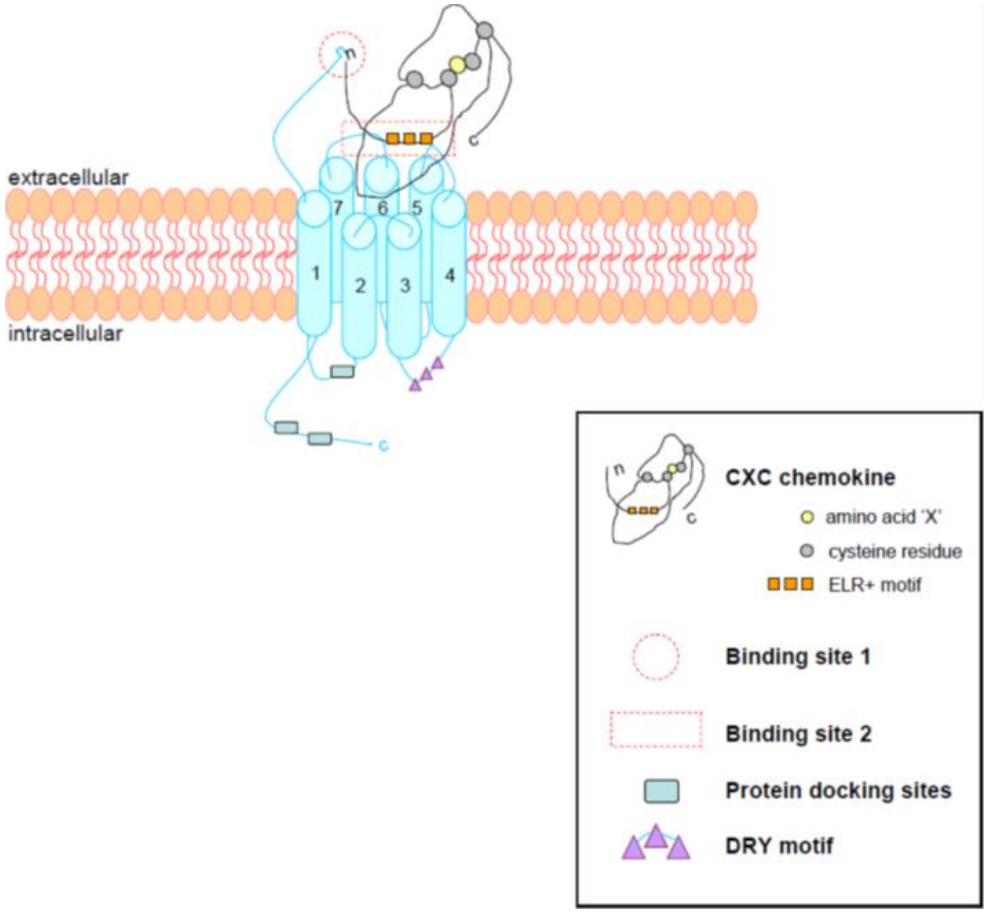

CXCR2 chemokine receptor structure. Representation of the binding sites of receptor, DRY motif and protein docking sites [117].

2. Aim of the work

In nanotechnology field, the selective targeting is still considered a challenge. It is very difficult to target in an active way cancer cells or a particular cell population, avoiding side effects on healthy cells. In particular, in my PhD project I decided to study and investigate this topic. The aim of my PhD project was to find a strategy to target in an active way a specific leukemia cell population (THP-1 cells). To get this goal, I adsorbed and covalently bound the chemokine CXCL5 on fluorescently labeled amino-functionalized and PEGylated SiO_2 NPs to precisely targeting CXCR2+ immune cells. My results provide the proof of principle that chemokine decorated nanomaterials enhance cellular uptake and allow precise cell subset localization. The possibility to aim at selective chemokine receptor-expressing cells can be beneficial for the different diseases involving immune system.

3. Results and discussion

3.1 Synthesis of 50 nm FITC-SiO_2 Nanoparticles

Silica (SiO_2) particles can be produced in a very precise manner in the nano-metric scale. Size, shape, and surface properties, such as charge or hydrophobicity, can be finely tuned to increase their biocompatibility [79]. Many features of SiO_2 NPs allow them to be used as reliable models for drug delivery systems [103]. Furthermore, fluorescent dyes or quantum dots can be easily entrapped or linked onto the NP surface for imaging purposes [103]. NP-coating polymers can also be used to reduce particle aggregation and increase their availability for target cells. Among the several biocompatible polymers, PEG shows many advantages, the most important of which are the reduced affinity to bind proteins [118] and the antifouling activity [119]. PEGylation of drugs and nanocarriers usually increase their circulation half-lives by decreasing their susceptibility to phagocytosis [77]. So, to endow NPs with "stealth" properties, the modification of their surfaces with PEG has become a popular method [120][121][122][123][9]. SiO_2 NPs were preferred as prototype particle due to the past and current expertise of the IIT-Nanobiointeractions and Nanodiagnostics Lab [103][124]. In particular fluorescent SiO_2 NPs were synthesized using the Stöber method [82] adding fluorescein isothiocyanate (FITC) that reacts with APTMS and creates a FITC-conjugate. The following reaction with TEOS forms the FITC-SiO_2 NPs (Figure 15).

Figure 15.

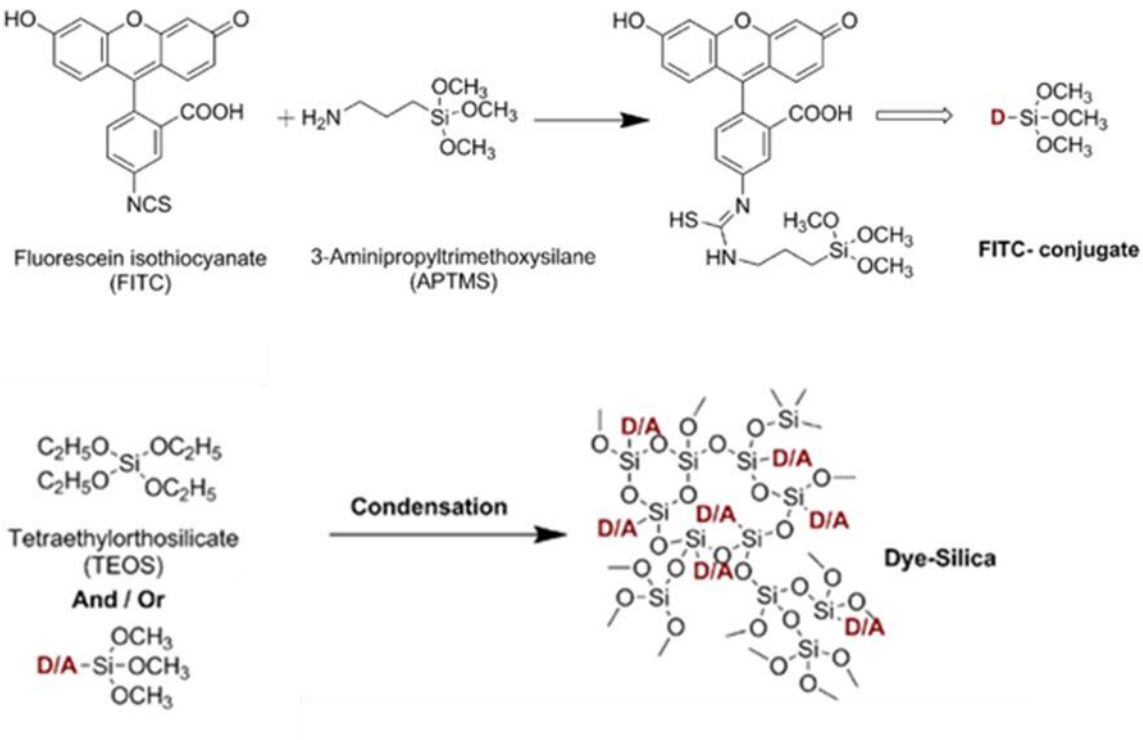

Synthesis of FITC-SiO_2 NPs using the Stöber method. Schematic representation of the different steps for the preparation of SiO_2 NPs [125].

3.2 SiO_2 NPs characterization

Synthesized SiO_2 NPs are characterized using different technique. To evaluate size and surface charge was used dynamic light scattering (DLS) analysis, for the morphology and the state of aggregation the transmission microscopy analysis (TEM). EDS analysis was used to evaluate the amount of N, C, O atoms present on NPs, CD to highlight important characteristics of protein secondary structure and conformational changes. To evaluate NPs uptake in cells was used the flow cytometry.

3.2.1 Transmission electron microscopy analysis

Transmission electron microscopy (TEM) is a microscopy technique in which a beam of electrons is transmitted through a specimen to form an image. The specimen is most often an ultrathin section less than 100 nm thick or a suspension on a grid. An image is formed from the interaction of the electrons with the sample as the beam is transmitted through

the specimen. The image is then magnified and focused onto an imaging device, such as a fluorescent screen [126]. In particular, I used this technique to evaluate the size, morphology and the state of aggregation of the SiO_2 NPs (Figure16). The images show that NPs are spheroidal, their size is 50 nm in average and are monodispersed.

Figure 16.

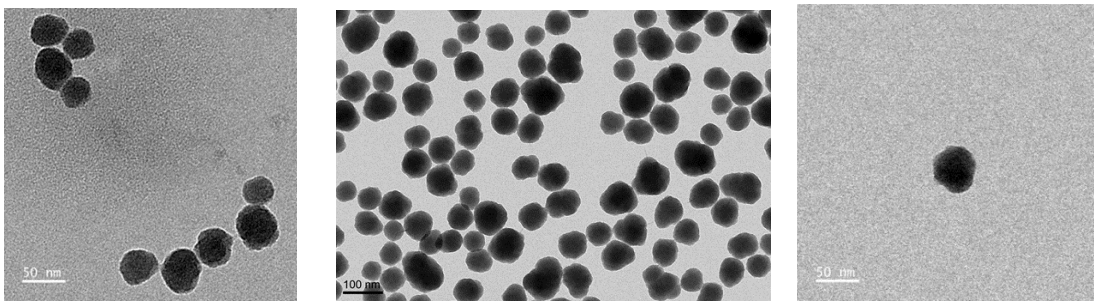

TEM analysis of SiO_2 NPs in ethanol.

3.2.2 Dynamic light scattering and zeta potential analysis

DLS is a technique that can be used to determine the size distribution profile of small particles in suspension or polymers in solution [127]. A monochromatic light source, usually a laser, is shot through a polarizer and into a sample. The scattered light then goes through a second polarizer where it is collected by a photomultiplier and the resulting image is projected onto a screen. In particular temporal fluctuations are usually analyzed by means of the intensity or photon auto-correlation function.

Figure 17.

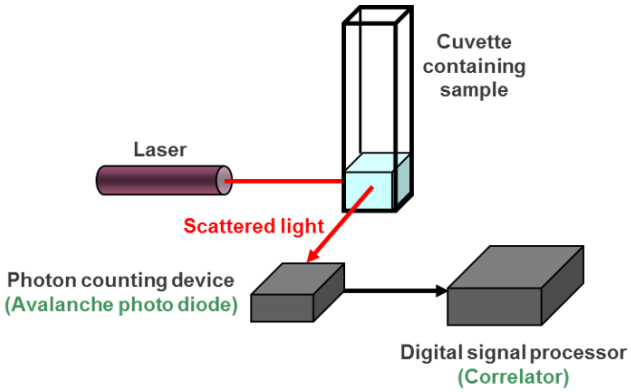

Schematic representation of DLS instrumentations [128]**.**

Zeta potential is a scientific term for electrokinetic potential in colloidal dispersions. The usual units are volts (V) or millivolts (mV). Zeta potential is the potential difference between the dispersion medium and the stationary layer of fluid attached to the dispersed particle. It is widely used for quantification of the magnitude of the charge and it is a key indicator of the stability of colloidal dispersions. The magnitude of the zeta potential indicates the degree of electrostatic repulsion between adjacent, similarly charged particles in a dispersion. For molecules and particles that are small enough, a high zeta potential will confer stability and dispersion will resist to the aggregation. When the potential is small, attractive forces may exceed this repulsion and the dispersion may break and flocculate. So, colloids with high zeta potential (negative or positive) are electrically stabilized while colloids with low zeta potentials tend to coagulate or flocculate [129][130]. DLS and Zeta potential analysis were performed to characterize the synthesized NPs in suspension. SiO_2 NP size was around 60 nm and have a negative surface charge. The size distribution was calculated measuring with Image J software the average diameter of NPs (500), confirming the size values obtained by DLS analysis.

Figure 18.

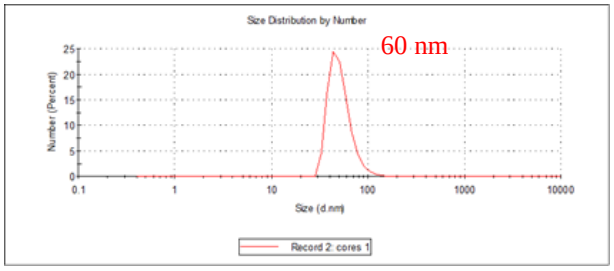

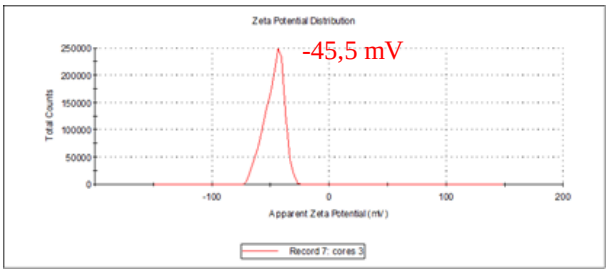

Evaluation of dispersion characteristics and surface charge of SiO_2 NPs.

Figure 19.

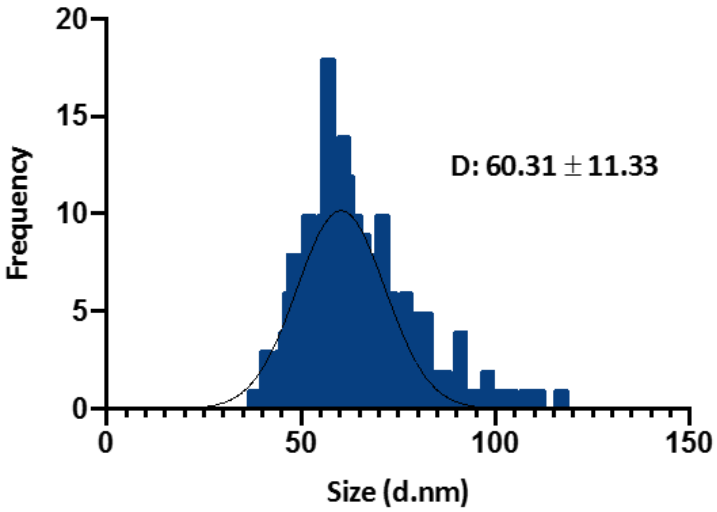

Histograms of size distribution in nm. D value (Diameter) reports the Average ± Standar deviation (SD) in nm [131].

3.3 Synthesis and characterization of PEGylated SiO_2 NPs

Coating nanoparticles surface with polymers like polyethylene glycol (PEG), polyethylene oxide hinders the binding of plasma proteins (opsonization) and prevents particle degradation. I functionalized SiO_2 NP surface with PEG hiding the silanol groups and stabilizing the colloidal particles with the final aim to avoid opsonization and reduce specific particle sequestration by macrophage. During the synthesis of SiO_2 NPs, the condensation/polymerization between the silanol groups or between silanol groups and

ethoxy groups creates siloxane bridges (Si–O–Si) that are able to form silica structure. In particular, Silane PEG-NH_2 was used to favor the reaction between the silane group on the PEG chain with the silane group on SiO_2 NPs. These particles were characterized by TEM and DLS. The images show the presence of a PEG shell around the silica surface (Fig. 21). Moreover, the graphs in Figure 21 highlight an increase of NP size and a positive shift in charge values when particles are functionalized with PEG moieties.

Figure 20.

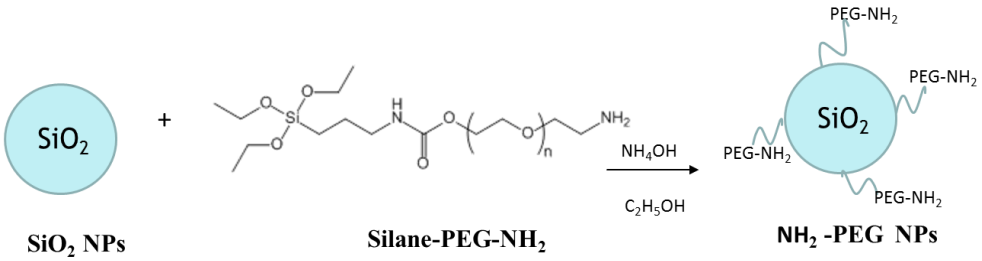

Schematic synthesis of PEGylated SiO_2 NPs using silane-PEG-NH_2. The reaction is conducted in ethanol using ammonium hydroxide as catalyst.

Figure 21.

Silane-PEG-NH_2 NPs

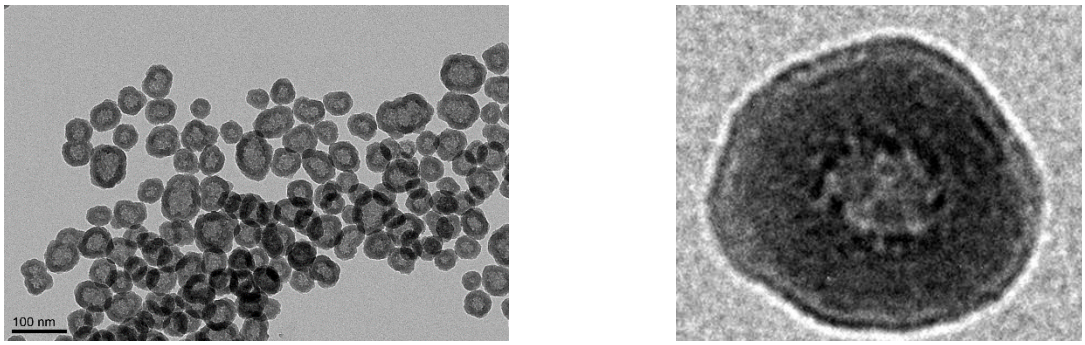

TEM analysis of PEG- NH_2 NPs previously resuspended in water. In the figure, it is possible to appreciate the presence of a PEG shell around NP surface.

Figure 22.

Silane-PEG-NH_2 SiO_2 NPs

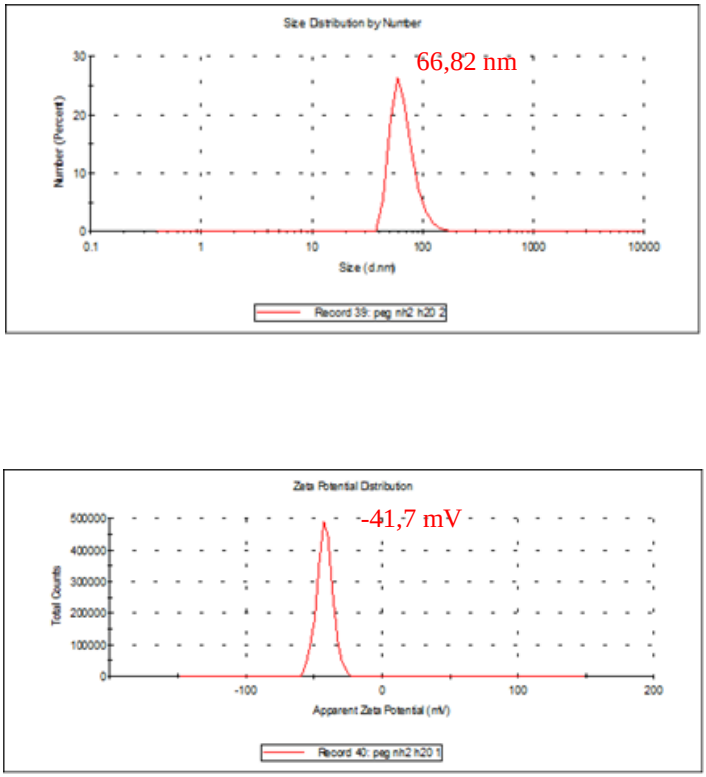

Evaluation of hydrodynamic diameter and surface charge of NH_2-PEG-SiO_2 NPs. After the coupling with PEG, the size increases and surface charge becomes less negative.

3.3.1 Ninhydrin assay

The ninhydrin assay was performed to evaluate the presence of amine groups in NH_2 – PEG NPs. Ninhydrin (2,2-dihydroxyindane-1,3-dione) is a chemical used to detect primary and secondary amines. When the compound reacts with free amines, a deep blue or purple color known as Ruhemann's purple is produced. To generate the ninhydrin chromophore (2-(1,3-dioxoindan-2-yl)iminoindane-1,3-dione), the amine is condensed with a molecule of ninhydrin to give a Schiff base. At this step, there must be a α hydrogen to form the Schiff base. Therefore, amines bound to tertiary carbons do not react further and thus are not detected. The reaction of ninhydrin with secondary amines gives an iminium salt, which is also colored, and this is generally yellow–orange in color [132]. Figure 24 shows that the samples containing NH_2 –PEG NPs, change color from yellow

to purple, due to the presence of amine in PEG chemical structure, confirming the presence of PEG on NPs. On the contrary, the SiO_2 NPs sample does not change color.

Figure 23.

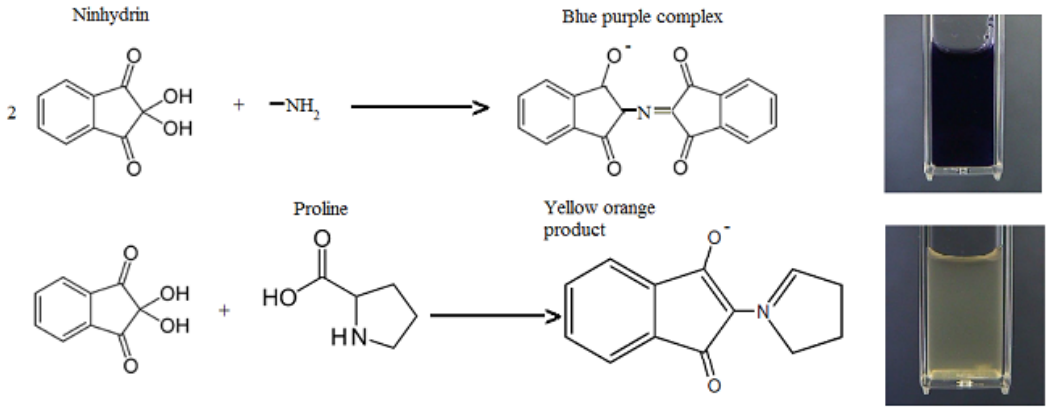

Schematic representation of ninhydrine reaction.

Figure 24.

Ninhydrine assay of SiO_2 and NH_2-PEG NPs to evaluate the presence of primary and secondary amines. The samples are dropped on a TLC and add to a solution of ninhydrin, butanol and acetic acid. The NH_2-positive sample (NH_2-PEG NPs) changes color from yellow to purple.

3.3.2 Coupling between Rhodamine isothiocyanate and Silane-PEG-NH_2 NPs

To further demonstrate the presence of PEG onto the SiO_2 NPs, the coupling between the amine group present on PEGylated NPs and the isothiocyanate group of the isothiocyanate-rhodamine was performed. The fluorescence was evaluated by confocal microscopy and PEGylated NPs resulted more fluorescent than SiO_2 NPs on average (Fig. 25). The different fluorescence intensity confirms the presence of PEG on NPs surface.

Figure 25.

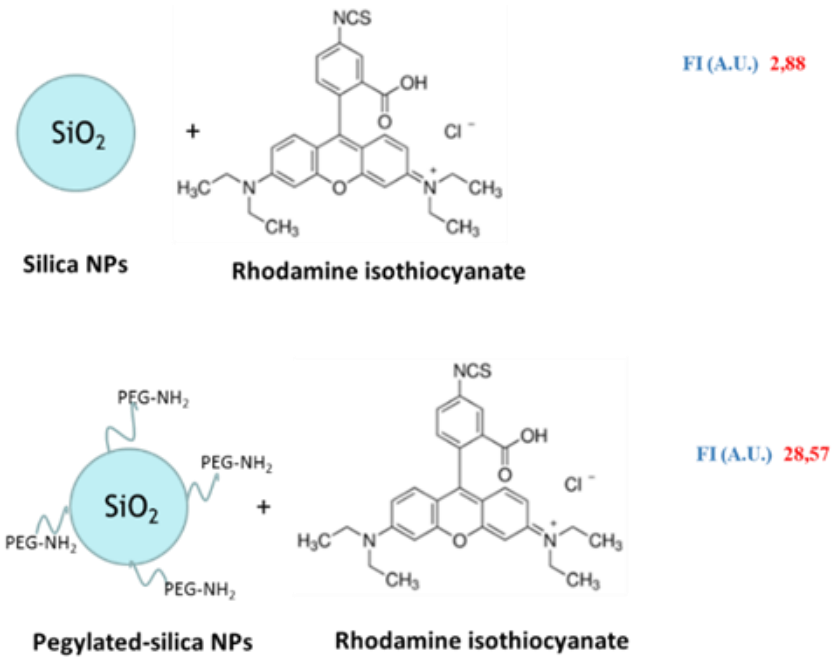

Schematic representation of the coupling between NH_2-PEG Nps and Rhodamine isothiocyanate. On the right, measurement of Rhodamine-induced fluorescence intensity.

3.3.3 EDS analysis to evaluate the presence of N atoms in NH_2-PEG NPs

Energy-dispersive X-ray spectroscopy (EDS, EDX, EDXS or XEDS) is an analytical technique used for the elemental analysis or chemical characterization of a sample. It is based on the interaction of X-rays with a sample containing elements with exclusive atomic structure allowing a unique set of peaks on its electromagnetic emission spectrum. At rest, an atom within the sample contains unexcited electrons in discrete energy levels or electron shells bound to the nucleus. The incident beam may excite an electron in one of the inner shells, ejecting it and creating an electron hole. An electron from an outer, higher-energy shell then fills the hole, and the difference in energy between the higher-energy shell and the lower energy shell may be released in the form of an X-ray. The number and energy of the X-rays emitted from a specimen can be measured by an energy-dispersive spectrometer and EDS allows the elemental composition of the specimen to be measured [133]. EDS analysis was used to further characterize the presence of Silane-PEG-NH_2 on Silica NPs evaluating the amount of N, C, O atoms present in the sample. Figure 26 shows the elemental analysis of NPs. N element is present only in NH_2 -PEG NPs and not in SiO_2 NPs, confirming the coupling with the polymer.

Figure 26.

Silica NPs	
Element	**Wt%**
C	44,27
N	0
O	55,73
Total: 100	

NH_2-PEG NPs	
Element	Wt%
C	5,29
N	22
O	72,72
Total: 100	

EDS analysis on silica and NH_2-PEG NPs. Quantification in percentage by weight of different atoms of C,O,N on SiO_2 NPs and NH_2-PEG NPs.

3.4 CXCL5 functionalization

The opportunity to choose specific polypeptides or proteins, whose cognate receptors are expressed by immune cells, can be exploited for specific immune cell targeting. To achieve this goal, I chose the chemokine CXCL5 to be bound onto the NPs. CXCL5 cognate receptor, CXCR2, is overexpressed in THP-1 cell line used as target cell model. I followed two strategies: CXCL5 was either covalently linked or absorbed on the PEG-NP surface. The covalent coupling (A) was chosen to favor the right orientation of the chemokine on NH_2-PEG NPs. The coupling reagent EDC/NHS allows the activation of the carboxylic groups of CXCL5 that reacts with the amine present of NPs surface. In this way, the amino terminal binding domain of CXCL5 can interact with CXCR2. In a second reaction (B) CXCL5 is adsorbed directly on NH_2-PEG NPs creating a CXCL5-protein corona around the NPs.

Figure 27.

A

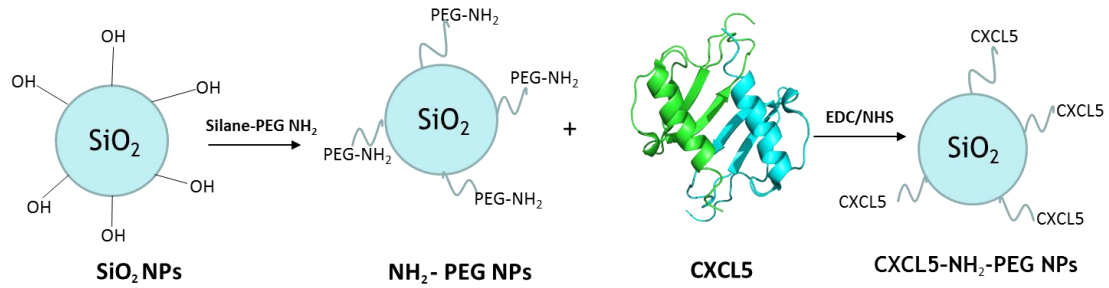

B

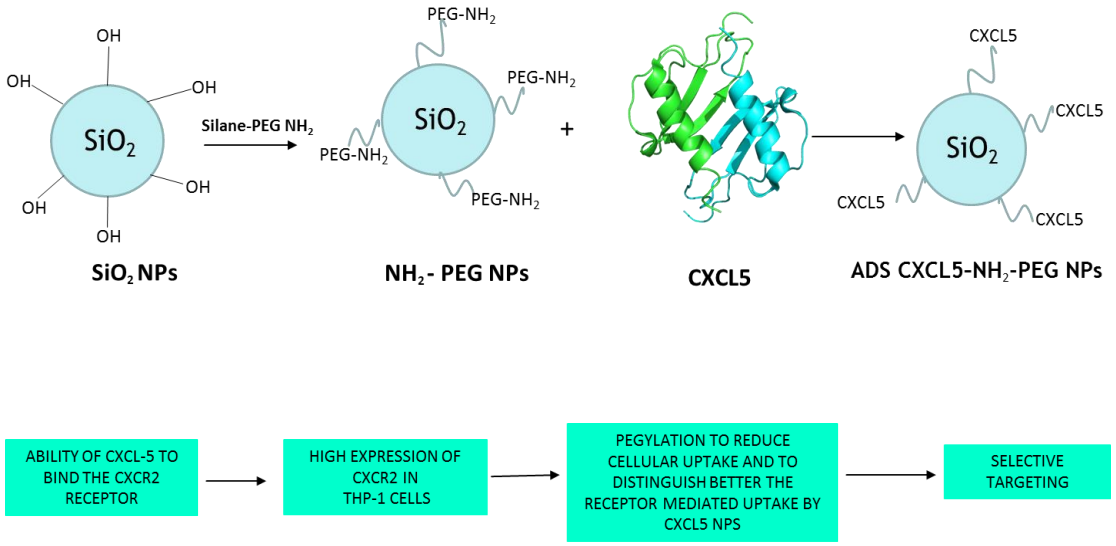

Schematic representation of CXCL5-PEG NPs synthesis.

3.5 Characterization of NH_2-PEG NPs

3.5.1 DLS and Zeta potential analysis

Dynamic light scattering (DLS) and Zeta potential analysis were performed to evaluate the dispersion characteristics and the surface charge of the synthesized NPs. SiO_2 NPs' size was around 60 nm on average. NH_2-PEG NP surface charge become more positive after the covalent coupling or adsorption of CXCL5 due to the presence of the chemokine on NP's surface (Fig. 28).

Figure 28.

NH_2-PEG NPs

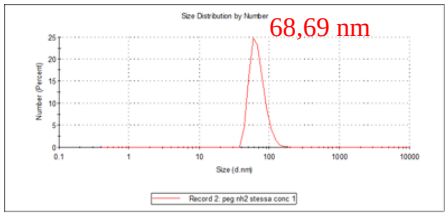

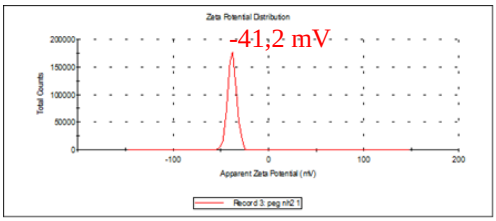

CXCL5 NH_2- PEG NPs

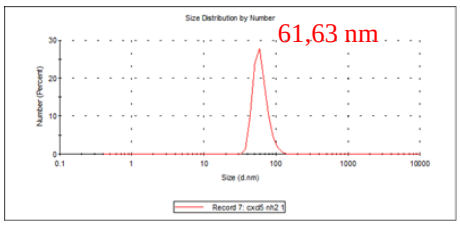

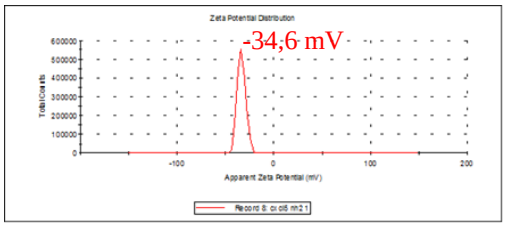

ADS CXCL5-NH_2-PEG NPs

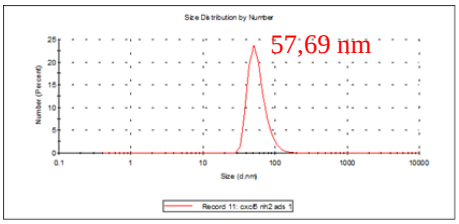

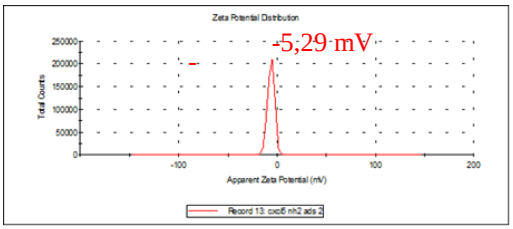

Evaluation of dispersion and surface charge of PEG-NH_2, CXCL-5 and adsorbed CXCL-5 NPs by DLS analysis.

3.5.2 Circular dichroism

Circular dichroism (CD) is a technique that evaluate the differential absorption of left- and right-handed light of optically active chiral molecules. CD spectroscopy has a wide range of applications in many different fields. Most notably, UV CD is used to investigate the secondary structure of proteins. UV/Vis CD is exploited to investigate charge-transfer transitions. Near-infrared CD is used to evaluate geometric and electronic structure by

probing metal d→d transitions. Vibrational circular dichroism, which uses light from the infrared energy region, is employed for structural studies of small organic molecules, and most recently proteins and DNA. In particular, the alpha helix of proteins and the double helix of nucleic acids have CD spectral signatures representative of their specific structures. The far-UV (ultraviolet) CD spectrum of proteins can reveal important characteristics of their secondary structure like the alpha-helix conformation, the beta-sheet and conformational changes [134].

Figure 29.

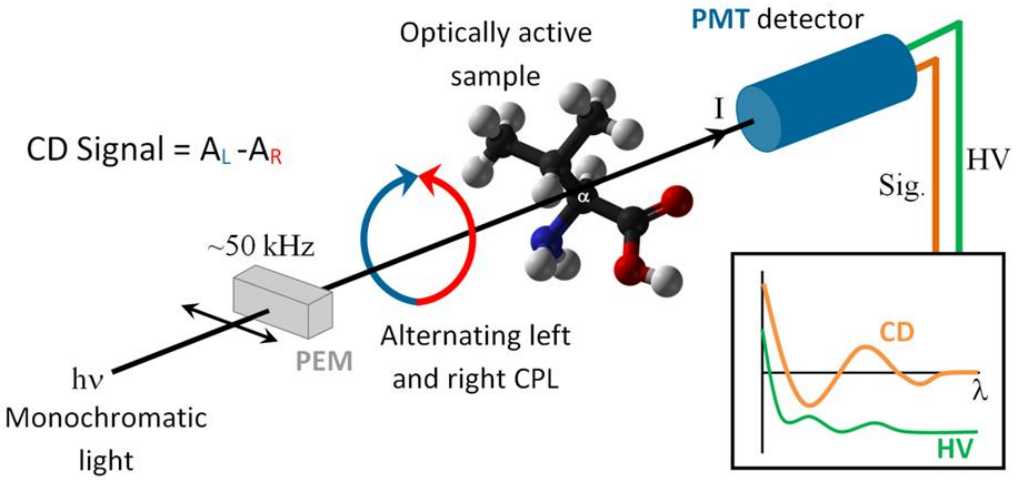

Schematic representation of CD spectroscopy technique. Monochrome light passed through a Photo Elastic Modulator (PEM), which converts the linear polarized light into alternating left and right-handed polarized light. The two polarizations are differently absorbed, and the difference in absorption is detected with a Photo Multiplier Tube (PMT) [135].

In my project, CD was performed to assess the presence of CXCL5 on NP surface and to evaluate its conformation through β-sheet and α-helix structure analysis. The results showed the presence of the chemokine on NPs, but with a different conformation compared to the native chemokine as effect of the several interactions with the nanomaterial (size, shape and charge). In Fig. 30 it is possible to appreciate the typical peaks of α- helix (negative bands at 222 nm and 208 nm and a positive band at 193 nm)

and β-sheets (bands at 218 nm and positive bands at 195 nm) in CXCL5-PEG NPs, which are not present in the non-functionalized NPs. In the case of adsorbed chemokine, the structure of the chemokine is similar to a random coil.

Figure 30.

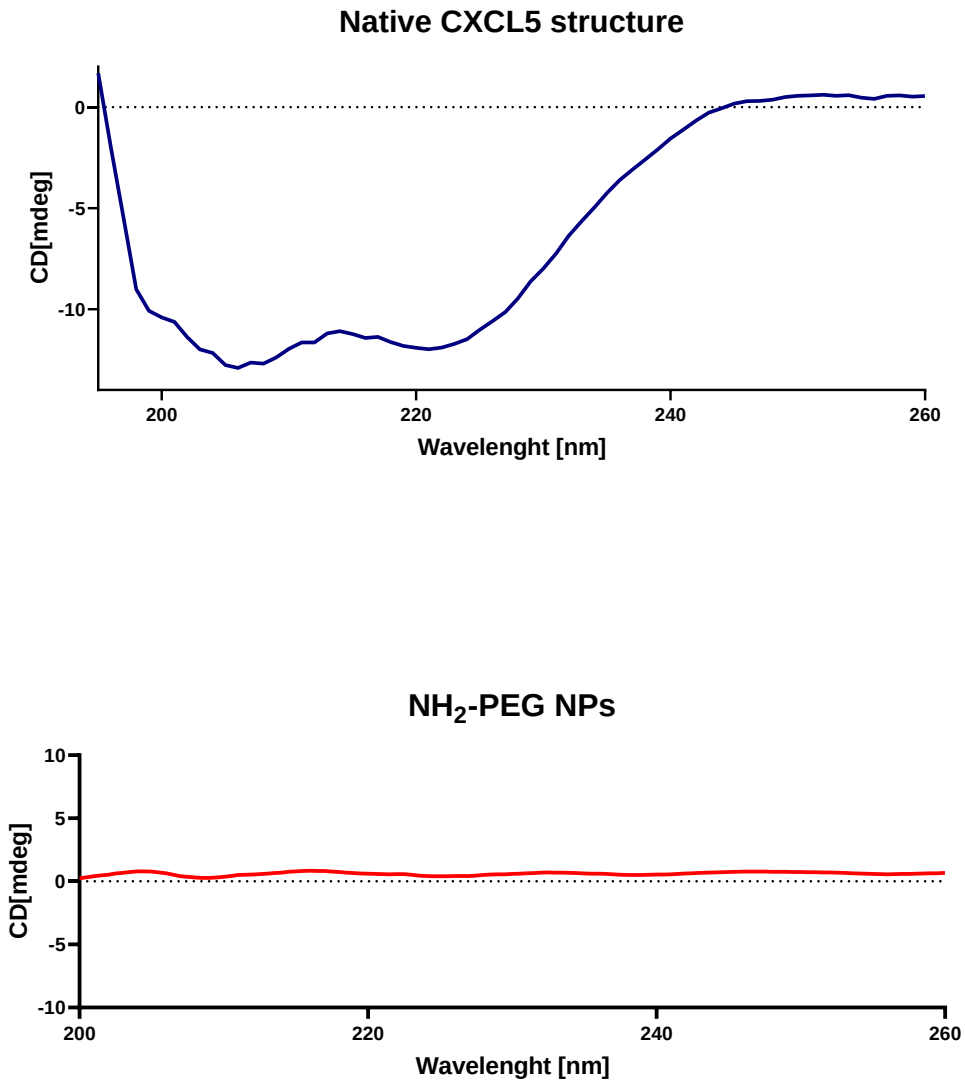

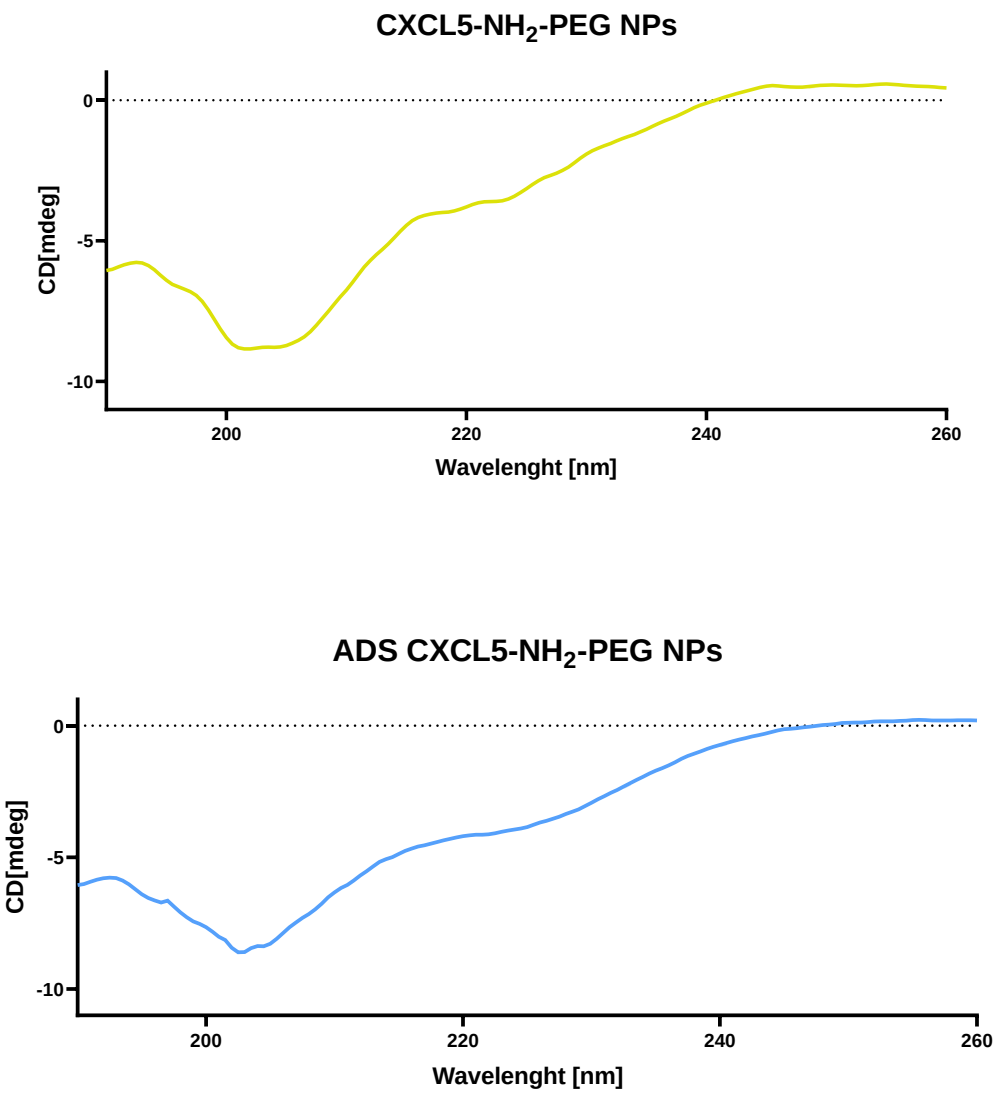

Circular dichroism analysis of different Silica NPs. Different CXCL5 conformation after the interaction with NH_2-PEG NPs.

3.6 Biological assays

3.6.1 Silica NPs uptake analysis by flow cytometry

Flow cytometry is a technique used to detect and measure physical and chemical characteristics of a population of cells or particles. Measurable cell parameters include: geometric properties, such as cell size (diameter, surface area, and volume); physiological properties, such as membrane potential, integrity, and vitality; and quantities of DNA, RNA, cytokines, surface antigens,nuclear antigens, enzymes, proteins. In particular, flow

cytometer is composed of five main components: a flow cell, a measuring system, a detector, an amplification system and a computer for analysis of the signals. The fluidics system includes a flow cell, where the sample fluid is injected. The flow cell requires sheath fluid to carry and align the cells or particles so that they pass through a narrow channel and into the laser intercept (light beam). The optics system consists of various filters, light detectors, and the light source, which is usually a laser line producing a single wavelength of light at a specific frequency. Lasers are available at different wavelengths ranging from ultraviolet to far red. The detector and analog-to-digital conversion (ADC) system converts analog measurements of forward-scattered light (FSC) and side-scattered light (SSC) into digital signals that can be processed by a computer. Forward scattered light is refracted by a cell in the flow, larger cells will have a stronger forward scatter signal. Side scattered light passes from the illumination source into the flow channel, is refracted by cells in a direction that is outside of the original light path and it is usually used to make a determination regarding the granularity and complexity of the cell. Highly granular cells with a large amount of internal complexity, like neutrophils, will produce more side-scattered light. The process of collecting data from samples using the flow cytometer is termed 'acquisition'. Acquisition is mediated by a computer physically connected to the flow cytometer and a software that is capable of adjusting parameters (e.g., voltage, compensation) for the sample [136].

Figure 31.

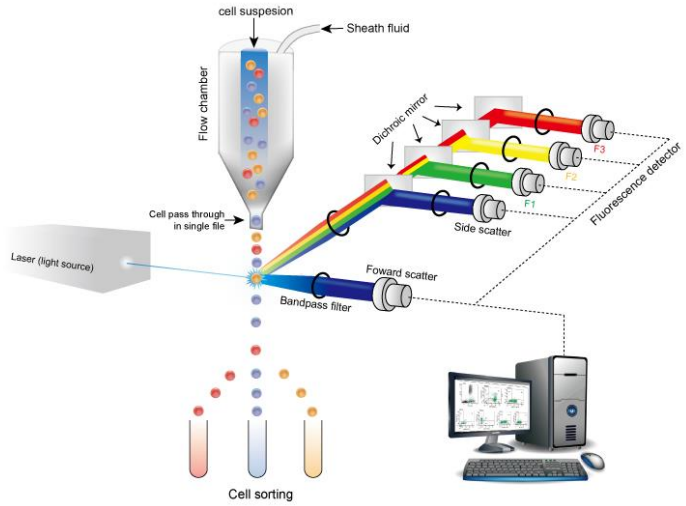

Schematic representation of flow cytometry instrument [137].

I used flow cytometry to study the interaction of fluorescent SiO_2 NPs with immune cells (THP-1). The cell fluorescence and side-scattered light increase after incubation with NPs and allowed us to define time and concentration dependence of nanoparticle-cell interaction.[104]. Fig. 32 shows the internalization of different SiO_2 NPs after 45 minutes of incubation in THP-1 cells. Cell uptake of CXCL5-NH_2 – PEG NPs is higher compared to NH_2 –PEG NPs due to the right disposition of the protein on NPs surface. When the protein is adsorbed on NPs internalization is reduced, possibly due to chemokine unfolding resulting in randomly orientated CXCL5 on the NP surface.

Figure 32.

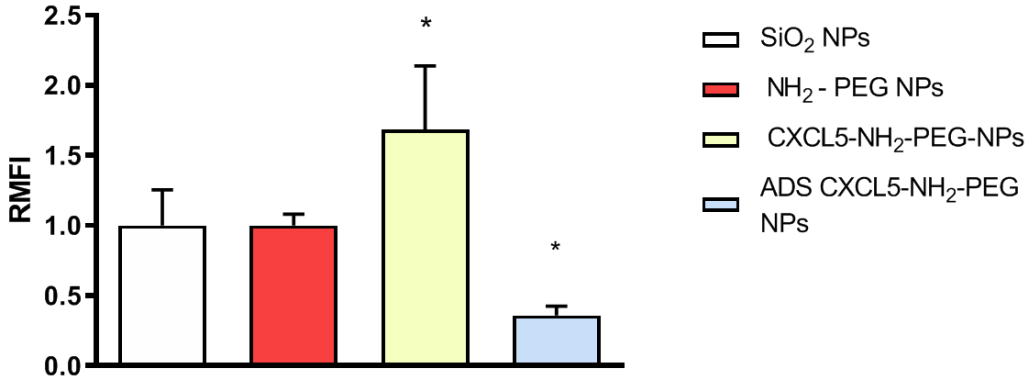

Uptake of different Silica NPs in THP-1 cells without serum evaluated by flow cytometry. The bars represent the fold increase fluorescence after the administration of 50 µg/ml of SiO_2 NPs. Error bars represent the mean at least of three independent experiments ± SD. * P< 0,05

3.7 Optimization of the coupling between CXCL5 chemokine and NH_2- SiO_2 NPs

Due to the difficult solubility of the Silane-PEG-NH_2 compound and NP aggregation after EDC/NHS reaction, CXCL5 NPs' synthesis was optimized by linking covalently CXCL5 directly onto the aminated surface of SiO_2 NPs. Since the receptor binding site of chemokines is at the N-terminus of the protein, I previously charged the NPs surface with positive amino groups to favorite the covalent binding of the COOH chemokine terminal group to the NP surface. Then, I functionalized NH_2-SiO_2 NPs with CXCL5 (Fig. 33).

The amination was obtained treating SiO_2 NPs with APTMS and acetic acid. Suddenly, the covalent coupling was achieved using a different coupling reagent to avoid NPs' aggregation. In particular NH_2-SiO_2 NPs were mixed with CXCL5 in the presence of 4-(4,6-dimethoxy-1,3,5-triazin-2-yl)-4-methyl-morpholinium chloride (DMTMM).

Figure 33.

Schematic representation of covalent coupling between NH_2 -SiO_2 NPs and CXCL5.

3.8 Adsorption of CXCL5 on NH_2-SiO_2 NPs

Numerous NMs show the intrinsic property to adsorb specific proteins present in biological fluids (e.g. blood) that can be used as targeting molecule to drive cell localization [64]. Although the formation of a selective protein corona is attractive, some concerns regarding the non-advantageous peptide orientation or the presence of conformational changes due to the chemical and physical interactions with the particle surface cannot excluded [65]. However, I also investigated the effect of the chemokine as a protein corona around NP Cores (A) and NH_2-SiO_2 NPs (B). In particular CXCL-5 adsorbed corona was prepared by mixing SiO_2 NPs with CXCL5 in water for 2h.

Figure 34.

A

Schematic representation CXCL5 adsorption onto NH_2 -SiO_2 NPs

B

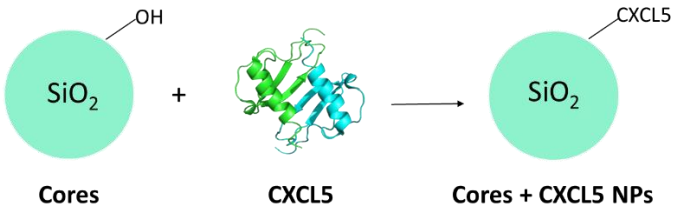

Schematic representation of CXCL5 adsorption onto Silica NP cores

3.9 SiO_2 NPs characterization

3.9.1 DLS analysis

DLS and Zeta potential analysis were performed to evaluate the dispersion characteristics and the surface charge of the synthesized NPs. SiO_2 NPs' size was around 90 nm and surface charge was negative (-50 mV), NH_2 – SiO_2 NPs show a positive zeta potential and when CXCL5 is linked to the NPs, there is an increase in size and a reduction in surface charge values from 29,8 to 16,8 mV according to the chemokine functionalization (Fig. 35).

Figure 35.

	Hydrodynamic diameter	**PDI**	**Zeta potential**
SiO_2 NPs	94,47 nm	0,12	-50,0 mV
NH_2 – SiO_2 NPs	99,4 nm	0,18	29,8 mV
CXCL5– SiO_2 NPs	121 nm	0,18	16,8 mV
Ads-CXCL5-SiO_2 NPs	145,8 nm	0,24	23,9 mV
Cores+CXCL5 NPs	116,8 nm	0,23	-1,48

Reported values of hydrodynamic diameters, polydispersion index and zeta potential of the NPs.

3.9.2 Immunogold

Immunogold labelling is a powerful technique to identify active sites and represents the best candidate probe to visualize proteins by TEM. In this technique gold nanoparticles conjugated with secondary antibodies bind primary antibodies that are able to recognize specific proteins [138].

Figure 36.

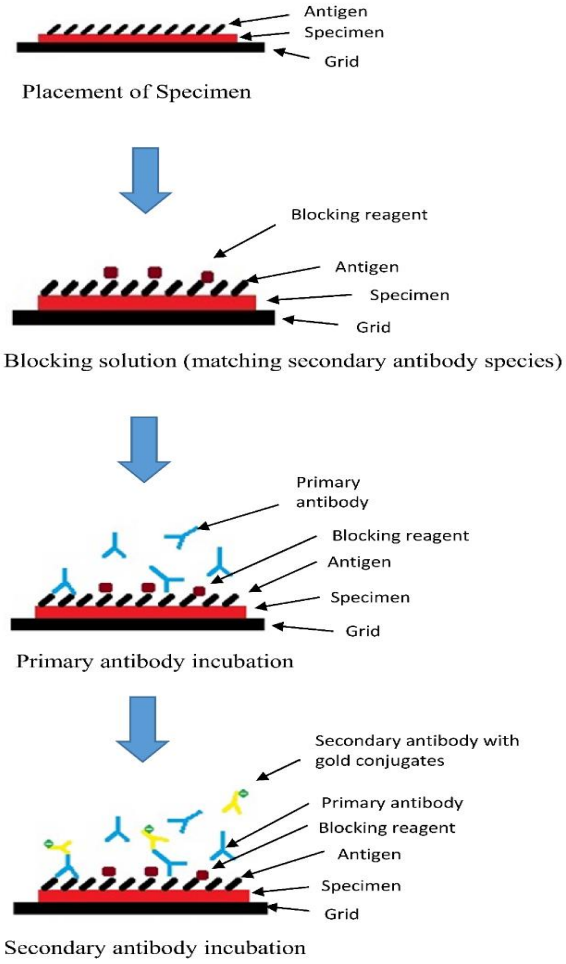

Representation of the whole process of immunogold labelling.

Immunogold staining was used to detect CXCL5 proteins on NH_2-SiO_2 NPs surface. Because of their electron density properties, gold nanoparticles (GNPs) can be easily revealed by electron microscopy and distinguished from the less electron-dense SiO_2. To visualize the fine localization of proteins present on NPs, I used 10 nm gold NPs linked to a secondary antibody against anti-CXCL5. Some spots in side view apparently seem detached from the NPs, although the distance is compatible with the antibody complex size (Fig.37).

Figure 37.

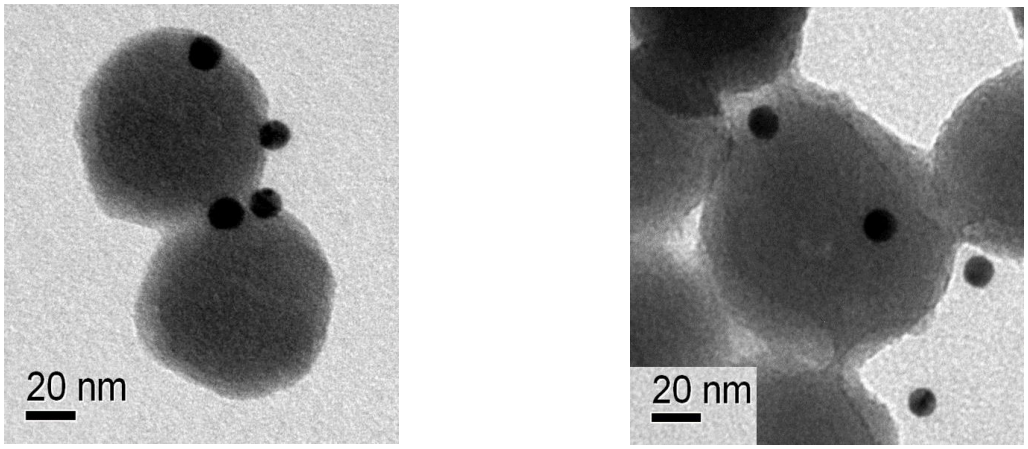

Nanoparticles immuno-labelling. TEM images showing the epitope mapping of covalently bound CXCL5 on NPs surface by 10 nm immune-gold NPs (dark spots) [131].

3.10 CXCR2 expression and internalization

To evaluate CXCR2 expression, THP-1 cultured in Fetal bovine serum (FBS) and Human Serum (HS) were incubated with fluorescently labelled antibody anti-CXCR2 and cell-associated fluorescence was analyzed by flow cytometry (Fig 38 A). The results show higher expression in HS enriched medium than in THP-1 cultured in FBS.

To evaluate receptor activity, THP-1 cells were starved in serum-free medium and then were treated with CXCL5 at different concentrations (100, 1000 nM). Subsequently the cells were incubated with fluorescently labelled antibody anti-CXCR2 and cell associated fluorescence was evaluated by flow cytometry (Fig. 38 B). The result highlight partial internalization (around 50%) of CXCR2 in THP-1 cells by CXCL5 at different concentrations (up to 1 μM).

Figure 38.

A **B**

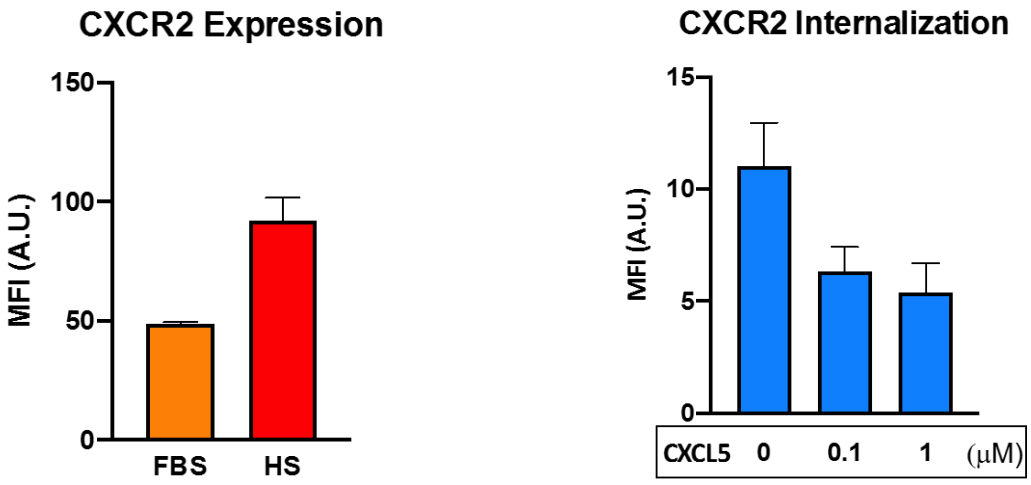

CXCR2 expression by flow cytometry on THP-1 cells cultured in different conditions (A). Bars represent the median fluorescence intensity. Error bars represent the mean at least of three independent experiments ± Standard error of the mean (SEM).

CXCR2 internalization (B). Bars represent the median fluorescence intensity (MFI) of APC-labelled anti-CXCR2 in the absence or presence of CXCL5. Error bars represent the mean at least of three independent experiments ± SEM [131].

3.11 SiO_2 NPs internalization in THP-1 cells cultured in HS and FBS

CXCL5-NP specific targeting properties were studied in CXCR2 expressing myeloid pro-monocytic THP-1 cells [139][140]. I compared the cellular uptake of the CXCL5-NPs with non-functionalized positively charged NPs, in the absence or in the presence of serum during the incubation time. The relatively short time incubation (45 minutes) has been chosen as longer time of cell exposure to NPs would have allowed unspecific internalization of both types of NPs invalidating the kinetic advantage of chemokine-receptor binding for the CXCL5-NPs. Flow cytometry results showed > 4 times increased uptake of the CXCL5-NPs vs. NH_2-NPs in serum-free medium (Fig.39 A). Internalization of CXCL5-NPs in complete medium was also noticeably enhanced, although less

pronounced than in serum-free condition. This reduction is likely due to the serum diverse protein corona reducing NPs interaction with cells.

In figure B is shown the same type of experiment using THP-1 cultured in HS enriched medium. Flow cytometry results showed increased uptake of the CXCL5-NPs vs. NH_2-NPs following incubation without serum. Internalization of CXCL5-NPs in THP-1 cells in complete medium was also enhanced but less pronounced than in serum-free condition (Fig. 39 B).

Figure 39.

A

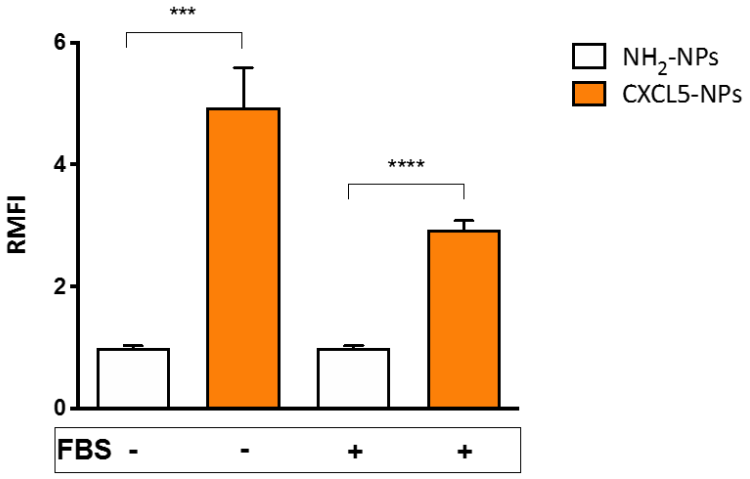

B

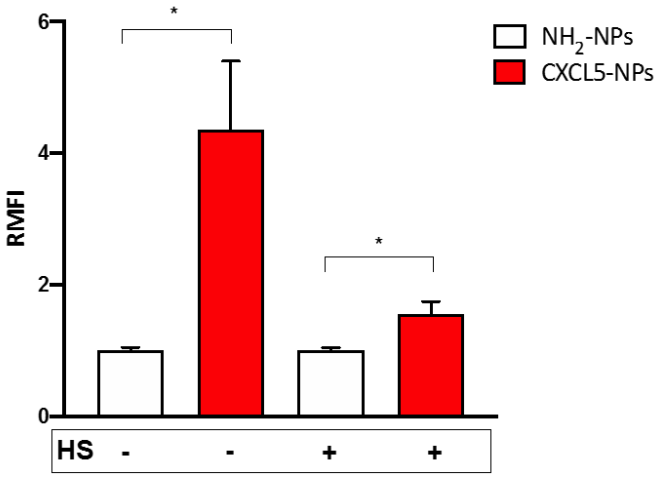

Silica NPs uptake in THP-1 cell lines in different medium conditions evaluated by flow cytometry. The bars represent the relative median fluorescence intensity (RMFI) after the administration of 50 μg/ml of SiO_2 NPs. Error bars represent the mean at least of three independent experiments ± SEM. **** P< 0,0001 *** P< 0,0005 * P< 0,05 [131].

It's very difficult to compare these results with other works present in literature, because is the first time that a chemokine is covalently linked to NPs surface to target in a selective way a receptor overexpressed in particular cell population. There are other works that have as main goal the targeting of receptors. In the work of Ying Xie et al. cyclam- and chloroquine-based polymeric CXCR4 antagonists are used to deliver functional siRNA and miRNA to cancer cells and block the CXCR4/ CXCL12 axis. These CXCR4 targeted nanomedicines carrying functional siRNA/miRNA represent a promising choice for combinational cancer therapy especially metastasis inhibition [141].

3.12 CXCL5 NPs displacement by CXCL5 pre-treatment.

A further proof of CXCL5-NPs interaction with CXCR2 has been underlined by NP uptake in cells pretreated with high concentration of free CXCL5. In particular I pre-treated THP-1 cells with 1μM CXCL5 and subsequently incubate the cells with both types of NPs. As shown in Fig. 40, CXCL5-NP internalization was reduced, whereas THP-1 uptake of NH_2-NPs revealed a statistically non-significant increase in average. I hypothesized that the presence of free chemokine in the medium could create a CXCL5 corona facilitating the entrance of NH_2-NPs. On the contrary, the moderate but statistically significant reduction of CXCL5-NPs internalization may be due to the agonist-mediated partial internalization of CXCR2 in THP-1 cells. As demonstrated in Fig 38 B, the administration of saturating concentrations (up to 1 μM) of CXCL5 internalizes less than 50% of the receptor expressed on the surface. This event maybe is due to saturation of intracellular internalization mechanisms, for example β-arrestins pathway desensitization [142] or aberrant expression of this receptor in THP-1 cell line. These data clearly show the different behavior of CXCL5-NPs and NH_2-NPs in the presence of receptor occupancy and desensitization by its cognate chemokine (Fig. 40).

Figure 40.

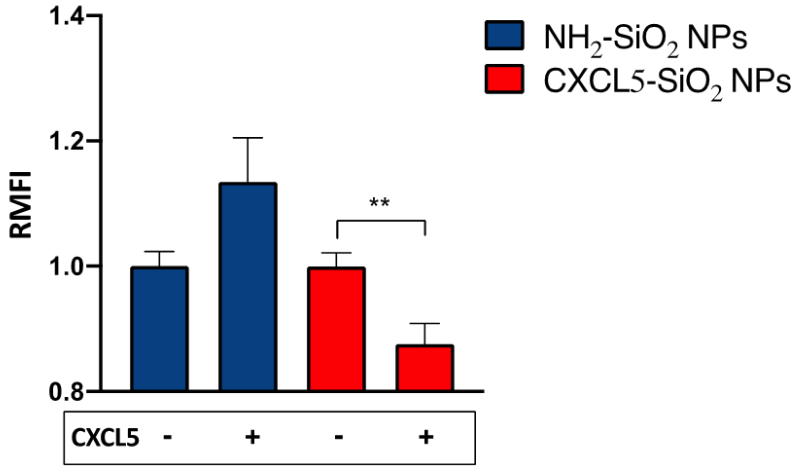

CXCL5 displacement by free CXCL5. Internalization of 50 µg/ml NPs in THP-1 cells pretreated or not with 1µM CXCL5. The bars represent RMFI of at least three independent experiments ± SEM. ** P< 0,001 [131].

3.13 CXCR2 expression and Silica NPs internalization in HeLa cells

In order to study the targeting selectivity of CXCR2+ cells, I compared the uptake of NPs in $CXCR2_{high}$ THP-1 cells vs. $CXCR2_{low}$ HeLa cells. THP-1 and HeLa cells were incubated with anti-CXCR2 antibody for 15 minutes and cell-associated fluorescence was analyzed by flow cytometry. The results show that HeLa cells present lower expression of CXCR2 compared to THP-1 (Fig 41 A).

In order to study the targeting selectivity of CXCR2+ cells, I compared the uptake of NPs in $CXCR2_{high}$ expressing THP-1 cells vs. $CXCR2_{low}$ HeLa cells (Fig 41 B). Incubation of these two cell lines with functionalized and non-functionalized NPs displayed opposite results. In $CXCR2_{low}$ HeLa cells, I could not detect increased CXCL5-NPs internalization in respect of the control NPs. The result shown by flow cytometry and confocal microscopy demonstrate the preferential targeting of CXCR2+ cell by CXCL5 decorated NPs.

Figure 41.

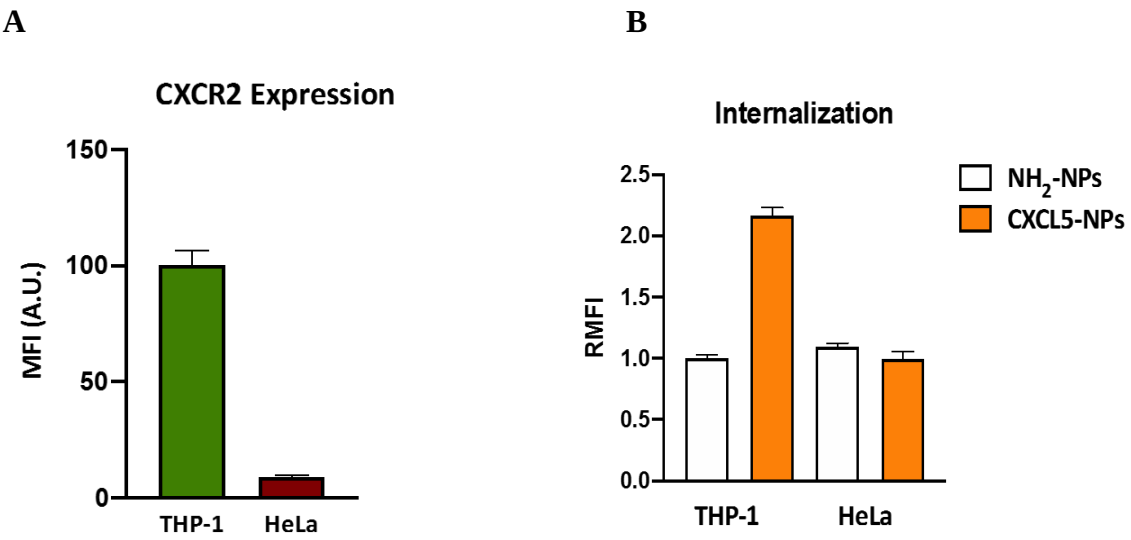

CXCR2+ cell preferential targeting of CXCL5-NPs. CXCR2 expression (A) and NPs uptake in THP-1 and HeLa cells in serum free conditions (B) evaluated by flow cytometry. The bars represent MFI and RMFI of at least three independent experiments ± SEM [131].

3.14 Confocal microscopy of NH_2-SiO_2 and CXCL5-SiO_2 NPs in THP-1 and HeLa cells

Confocal microscopy is used to resolve the detailed structure of specific object within the cells. In particular, biological samples are often treated with fluorescent dyes to make selected objects visible. Confocal laser-scanning microscope (CLSM) illuminates the sample with lasers of various wavelengths (available from UV to infrared) that produce an intense beam that can be focused down to a tiny spot. Galvanometer mirrors within the scan head guide the laser beam through the objective lens and back and forth and up and down across the specimen. To form a 3D data set, the focus can then be changed and another image generated at the new focal depth. Successive images are collected at various focus depths to generate a 3D image stack. Modern confocal microscopes use acousto-optic tunable filters (AOTFs) to rapidly turn lasers on and off, attenuate laser light, and to select which color of laser light is exciting the sample. To visualize the specimen by eye or using a camera, the fluorescence from the sample is collected by the objective lens, rescanned by the galvanometric mirrors, and then focused through a confocal pinhole onto a photomultiplier tube (PMT).The PMT has a light-sensitive

photocathode that converts photons into photoelectrons that are then amplified by a series of dynodes. As the PMT detects the fluorescence pixel by pixel across the sample, the computer builds up an image of the specimen on the computer screen [143].

Figure 42.

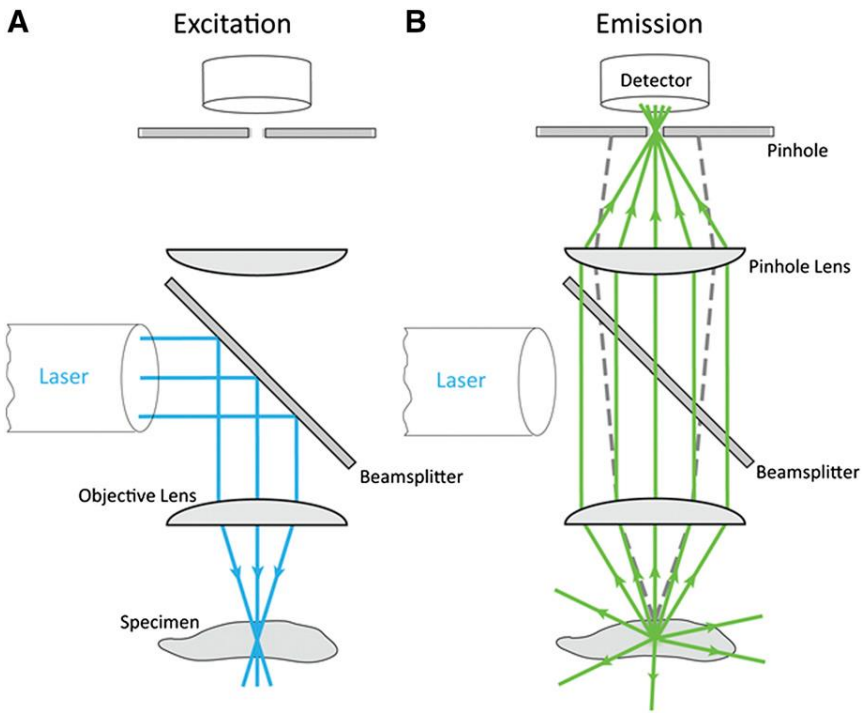

Schematic diagram of the confocal laser-scanning microscope (CLSM). The excitation laser beam light path (A) and emission light path (B). The solid blue lines in (A) represent the excitation laser that is focused onto the specimen. The solid green lines in (B) show that emission light from the focal plane passes through the pinhole aperture and is detected by the photomultiplier tube (PMT). The dashed gray lines show that out-of-focus light will be blocked, will not pass through the pinhole, and will not be detected by the PMT [143].

Figure 43.

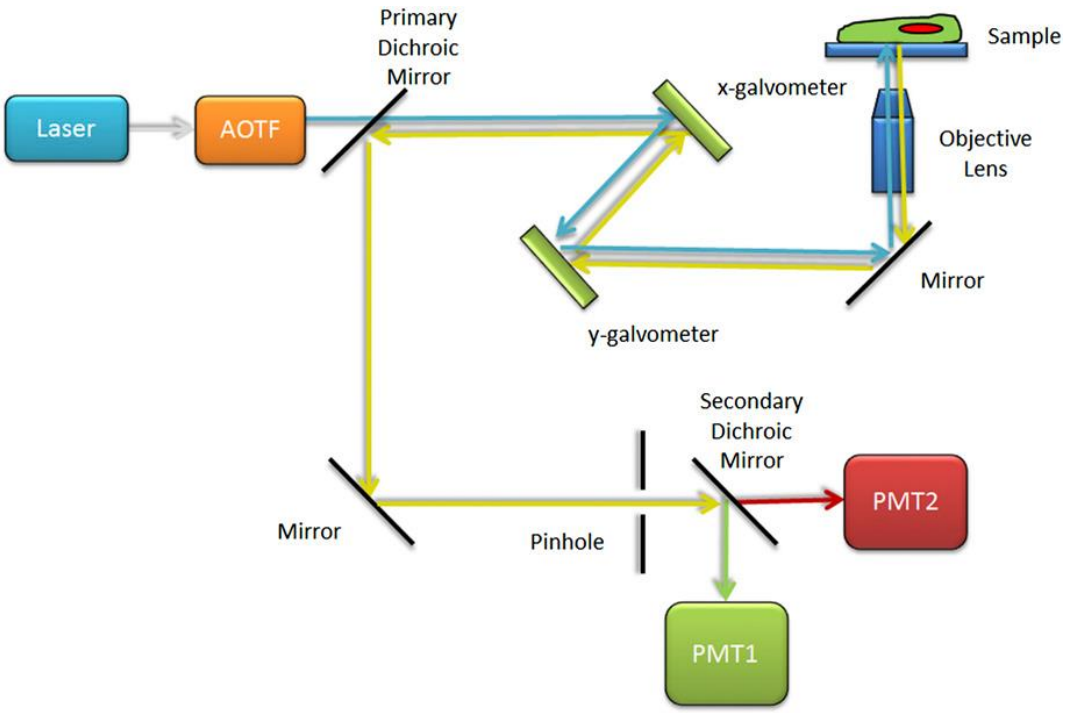

Basic CLSM light path. Schematic diagram of the CLSM light path with blue excitation light selected by the AOTF. The light is focused onto the sample by the objective lens and then scanned across the sample by the x and y galvanometer mirrors. Emission light is focused by the objective lens, descanned by the mirrors and reflected toward the detection light path by the primary dichroic mirror. In-focus light is selected by the pinhole aperture. The secondary dichroic mirror splits the green emission light and directs it to be detected by PMT1, and the red emission light passes and is detected by PMT2 [143].

I used confocal microscopy to visualize the presence of fluorescent SiO_2 NPs inside the cells. In particular, to confirm the data obtained by flow cytometry, THP-1 and HeLa cells were treated with NH_2 – SiO_2 and CXCL5-NPs for 45 minutes and the internalization was evaluated by confocal microscopy. Figures A-C show THP-1 and HeLa pre-treated with NH_2–SiO_2 NPs. The nuclei were stained with Hoersch dye and lysosomes with lysotracker for THP-1 instead for HeLa the cytoscheleton was stained with phalloidin red. Both the cell lines don't internalized NH_2 – SiO_2 NPs. Maybe it is due to the fact that 45

minutes are a short time to favor the internalization of nanoparticles that enter the cells by endocytosis.

Figures B-D show the cells pre-treated with fluorescent CXCL5-NPs. In THP-1 cells it's possible to observe the presence of nanoparticles inside the cells because they enter the cells through the receptor mediated uptake and as demonstrated before, CXCR2 is very high expressed on THP-1 cell membranes. Instead for HeLa cells, because of the very low expression of CXCR2, these cells don't internalize CXCL5-NPs demonstrating the preferential targeting of CXCR2+ cell by CXCL5 decorated NPs.

The intracellular localization of the particles was also confirmed by 3D confocal microcopy (Fig.45) highlighting the presence of CXCL5-NPs inside the cells, many of them not co-localize with lysosomes, as predictable by the short time incubation.

Figure 44.

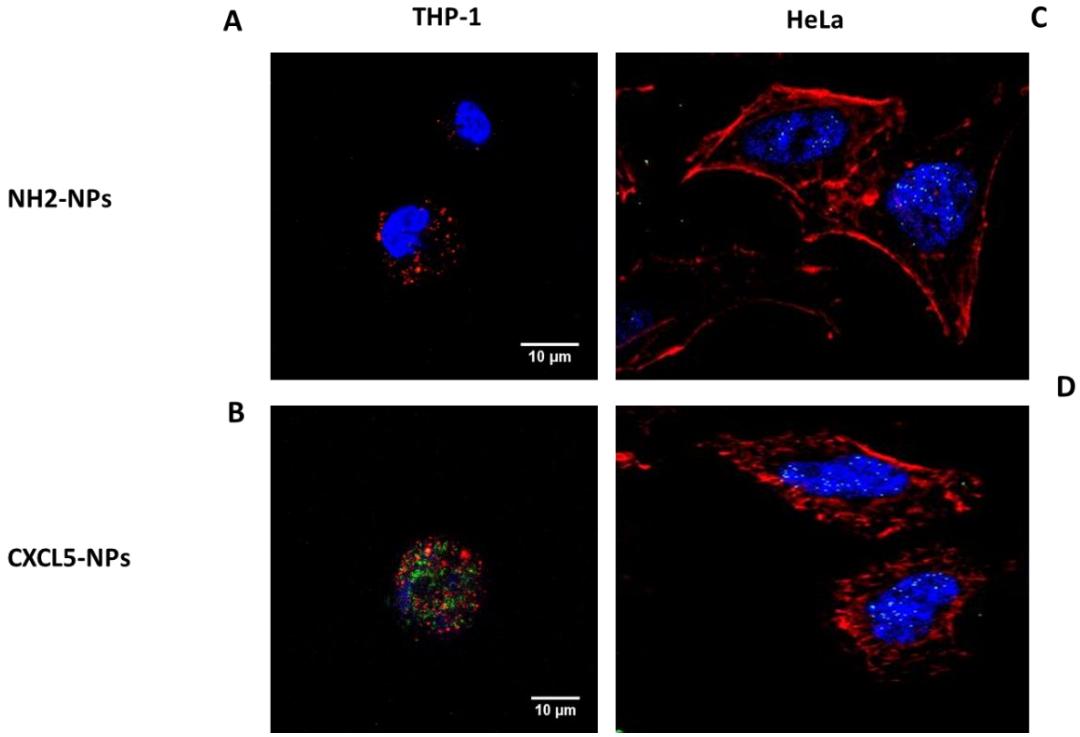

A-B: Confocal microscopy of THP-1 cells treated with 50 µg/ml of NH_2 SiO_2–NPs and CXCL5-SiO_2 NPs for 45 minutes. Blue: nuclei; red: lysosomes; green: NPs. **C-D**: Confocal microscopy of HeLa cells treated with 50 µg/ml of NH_2– SiO_2 NPs and CXCL5-SiO_2 NPs for 45 minutes. Blue: nuclei; red: cytoskeleton; green: NPs [131].

Figure 45.

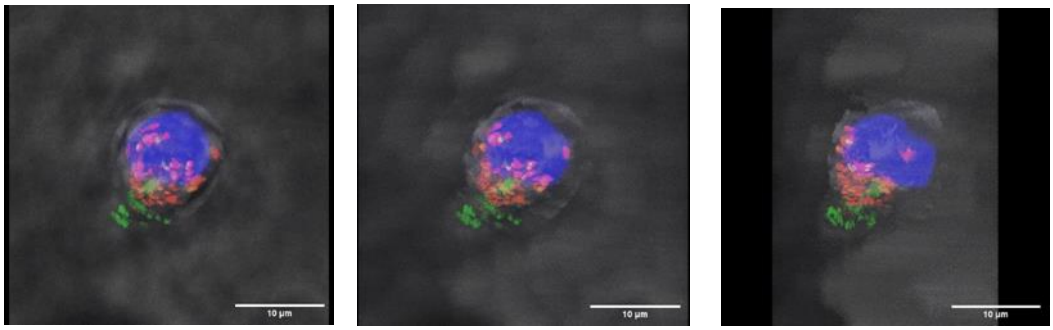

3d images obtained by confocal analysis of CXCL5 SiO_2 NPs uptake in THP-1 cells.

3.15 Uptake of NH_2-SiO_2 and Ads CXCL5-SiO_2 NPs in THP-1 cells cultured in FBS and HS

The internalization of NH_2 –SiO_2 and Ads CXCL5-SiO_2 NPs in THP-1 cells cultured in FBS and HS was evaluated by flow cytometry. The results (Figure 46 A) demonstrate that both without and with serum Ads CXCL5-SiO_2 NPs show an increased internalization compared with the NH_2-SiO_2 NPs due to the presence of the protein on NPs surface. In particular, without the presence of serum there is an increase in cell fluorescence, maybe due to the presence of NPs aggregates, instead with serum, the colloidal system became more stable due to the presence of protein in serum avoiding the formation of aggregates. Even if the protein is adsorbed on the surface in a randomly way, it is able to interact with its cognate receptor, favoring NPs uptake.

In Figure 46 B when cells are cultured in HS, internalization of Ads CXCL5-SiO_2 NPs was noticeably enhanced than NH_2-SiO_2 NPs. Ads CXCL5-SiO_2 NPs in cells treated without serum present an opposite behavior compared with the cells cultured in FBS. It is due to the different condition in which cells are cultured, because the proteins contained in HS are different from the ones that are present in FBS and this fact could affect the behavior of cells.

Figure 46.

A

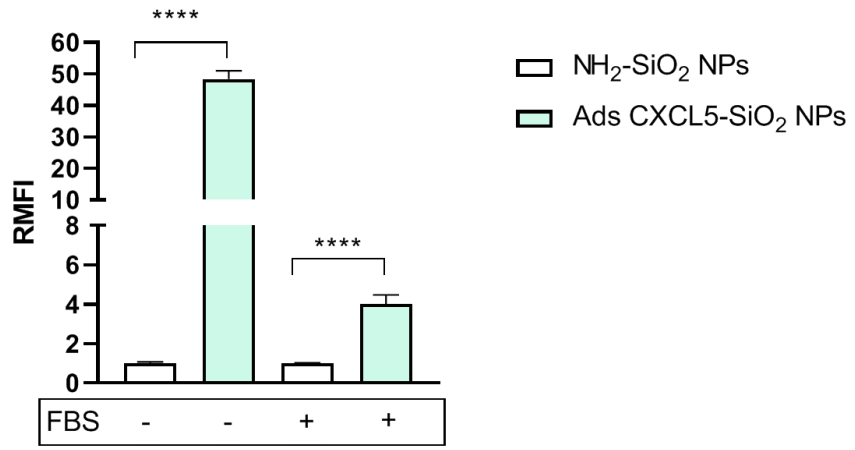

B

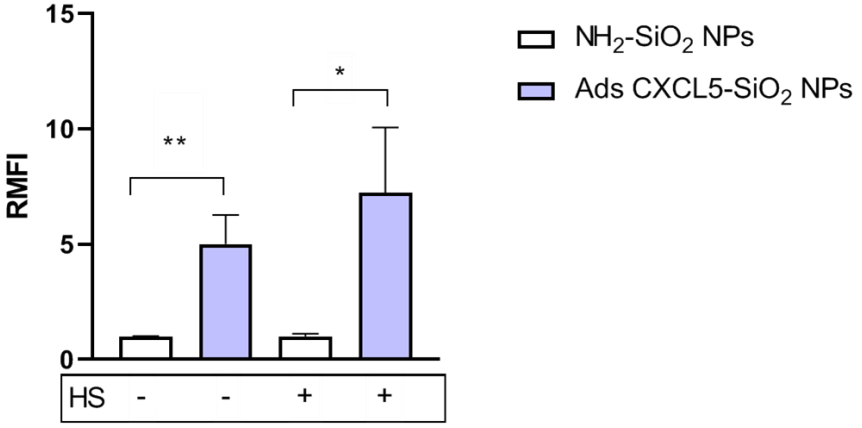

Silica Nps uptake in Thp-1 cell lines in different medium conditions evaluated by flow cytometry. The bars represent the RMFI after the administration of 50 µg/ml of SiO_2 NPs. Error bars represent the mean at least of three independent experiments ± SEM. **** P< 0,0001 ** P< 0,01 * P< 0,05

3.16 Uptake of Cores and Cores + CXCL5-SiO_2 in THP-1 cells cultured in FBS and HS

In Fig. 47 A CXCL5 was adsorbed on SiO_2 NPs (Cores) and the internalization in THP-1 cultured in FBS was evaluated by flow cytometry. The results show that internalization

of functionalized NPs was compared with the silica cores as expected by chemokine functionalization. In particular, due to the different surface charge of SiO_2 NPs vs NH_2 SiO_2 NPs, in presence of serum functionalized NPs show a higher internalization compared with the condition in which cells are cultured without serum. Maybe, the presence of serum destabilizes the colloidal suspension of NPs creating aggregates in cells.

In Fig. B, when cells are cultured in HS, NPs present the same behavior of the previous experiment. Interestingly, because of the presence of human CXCL5 in the medium, the uptake of functionalized NPs is reduced because human CXCL5 screens the effect of CXCL5 present on NPs surface.

Figure 47.

A

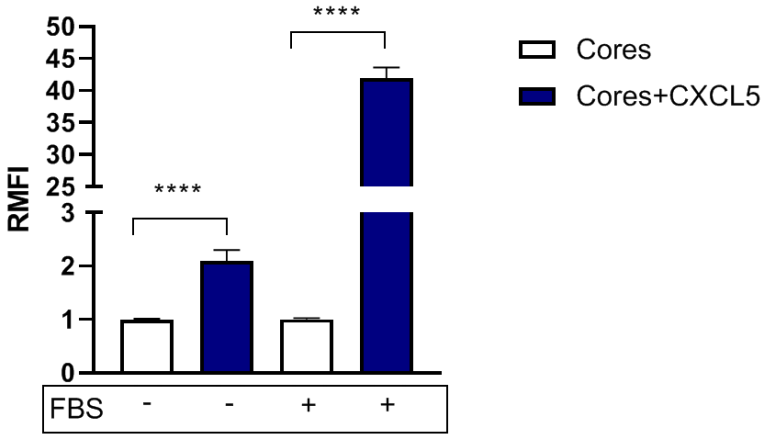

B

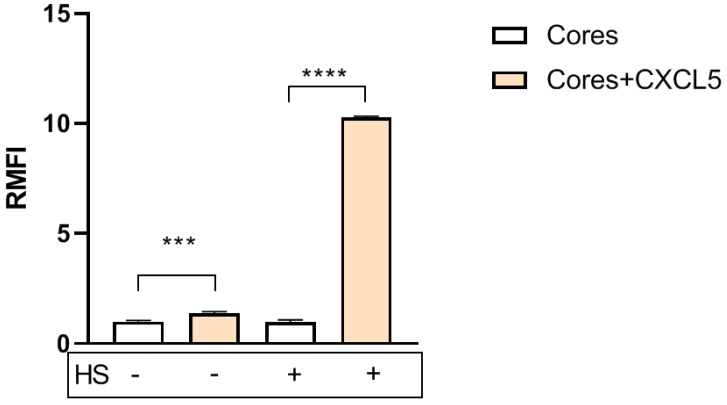

Silica NPs uptake in Thp-1 cell lines in different medium conditions evaluated by flow cytometry. The bars represent the RMFI after the administration of 50 µg/ml of SiO_2 NPs. Error bars represent the mean at least of three independent experiments ± SEM. **** P< 0,0001 *** P< 0,0005

My results demonstrated a big increase in NPs internalization after the adsorption of CXCL5 on NPs surface. Similar results are shown in the work of Melissa Santi et al. [144]. The transferrin receptor (TfR) is a promising target in cancer therapy owing to its overexpression in most solid tumors and on the blood−brain barrier. In the work, transferrin-mediated endocytosis of gold nanoparticles by modifying their protein corona of transferrin is promoted. The internalization of gold nanoparticles is strongly dependent on the amount of the peptide PepN-Tf2 on the surface, in fact the internalization of AuNP-10 (10% w/w of peptide) was 44-fold greater compared with what observed for AuNP not functionalized. The advantage, in my project to use Ads CXCL5 NPs is that these protein-decorated nano-tools showed enhanced uptake and precise receptor-mediated cell subset localization. Instead, in the work mentioned above, NPs could be used for different types of cancer but not for a specific cell population.

4. Methods and Materials

4.1 SiO_2 Nanoparticles preparation, functionalization and characterization

4.1.1 Synthesis of 50 nm FITC-SiO_2 NPs

Briefly, N-1-(3-trimethoxysilylpropyl)-N‘-fluoresceyl thiourea (FITC-APTMS) conjugate solution was prepared by dissolving 2 mg fluorescein isothiocyanate (FITC) in 1 ml anhydrous ethanol and immediately mixed with 10 µl of (3-Aminopropyl) trimethoxysilane (APTMS) under shaking at room temperature for 4 h in the dark. Under nitrogen atmosphere, 25 ml of ethanol was added to 1 ml of aqueous ammonia (28%) and stirred. 950 µl Tetraethyl orthosilicate (TEOS) was then mixed with the conjugate solution and the reaction was stirred at 600 rpm at room temperature for further 20 h in darkness. The resulting particles were washed three times by centrifugation and resuspension in Ethanol using bath sonication and ultimately resuspended in ethanol to reach a final particle concentration of 10 mg/ml [131].

4.1.2 Nanoparticles surface amination

FITC-SiO_2 NPs were centrifuged and redispersed in water, then 0,5% of acetic acid and 1% of APTMS were added. The reaction was taken under stirrer for 1 h at room temperature. NPs were washed twice and redispersed in water [131].

4.1.3 Pegylation of Silica NPs

4 ml of 50 nm FITC-SiO_2 NPs were centrifuged and redispersed in 1,6 ml of ethanol anhydrous, then was added 1,6 ml of Silane-PEG-NH_2 (400 µM final concentration) and 800 µL of ammonia (28%). The reaction was taken under nitrogen atmosphere for 16 h. NPs were centrifuged and washed twice with a solution of ethanol/dimethyl sulfoxide (DMSO) 1:1, once with ethanol and redispersed in water .

4.1.4 Ninhydrine assay

To evaluate the presence of secondary amine in NH_2-PEG NPs, ninhydrine assay was performed. Ninhydrine is able to bind the primary and secondary amines, changing the color from yellow to purple in presence of amino groups. The samples are dropped on a TLC and then they are put in a solution of ninhydrine, butanol and acetic acid. The samples changes the color from yellow to purple in the presence of PEG.

4.1.5 Coupling between Rhodamine isothiocyanate and NH_2 –PEG NPs

200 µl of NH_2-PEG NPs and SiO_2 NPs were centrifuged and redispersed in 200 µl of ethanol, then was added 50 µl of Rhodamine Isothiocyanate (200 nM final concentration). The reaction was stirred for 3,30h and then the particles were centrifuged and washed once in ethanol and three times in water. To evaluate FITC and Rhodamine fluorescence, images are acquired using the laser 488 for FITC, and the laser 543 for Rhodamine isothiocyanate, using the confocal LSM710 ZEISS with oil objective 100X.

4.1.6 Coupling with chemokine CXCL5

NH_2-PEG NPs were mixed with the chemokine CXCL5, then 1-ethyl-3-(3-dimethylaminopropyl)carbodiimide hydrochloride) (EDC) and N-Hydroxysuccinimide (NHS) were added in MES (2-(N-morpholino)ethanesulfonic acid) and stirred at room temperature for 2h. The solution was centrifuged once and washed many times with water. Finally NPs were redispersed in water.

4.1.7 Optimization of Covalent Coupling with CXCL5 chemokine

NH_2-SiO_2 NPs (500 µg/ml) were mixed with CXCL5 (4 µM) in water, then 4-(4,6-Dimethoxy-1,3,5-triazin-2-yl)-4-methylmorpholinium chloride (DMTMM 10 µM) was added and the reaction was stirred at room temperature for 4h. The solution was then centrifuged twice (1100 rpm for 1,5 minutes) using 100 kDa Amicon tubes (Merck Millipore) and the NPs were redispersed in water at the same initial concentration [131].

4.1.8 Adsorption of CXCL5 on Silica NPs

Silica NPs (500µg/ml) and NH_2- SiO_2 NPs were mixed with CXCL5 (4µM), in water and stirred at room temperature for 2h.

4.1.9 Transmission electron Microscopy

NPs were characterized by TEM using a JEOL JEM-1400 Plus (Jeol, Akishima-shi, Japan), with LaB6 thermionic source with an acceleration voltage of 120 kV. Images were acquired using a Gatan CCD camera Orius 830 (2048 x 2048 active pixels). The particle size distribution was obtained by manually measurement of the diameter of at least 500 NPs using ImageJ software.

4.1.10 Size and electrophoretic mobility.

Dynamic light scattering (DLS) measurements were performed on a Zetasizer Nano ZS90 (Malvern, USA). 20 µl of nanoparticle dispersion sample were taken and dispersed in 980 µl Milli Q water. Measurements were made at 25 °C using disposable polystyrene cuvettes. The refractive index (Ri) and the adsorption index (Rabs) of silica material were 1,47 and 0.000 respectively, according to the standard operating procedure (SOP) for measurement of hydrodynamic Size-Distribution and Dispersion Stability by Dynamic Light Scattering (DLS). After size measurement, particles were transferred to zeta potential cuvette (disposable capillary zeta cell) and the measurements were made used the Smoluchowski model [131].

4.1.11 Nanoparticle Immunolabelling

Plasma-cleaned formvar carbon film-coated 300 mesh copper grids (Electron Microscopy Sciences) were incubated 2 min with 5-µL drops containing CXCL5-SiO_2 NPs. Dilutions were optimized for each SiO_2 NPs concentration. After two washing steps with 50-µL drops of washing buffer (0.1% BSA in PBS), samples were incubated with 50-µL drops

containing buffer A (1% BSA in PBS) for negative control or Rabbit Anti-Human CXCL5 primary antibody (Peprotech, USA) (8 μg/mL in buffer A) in a wet chamber for 3 h at room temperature. After five washes with washing buffer, SiO_2 NPs were incubated with 20-μL drops of 1:40 dilutions of the secondary antibody (goat anti-rabbit IgG-gold conjugate, (H&L) EM-grade, 10-nm particle size (Electron microscopy science) for 30 minutes in washing buffer. The system was then washed five times with five drops of washing buffer, followed by five washes with water drops [131].

4.1.12 EDS analysis

EDS characterization was performed on a high resolution scanning electron microscope (SEM) Jeol JSM-7500F equipped with a cold field emission gun using an Oxford X-Max 80 system with a silicon drift detector (SDD) having an 80 mm2 effective area. The analyses were done with an accelerating voltage of 5/10 kV.

4.1.13 Circular Dichroism

CD spectra were recorded using a JascoJ-1500 spectropolarimeter in a 1.0 cm quartz cell at room temperature. The spectra were recorded from 300 to 190 nm, with a band width of 1 nm, a time constant of 16 s, and a scan rate of 10 nm/min. Spectra were recorded subtracting them from blank samples.

4.2 Biological assays

4.2.1 Cell culture

THP-1 cells (ATCC Manassas, VA, USA) were cultured in RPMI-1640 (Thermo Fisher Scientific) supplemented with 10% fetal bovine serum (FBS) or 5% human serum (HS) (Thermo Fisher Scientific, Waltham, MA, USA), 1% Penicillin-Streptomycin (Sigma-Aldrich, Saint Louis, MO, USA) and 0.05 mM 2-mercaptoethanol (Thermo Fisher Scientific, Waltham, MA, USA). HeLa cells (ATCC Manassas, VA, USA) were cultured in DMEM (Thermo Fisher Scientific) supplemented with 10% FBS and 1% Penicillin-Streptomycin. Both the cell lines were grown at 37°C in a 5% CO_2 humidified atmosphere [131].

4.2.2 Confocal microscopy

THP-1 and HeLa cells were seeded on a 4 well NUNC Lab-Tek Chambered Coverglass (Thermo Fisher Scientific) and incubated in serum free medium with the proper SiO_2 NPs

at the concentration of 50 µg/ml for 45 minutes, then washed twice. THP-1 cells were incubated with LysoTracker and Hoechst 33342 (Thermo Fisher Scientific) at a concentration of 5 µg/mL for 15 minutes at 37 °C. After the staining, the cells were washed twice and Live Cell Imaging Medium (Thermo Fisher Scientific) was added for living cell analysis. HeLa cells were fixed with 4% paraformaldehyde for 15 minutes at room temperature, permeabilized with 0.1% Triton for 30 minutes and blocked with PBS/1% BSA for 30 minutes. The cells were then incubated with 0.1 nM Rhodamine Phalloidin for actin microfilaments staining and 5 µg/mL Hoechst 33342 (Thermo Fisher Scientific) for 2 h at room temperature in the dark. Confocal microscopy images were acquired by a Leica SP5 Inverted confocal microscope with a 63 × oil immersion objectives, 405, 495 and 561 nm excitation laser wavelengths and a resolution 1024 × 1024 pixels [131].

4.2.3 CXCR2 receptor expression

THP-1 cells (5 x 10^5 cells ml-1) cultured both in FBS and HS and HeLa cells, were centrifuged at 300 g for 5 min, resuspended in RPMI 0.5% BSA (Miltenyi Biotec) and incubated with APC-conjugated mouse anti-human CXCR2 antibody (Miltenyi Biotec) at the manufacturer's recommended concentration for 15 min on ice in the dark, then washed and resuspended in RPMI. Cell-associated fluorescence was analyzed by flow cytometry with MACS Quant Analyzer, gating the living cells based on light forward scattering (FSC) and side scattering (SSC). 100 000 events per sample were acquired [131].

4.2.4 Internalization capability of CXCR2 receptor

THP-1 cells (2 x 10^5) were starved in serum-free medium containing 0,5% of BSA for 1h. Then the cells were treated with CXCL5 at different concentrations (0,1; 1 µM) for 1,30h, washed and incubated for 15 minutes with APC-conjugated mouse anti-human CXCR2 antibody (Miltenyi Biotec). Then the cells were washed and analyzed by FACS MACS Quant Analyzer (Miltenyi Biotec, Bergish, Germany) using MACS Quantify software. Living cells were gated based on light forward scattering (FSC) and side scattering (SSC).

4.2.5 Uptake of Silica NPs

2 x 10^5 THP-1 cells cultured both in FBS and HS, were placed inside a 48 -well plate and incubated with 50 µg/mL of different Silica NPs at 37 °C and 5% CO_2 for 45 minutes in different types of culture media. After incubation, samples were washed twice at 4°C with RPMI medium to remove non-internalized NPs. The effect of Silica NPs internalization was evaluated by flow cytometry with MACSQuant Analyzer (Miltenyi Biotec, Bergish, Germany) using MACSQuantify software [131].

4.2.6 CXCL5 NPs displacement by CXCL5 pre-treatment.

THP-1 cells (2 x 10^5 cells ml -1) were treated with 1 µM CXCL5 in serum free medium containing 0,1 % of bovine serum albumin (BSA) for 45 minutes and incubated with 50 µg/ml of NH_2– SiO_2 NPs and CXCL5- SiO_2 NPs for 45 minutes. After incubation, samples were washed twice to remove non-internalized NPs and resuspended in RPMI 0,1% BSA. Cell-associated fluorescence was analyzed by flow cytometry with FACS MACS Quant Analyzer (Miltenyi Biotec, Bergish, Germany) using MACS Quantify software.

4.2.7 Uptake of Silica NPs in THP-1 and HeLa cells

2 x 10^5 THP-1 cells and HeLa , were incubated with 50 µg/mL of different Silica NPs at 37 °C and 5% CO_2 for 45 minutes in medium without serum. After incubation, samples were washed twice at 4°C with RPMI medium to remove non-internalized NPs. The effect of SiO_2 NPs internalization was evaluated by flow cytometry with MACSQuant Analyzer (Miltenyi Biotec, Bergish, Germany) using MACSQuantify software [131].

4.3 Statistical analysis

Data were expressed as mean ± SEM. For statistical analysis GraphPad Prism 8 software wad used (San Diego, California, USA). p-values were calculated using two-tailed t-test and ordinary one way ANOVA [131].

5. Conclusions

One major challenge in nanomedicine is to find a way to selectively deliver NPs to diseased tissues. Functionalizing nanoparticles is a widely-used technique that allows the conjugation with targeting ligands, which possess inherent ability to direct selective binding to cell types or states and, therefore, confer "smartness" to NPs. These targeting ligands fall into several general classes: small molecules, polypeptide-based peptides, protein domains, antibodies, and nucleic acid-based aptamers. During my PhD I produced a novel functionalization of potential nano-delivery systems using chemokines and I evaluated their cell targeting performances. To achieve this challenging goal, the chemokine CXCL5 has been chosen as model protein to be adsorbed or covalently bound onto fluorescently labelled SiO_2 NPs to precisely targeting CXCR2+ immune cells like THP-1 cell lines used as monocyte cell model. I demonstrated CXCR2+ cell preferential targeting by comparing particle uptake in THP-1 vs. low-CXCR2 expressing HeLa cells. In particular the covalent coupling of CXCL5 shows an advantage in cellular uptake compared with the adsorbed method due to the right disposition of the chemokine on NP surface that avoid aggregation phenomena. My results provide the proof of principle that chemokine decorated NMs enhance uptake through the fast chemokine-receptor binding allowing precise cell subset localization. The possibility to aim at selective chemokine receptor-expressing cells can be beneficial for the different pathological conditions involving immune reactions.

Effect of PtNPs on undifferentiated and differentiated HL60

1. Introduction

The strong antioxidant activity exhibited by some nanoparticles is considered a new tool to develop novel therapies. Pt NPs have been poorly explored in nanomedicine, despite their well-known catalytic and antioxidant properties. Different studies aimed at improve their catalytic properties by synthesizing PtNPs with different shape. In particular, the surface structure is important for determining and controlling the electrocatalytic properties of the material [145]. It is known that PtNPs could play an important role in nanomedicine because of their catalytic activity and ROS scavenging ability. Citrate-capped Pt NPs of two sizes (5 and 20 nm) are endowed with strong catalase-, peroxidase, and superoxide dismutase-like activities. They are cytocompatible and can counteract molecular dysfunctions that cause the accumulation of intracellular ROS, suggesting potential applications in stress-related diseases.

Figure 1.

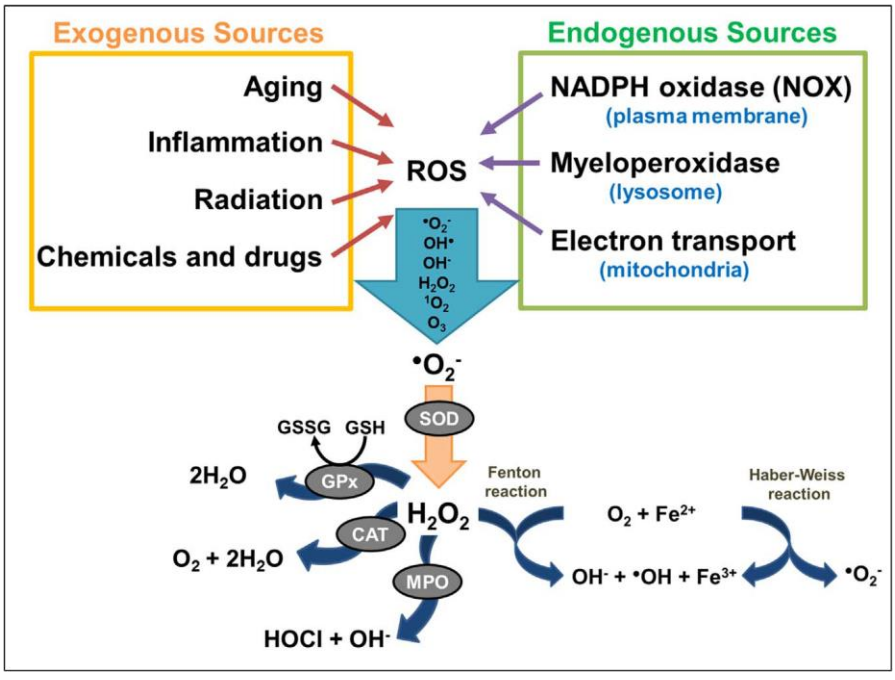

Sources of ROS and key ROS molecules in signaling. ROS generation is a cascade of reaction initiated by the production of O_2 [146].

However, metallic NPs have often create interest about their potential toxicity, mostly induced by the loss of toxic ions, the presence of synthesis by products or the use of unsafe coating materials [147]. NP coatings have an important role for the potential immunotoxicity of the NPs, since they can directly bind to immune receptors or adsorb active molecules that change the immunological identity of the particles [148][89]. My group recently synthesized citrate-coated PtNPs demonstrating efficient intracellular ROS scavenging activity and a high degree of cytocompatibility [149]. The particle physicochemical properties like surface chemistry, size and shape regulate their biological fate and eventually the potential toxicity. All these parameters influence the NP delivery and its toxicological profile, often produces unexpected immune reactions. Immunity is characterized by innate and acquired defense systems that allow protection against pathogenic hazards [150]. Several active molecules and fast-responding leukocytes belong to the innate immune system, such as neutrophils, NK cells and monocyte/macrophage phagocytes. In particular, monocytes circulating in the bloodstream react to chemo-attractant inflammatory stimuli by migrating to the site of infection, where they differentiate into tissue-specific macrophages able to phagocyte and eliminate the threats. The response of the immune system to PtNPs is poorly investigated and part of my PhD thesis is aimed at studying the nano-bio-interactions between PtNPs and the immune cell line HL60 (Human promyelocytic leukemia cells). The HL60 cell line was established in 1977 from a patient with acute myeloid leukemia. The cells largely resemble promyelocytes but can be induced to differentiate terminally in vitro. Some reagents cause HL60 cells to differentiate into granulocyte-like cells, others to monocyte/macrophage-like cells. Compounds such as dimethyl sulphoxide (DMSO), and other compounds as diverse as retinoic acid and actinomycin D, all induce differentiation to granulocytes, while 1,25-dihydroxyvitamin D3, phorbol esters and sodium butyrate induce monocyte/macrophage differentiation [151]. The course of the differentiation induced by any of these agents is accompanied by a large number of changes in the cells [152] and is easily monitored by morphological, histochemical and immunological criteria. Thus, incubation with DMSO or retinoic acid leads, over a period of 5 days, to a progressive decrease in the size of HL60 cells and condensation of nuclear material with the appearance of kidney-shaped nuclei characteristic of the myelocyte and, later, lobed nuclei characteristic of banded and segmented neutrophils.

In particular I evaluated the potential interference of PtNPs with human HL60 undifferentiated and differentiated cells, demonstrating that citrate-coated PtNPs are not toxic and cytocompatible for these immune cells.

2. Results

2.1 Interaction of PtNPs with Undifferentiated and Differentiated HL60

In vitro neutrophil-like granulocyte differentiation was obtained by administration of retinoic acid for 9 days. Fully differentiated non-adherent HL60 was investigated by flow cytometry. The results show higher values of side SSC and lower values of forward FSC, as reported in Figure 2. The increase of SSC agrees with the higher number of granules in the neutrophil-like phenotype, whereas lower FSC describes the smaller size of the differentiated cells. I considered differentiation of HL60 to be complete when >95% of cells were gating within arbitrarily fixed parameters of SSC and FSC corresponding to granulocyte morphology analysis by TEM.

To evaluate the potential cytotoxicity of PtNPs in both non-adherent HL60 phenotypes, an AnnV/PI assay was performed by flow cytometry (Fig.3). I measured the number of necrotic/PI-positive cells and apoptotic/AnnV-positive cells, in particular 25nm, 100 μg/mL PtNPs were added to the cell cultures for 6 h without inducing any significant necrotic or apoptotic cell death in both the HL60 phenotypes.

Figure 2.

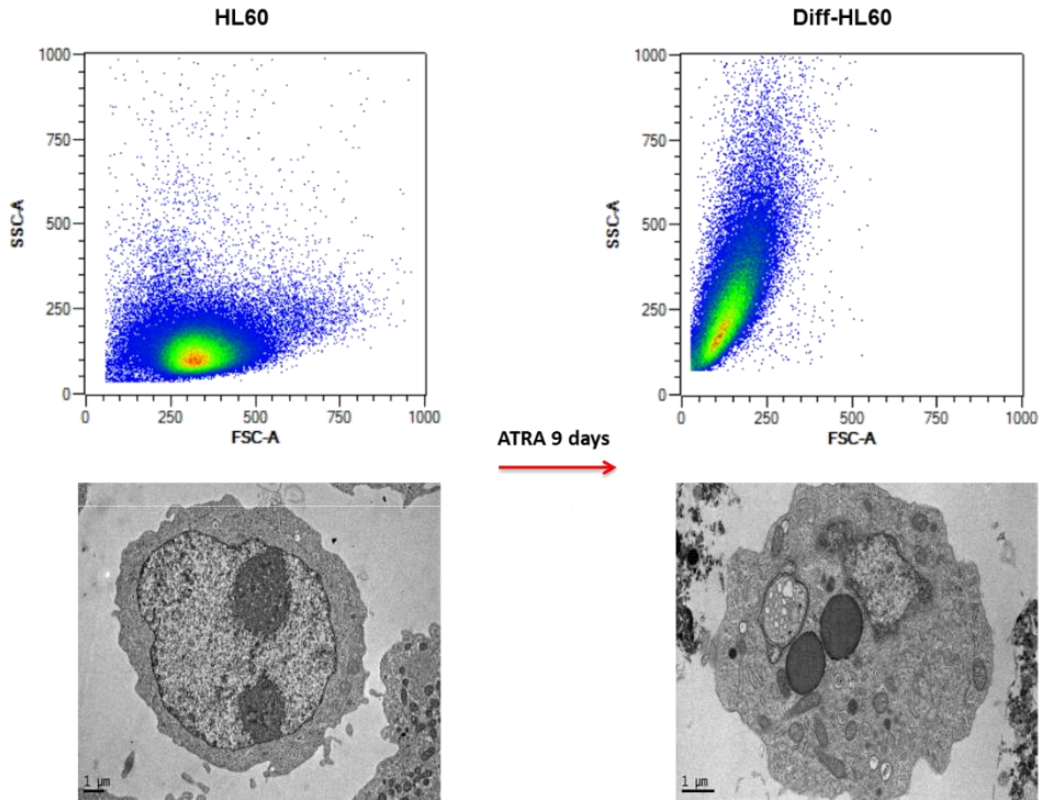

Flow cytometer dot plots and TEM images of internalized undifferentiated and differentiated HL60. Representation of the different cell FSC and SSC of HL60 and differentiated HL60 after 9 days of treatment with retinoic acid. TEM displays intracellular structures in HL60 and differentiated HL60 cells, showing morphological changes induced by retinoic acid treatment [153].

Figure 3.

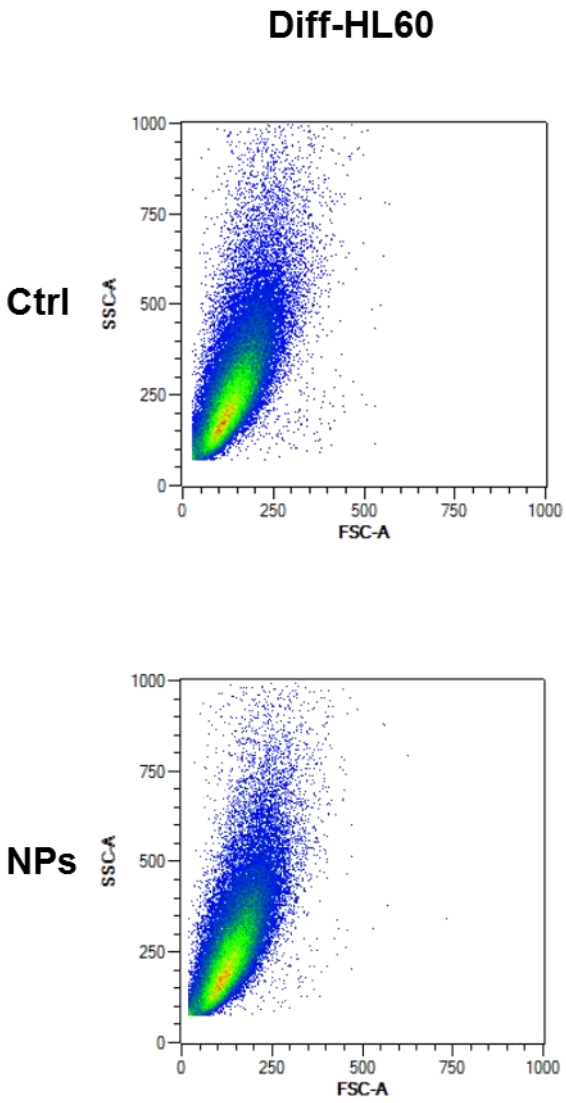

Dot plots show the comparison between untreated and PtNP-treated differentiated HL60 for 24h. Treatment with NPs don't affect cell viability [153].

Figure 4.

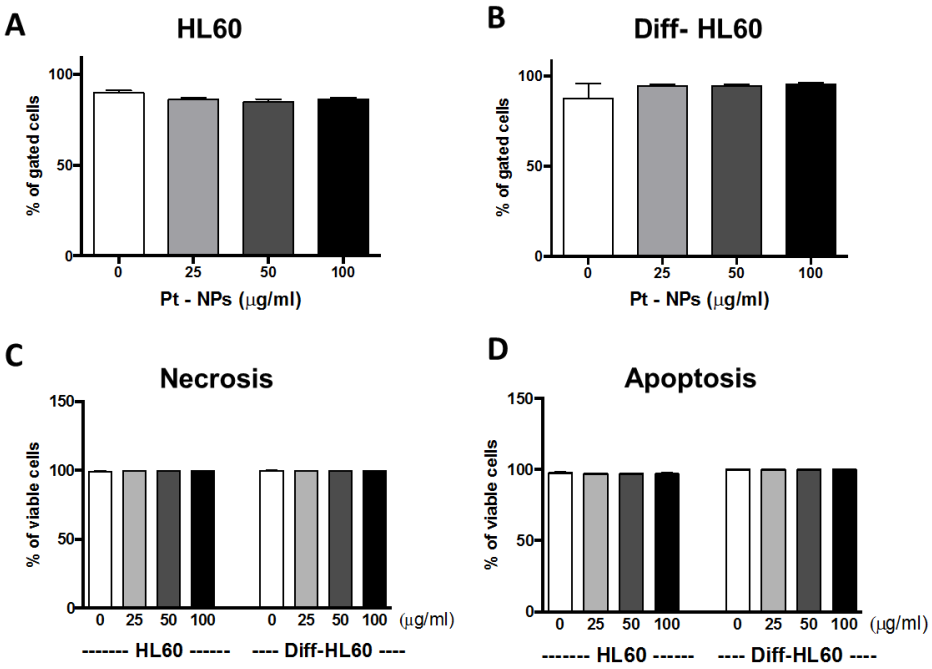

Evaluation of cells viability after the treatment with PtNPs evaluated by flow cytometry. (A,B) The bar graphs show the percentages of living undifferentiated (A) and differentiated (B) cells after 6 h incubation with 25, 50 and 100 μg/mL 5 nm-PtNPs. (C,D) AnnV/PI assay by flow cytometry. (C,D) Bars show necrosis (C) and apoptosis (D) of undifferentiated and differentiated HL60 cells, untreated or treated with PtNPs at different concentrations for 6 h. All the data represent the mean ± SD of three independent experiments [153].

2.2 PtNPs Internalization in Undifferentiated and Differentiated HL60

TEM analysis of undifferentiated and differentiated HL60 cells treated with 5 nm citrate-coated PtNPs was performed (Figure 4) to visualize the presence of NPs in cells and to evaluate their fate in cellular compartments. Low NP internalization in both non-adherent phenotypes was observed, although stimulation with retinoic acid induced a granulocytic/phagocytic neutrophil-like HL60.

Figure 5.

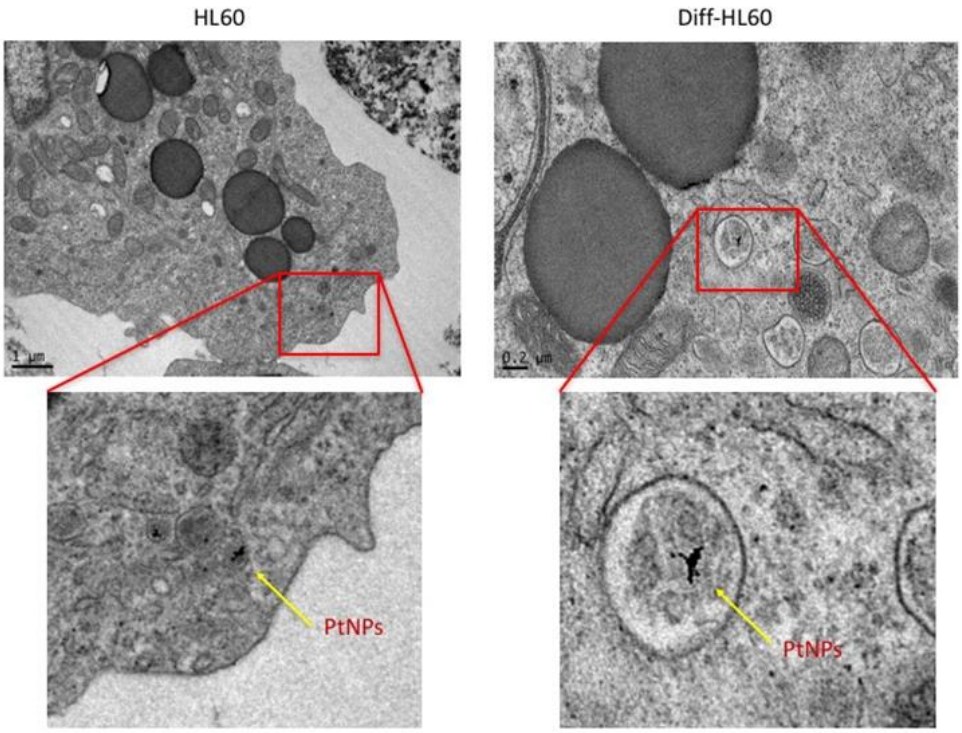

TEM images of undifferentiated and differentiated HL60 treated with 50 µg/mL of PtNPs. Magnification shows highlighted endocytotic vesicles retaining PtNPs[153].

3. Discussion

The development of NPs as drug delivery system requires deep investigation of particle-cell interactions, and their potential impairment of cell-cycle processes. Special attention must be given to the absence of immunogenicity and toxicity of NPs to avoid immune system reactions and to favor the application in several fields of medicine [154][155]. My group have already proposed PtNPs as novel catalytic nanomaterials for biomedical applications [149]. Their surface chemistry allows intracellular ROS scavenging and impairment of inflammatory pathways [156] suggesting PtNPs as antioxidant and anti-inflammatory "nanoenzymes". To extend the observation of PtNP effects on innate immune cells, human promyelocytic HL60 cells, are induced, using retinoic acid, to differentiate into granulocytes that express morphologic and functional features of mature neutrophils (Figure 2). Moreover, to evaluate NPs cytotoxicity on HL60 cells, was

performed the Annexin V/PI assay by flow cytometry-based methods. Propidium iodide (PI) is widely used in conjunction with Annexin V to determine if cells are viable, apoptotic, or necrotic through differences in plasma membrane integrity and permeability [157]. PI is used as nuclear stains because it is stable and a good indicator of cell viability, based on its capacity to exclude dye in living cells [158]. The ability of PI to enter a cell is dependent upon the permeability of the membrane; PI does not stain live or early apoptotic cells due to the presence of an intact plasma membrane. In late apoptotic and necrotic cells, the integrity of the plasma and nuclear membranes decreases, allowing PI to pass through the membranes, intercalate into nucleic acids, and display red fluorescence [159]. As reported in Figure 4, 5 nm citrate-coated PtNPs do not show toxicity in fact NPs do not induce necrosis or apoptosis in both HL60 phenotypes. Interestingly, PtNPs internalization in differentiated and undifferentiated cells is similarly low (Figure 5), indicating that it is not increased by the phagocytic phenotype. This may be due to the non-adherent nature of these cell lines, and the shorter time of PtNP exposure. I chose a 6 h treatment for HL60, because the fast proliferation time of undifferentiated cells [160] would have diluted the initial NP concentration-per-cell over 24 h. Therefore, the results shows that PtNPs do not induce toxicity for HL60 cells, exhibiting low NP internalization ability. These results are in contrast with the work of Daniela Guarnieri et al. [161] in which PtNPs of different diameters (2,5 5 20 nm) are linked to the cell penetrating peptides (CPP) gH625, to escape the endo-lysosomal compartment and deliver NPs within the cytoplasm, as a function of the NP size. The uptake was evaluated on human cervix epithelioid carcinoma (HeLa) cells demonstrating a 4-fold increase for gHPt5 and gHPt20 NPs and a 12-fold increase for gHPt2.5 NPs with respect to pristine particles. These results suggest that the ability of gH625 peptide to enhance NP cellular uptake is strongly limited by the size of the NP cargo. In my project PtNps penetrate very low in THP-1 cells because they are cells in suspension, not adherent like HeLa cells, therefore it’s more difficult for cells to come in contact with NPs.

4. Materials and Methods

4.1 Nanoparticles

5 nm Citrate-capped PtNPs, synthesized and characterized as previously reported [162].

4.2 Cell Culture

HL60 cells (ATCC Manassas, VA, USA) were grown in RPMI-1640 (Thermo Fisher Scientific) supplemented with 10% FBS (Thermo Fisher Scientific), 1% Penicillin-Streptomycin (Sigma-Aldrich) in a 5% CO2 humidified atmosphere at 37°C [153].

4.3 Differentiation Assay

HL60 cells were incubated with 1 μM all-trans retinoic acid (ATRA) (Sigma-Aldrich, Saint Luis, MO, USA) for 9 days to obtain complete differentiation in neutrophil-like cells. Differentiation along the granulocytic pathway was monitored by characteristic changes in morphology using the flow cytometry with MACSQuant Analyzer (Miltenyi Biotec, Bergish, Germany) [153].

4.4 Transmission Electron Microscopy

Suspension cells (HL60 and differentiated HL60) were incubated with 50 μg/mL PtNPs for the proper time, then washed twice with RPMI and fixed for 45 min in a fixative solution (2% Glutaraldehyde in complete culture medium). The samples were centrifuged and the pellet fixed again with 1.5% Glutaraldehyde solution in Na-Cacodylate buffer 0.1 M. A final post-fixation (2 h) in 1% OsO4 solution in Na-Cacodylate buffer 0.1 M was performed. The fixed samples were stained overnight in a 1% Uranyl acetate aqueous solution at 4°C. Samples were washed in water and completely dehydrated with a scale of Ethanol, transferred in Propylene Oxide and finally infiltrated with epoxy Spurr™ (SPI-Chem, West Chester, PA, USA) resin. Once the resin had hardened for 48 h in oven at 65°C, thin sections were cut with a Leica EM UC6 ultra-microtome. TEM images were collected with a Jeol JEM 1011 (Jeol, Tokyo, Japan) electron microscope (Electron Microscopy Facility—Fondazione Istituto Italiano di Tecnologia, Genova, Italy), operating at an acceleration voltage of 100 kV, and recorded with an 11 Mp fiber optical charge-coupled device (CCD) camera (Gatan Orius SC-1000) [153].

4.5 Annexin-PI Assay

Cell viability was quantified by using Annexin V-PI assay (Miltenyi Biotec, Bergish, Germany) according to the manufacturer's instructions. In brief, HL60 and differentiated HL60 cells were incubated with 50 μg/mL PtNPs for 6 h. After the treatments, the cells were washed and incubated with Annexin V-FITC for 15 min in the dark at room temperature. Subsequently, the cells were washed and propidium iodide (PI) solution

was added immediately prior to analysis by flow cytometry with MACSQuant Analyzer. The percentage of necrotic or apoptotic cells was evaluated using MACSQuantify software [153].

4.6 Flow Cytometry

For the evaluation of cell viability, HL60 and differentiated HL60 cells were incubated with 50 μg/mL of 5 nm PtNPs. After 6 h incubation, the effect of PtNP internalization on cell viability was evaluated by flow cytometry with MACSQuant Analyzer (Miltenyi Biotec, Bergish, Germany) using MACSQuantify software [153].

5. Conclusions

In this project, I evaluated PtNPs effects on innate immune cells, in particular I exploited undifferentiated human HL60 cells, and differentiated them into a neutrophil-like phenotype to demonstrate that cells viability is not affected by the treatment with PtNPs. The particles internalized within these cells seem very few, emphasizing the specificity of PtNPs-immune cell type interaction. All these results highlight the influence PtNPs interaction with immune cells in view of their potential applications in nanomedicine.

6. Acknowledgments

Undertaking this PhD has been a truly life-changing experience for me and it would not have been possible to do without the support and guidance that I received from many people.

Firstly, I would like to express my sincere gratitude to my supervisors Prof. Pier Paolo Pompa and Dr. Giuseppe Bardi for the continuous support of my PhD study and related research. Their guidance helped me in all the time of research and writing of this thesis.

Then, I would like to express my sincere gratitude to my colleague Francesca Gatto for the continuous support of my PhD study and related research and for her sincere friendship.

I would like to thank the Post-doc Paola Sanchez Moreno for all the scientific support and encouragement she gave me during the first years of my PhD.

I am also very grateful to all those of my group, who were always so helpful and provided me with their assistance throughout my PhD period.

Last but not the least, I would like to thank my parents, my twin and my friend Alessandra for supporting me spiritually throughout writing this thesis and for always believing in me and encouraging me to follow my dreams.

7. References

1. Biswas, A.K.; Islam, M.R.; Choudhury, Z.S.; Mostafa, A.; Kadir, M.F. Nanotechnology based approaches in cancer therapeutics. *Adv. Nat. Sci. Nanosci. Nanotechnol.* 2014, *5*.

2. Kohane, D.S. Microparticles and nanoparticles for drug delivery. *Biotechnol. Bioeng.* 2007, *96*, 203–209.

3. Zhang, J.; Saltzman, M. *Engineering biodegradable nanoparticles for drug and gene delivery*; Chem Eng Prog. 2013 Mar;109(3):25-30.

4. Khanbabaie, R.; Jahanshahi, M. *Send Orders of Reprints at reprints@benthamscience.org 370 Current Neuropharmacology*; 2012; Vol. 10;.

5. Kou, L.; Sun, J.; Zhai, Y.; He, Z. The endocytosis and intracellular fate of nanomedicines: Implication for rational design. *Asian J. Pharm. Sci.* 2013, *8*, 1–10.

6. Li, S.-D.; Huang, L. Stealth Nanoparticles: High Density but Sheddable PEG is a Key for Tumor Targeting 2010 Aug 3;145(3):178-81

7. Baas, J.; Senninger, N.; Elser, H. [The reticuloendothelial system. An overview of function, pathology and recent methods of measurement]. *Z. Gastroenterol.* 1994, *32*, 117–23.

8. Wani, T.U.; Raza, S.N.; Khan, N.A. Nanoparticle opsonization: forces involved and protection by long chain polymers. *Polym. Bull.* 2019.

9. Bargheer, D.; Nielsen, J.; Gébel, G.; Heine, M.; Salmen, S.C.; Stauber, R.; Weller, H.; Heeren, J.; Nielsen, P. The fate of a designed protein corona on nanoparticles in vitro and in vivo. *Beilstein J. Nanotechnol* 2015, *6*, 36–46.

10. Ladj, R.; Bitar, A.; Eissa, M.; Mugnier, Y.; Le Dantec, R.; Fessi, H.; Elaissari, A. Individual inorganic nanoparticles: Preparation, functionalization and in vitro biomedical diagnostic applications. *J. Mater. Chem. B* 2013, *1*, 1381–1396.

11. Ealias, A.M.; Saravanakumar, M.P. A review on the classification, characterisation, synthesis of nanoparticles and their application. *IOP Conf. Ser. Mater. Sci. Eng.* 2017, *263*.

12. McNamara, K.; Tofail, S.A.M. Nanosystems: The use of nanoalloys, metallic, bimetallic, and magnetic nanoparticles in biomedical applications. *Phys. Chem. Chem. Phys.* 2015, *17*, 27981–27995.

13. Akbarzadeh, A.; Rezaei-Sadabady, R.; Davaran, S.; Woo Joo, S.; Zarghami, N.; Hanifehpour, Y.; Samiei, M.; Kouhi, M.; Nejati-Koshki, K. *Liposome: classification, preparation, and applications*; Nanoscale Res Lett. 2013; 8(1): 102

14. Sahu, R.K.; Hiremath, S.S. A review on the classification, characterisation, synthesis of nanoparticles and their application Related content Synthesis of Aluminium Nanoparticles in A Water/Polyethylene Glycol Mixed Solvent using-EDM, Materials Science and Engineering 263 (2017) 032019

15. Vallet-Regí, M.; Balas, F.; Arcos, D. Mesoporous Materials for Drug Delivery. *Angew. Chemie Int. Ed.* 2007, *46*, 7548–7558.

16. Slowing, I.I.; Vivero-Escoto, J.L.; Wu, C.W.; Lin, V.S.Y. Mesoporous silica nanoparticles as controlled release drug delivery and gene transfection carriers. *Adv. Drug Deliv. Rev.* 2008, *60*, 1278–1288.

17. Hergt, R.; Dutz, S.; Zeisberger, M. Magnetic particle hyperthermia: nanoparticle magnetism and materials development for cancer therapy. *J. Phys. Condens. Matter* 2006, *18*, 2919–2934.

18. Tang, L.; Cheng, J. Nonporous Silica Nanoparticles for Nanomedicine Application, Nano Today. 2013 Jun;8(3):290-312.

19. Yang, P.; Gai, S.; Lin, J. Functionalized mesoporous silica materials for controlled drug delivery. *Chem. Soc. Rev.* 2012, *41*, 3679–3698.

20. Singh, A.P.; Biswas, A.; Shukla, A.; Maiti, P. Targeted therapy in chronic diseases using nanomaterial-based drug delivery vehicles. *Signal Transduct. Target. Ther.* 2019, *4*.

21. Faraji, A.H.; Wipf, P. Nanoparticles in cellular drug delivery. *Bioorganic Med. Chem.* 2009, *17*, 2950–2962.

22. Patra, J.K.; Das, G.; Fernandes Fraceto, L.; Vangelie, E.; Campos, R.; Del Pilar Rodriguez-Torres, M.; Acosta-Torres, L.S.; Armando Diaz-Torres, L.; Grillo, R.; Kumara Swamy, M.; et al. Nano based drug delivery systems: recent developments

and future prospects. *J Nanobiotechnol* 2018, *16*, 71.

23. Kim, J.H.; Pham, T.V.; Hwang, J.H.; Kim, C.S.; Kim, M.J. Boron nitride nanotubes: synthesis and applications. *Nano Converg.* 2018, *5*, 17.

24. -Uwe, J.; Junghanns, A.H.; Müller, R.H. *Nanocrystal technology, drug delivery and clinical applications*; Int J Nanomedicine. 2008 Sep; 3(3): 295–310.

25. Prasad, P.N. *Nanophotonics, 2004, p.418*; John Wiley & Sons, Inc., 2004; ISBN 978-0-471-64988-5.

26. Figuerola, A.; Di Corato, R.; Manna, L.; Pellegrino, T. From iron oxide nanoparticles towards advanced iron-based inorganic materials designed for biomedical applications. *Pharmacol. Res.* 2010, *62*, 126–143.

27. Tan, A.; Wang, Z.; Lust, R.; Hua, S.; Sercombe, L.; Veerati, T.; Moheimani, F.; Wu, S.Y.; Sood, A.K. Advances and Challenges of Liposome Assisted Drug Delivery. *Front. Pharmacol.* | *www.frontiersin.org* 2015, *6*, 286.

28. Formulations, N.; Yadav, D.; Anwar, M.F.; Suri, S.; Kardum, H. Novel Strategies in the Drug Delivery Development of Anticancer Drugs: The Nanoparticulate Formulations. *Front. Anti-Cancer Drug Discov.* 2014, 233–261.

29. Çağdaş, M.; Sezer, A.D.; Bucak, S. Liposomes as Potential Drug Carrier Systems for Drug Delivery. In *Application of Nanotechnology in Drug Delivery*; InTech, 2014.

30. Nano- and Microscale Drug Delivery Systems: Design and Fabrication - Alexandru Mihai Grumezescu - Google Libri Available online: https://books.google.it/books?id=WpIxDQAAQBAJ&pg=PA439&lpg=PA439&dq=Swati+Pund,+Amita+Joshi,+in+Nano-+and+Microscale+Drug+Delivery+Systems,+2017&source=bl&ots=hRrav6-mEW&sig=ACfU3U0V_kkTpcejoP3wWrNvom2tWYMkKw&hl=it&sa=X&ved=2ahUKEwiEtImXgaHmAhUFKlAKHQ9MDd (accessed on Dec 6, 2019).

31. Gombotz, W.R.; Wee, S.F. Protein release from alginate matrices. *Adv. Drug Deliv. Rev.* 1998, *31*, 267–285.

32. Smidsrød, O.; Skjåk-Bræk, G. Alginate as immobilization matrix for cells. *Trends Biotechnol.* 1990, *8*, 71–78.

33. Pan, Y.; Li, Y.J.; Zhao, H.Y.; Zheng, J.M.; Xu, H.; Wei, G.; Hao, J.S.; Cui, F. De Bioadhesive polysaccharide in protein delivery system: Chitosan nanoparticles improve the intestinal absorption of insulin in vivo. *Int. J. Pharm.* 2002, *249*, 139–147.

34. Mladenovska, K.; Cruaud, O.; Richomme, P.; Belamie, E.; Raicki, R.S.; Venier-Julienne, M.C.; Popovski, E.; Benoit, J.P.; Goracinova, K. 5-ASA loaded chitosan-Ca-alginate microparticles: Preparation and physicochemical characterization. *Int. J. Pharm.* 2007, *345*, 59–69.

35. Kotzé, A.F.; Thanou, M.M.; Lueben, H.L.; De Boer, A.G.; Verhoef, J.C.; Junginger, H.E. Enhancement of paracellular drug transport with highly quaternized N- trimethyl chitosan chloride in neutral environments: In vitro evaluation in intestinal epithelial cells (Caco-2). *J. Pharm. Sci.* 1999, *88*, 253–257.

36. Sarmento, B.; Ribeiro, A.; Veiga, F.; Sampaio, P.; Neufeld, R.; Ferreira, D. Alginate/chitosan nanoparticles are effective for oral insulin delivery. *Pharm. Res.* 2007, *24*, 2198–2206.

37. Polymeric Nanoparticles - an overview (pdf) | ScienceDirect Topics Available online: https://www.sciencedirect.com/topics/engineering/polymeric-nanoparticles/pdf (accessed on Nov 30, 2019).

38. Augustus, E.N.; Allen, E.T.; Nimibofa, A.; Donbebe, W. A Review of Synthesis, Characterization and Applications of Functionalized Dendrimers. *Am. J. Polym. Sci.* 2017, *7*, 8–14.

39. Menjoge, A.R.; Kannan, R.M.; Tomalia, D.A. Dendrimer-based drug and imaging conjugates: design considerations for nanomedical applications. *Drug Discov. Today* 2010, *15*, 171–185.

40. Heinz, H.; Pramanik, C.; Heinz, O.; Ding, Y.; Mishra, R.K.; Marchon, D.; Flatt, R.J.; Estrela-Lopis, I.; Llop, J.; Moya, S.; et al. Nanoparticle decoration with surfactants: Molecular interactions, assembly, and applications. *Surf. Sci. Rep.* 2017, *72*, 1–58.

41. Varshosaz, J.; Farzan, M. Nanoparticles for targeted delivery of therapeutics and small interfering RNAs in hepatocellular carcinoma. *World J. Gastroenterol.* 2015, *21*, 12022–12041.

42. Danhier, F.; Feron, O.; Préat, V. To exploit the tumor microenvironment: Passive and active tumor targeting of nanocarriers for anti-cancer drug delivery. *J. Control. Release* 2010, *148*, 135–146.

43. Friedman, A.D.; Claypool, S.E.; Liu, R. *The Smart Targeting of Nanoparticles*; Curr Pharm Des. 2013;19(35):6315-29.

44. Zhao, X.; Li, H.; Lee, R.J. Targeted drug delivery via folate receptors. *Expert Opin. Drug Deliv.* 2008, *5*, 309–319.

45. Duskey, J.T.; Rice, K.G. Nanoparticle Ligand Presentation for Targeting Solid Tumors, AAPS PharmSciTech. 2014 Oct;15(5):1345-54.

46. Bonoiu, A.C.; Mahajan, S.D.; Ding, H.; Roy, I.; Yong, K.-T.; Kumar, R.; Hu, R.; Bergey, E.J.; Schwartz, S.A.; Prasad, P.N. *Nanotechnology approach for drug addiction therapy: Gene silencing using delivery of gold nanorod-siRNA nanoplex in dopaminergic neurons*; Proc Natl Acad Sci U S A. 2009 Apr 7;106(14):5546-50.

47. Mcbain, S.C.; Hp, H.; Dobson, Y.J.; Dobson, J. *Magnetic nanoparticles for gene and drug delivery*; Int J Nanomedicine. 2008 Jun; 3(2): 169–180.

48. Kwon, H.J.; Cha, M.-Y.; Kim, D.; Kim, D.K.; Soh, M.; Shin, K.; Hyeon, T.; Mook-Jung, I. Mitochondria-Targeting Ceria Nanoparticles as Antioxidants for Alzheimer's Disease. *ACS Nano* 2016, *10*, 2860–2870.

49. Aouadi, M.; Tesz, G.J.; Nicoloro, S.M.; Wang, M.; Chouinard, M.; Soto, E.; Ostroff, G.R.; Czech, M.P. Orally delivered siRNA targeting macrophage Map4k4 suppresses systemic inflammation, Nature. 2009 Apr 30;458(7242):1180-4.

50. Farokhzad, O.C.; Jon, S.; Khademhosseini, A.; Tran, T.N.T.; LaVan, D.A.; Langer, R. Nanoparticle-aptamer bioconjugates: A new approach for targeting prostate cancer cells. *Cancer Res.* 2004, *64*, 7668–7672.

51. Bhaskar, S.; Tian, F.; Stoeger, T.; Kreyling, W.; De La Fuente, J.M.; Grazú, V.; Borm, P.; Estrada, G.; Ntziachristos, V.; Razansky, D. *Multifunctional Nanocarriers for diagnostics, drug delivery and targeted treatment across blood-brain barrier: perspectives on tracking and neuroimaging*; Part Fibre Toxicol. 2010 Mar 3;7:3

52. Kumar, R.; Roy, I.; Ohulchanskyy, T.Y.; Goswami, L.N.; Bonoiu, A.C.; Bergey, E.J.; Tramposch, K.M.; Maitra, A.; Prasad, P.N. Covalently Dye-Linked, Surface-Controlled, and Bioconjugated Organically Modified Silica Nanoparticles as Targeted Probes for Optical Imaging. *ACS Nano* 2008, *2*, 449–456.

53. Shang, H.; Chang, W.-S.; Kan; Majetich, S.A.; Lee, G.U. Synthesis and Characterization of Paramagnetic Microparticles through Emulsion-Templated Free Radical Polymerization. *Langmuir* 2006, *22*, 2516–2522.

54. Saha, K.; Agasti, S.S.; Kim, C.; Li, X.; Rotello, V.M. Gold Nanoparticles in Chemical and Biological Sensing, Chem Rev. 2012 May 9;112(5):2739-79

55. Bart, J.; Tiggelaar, R.; Yang, M.; Schlautmann, S.; Zuilhof, H.; Gardeniers, H. Room-temperature intermediate layer bonding for microfluidic devices. *Lab Chip* 2009, *9*, 3481–3488.

56. Binder, W.; Kluger, C. Azide/Alkyne-“Click” Reactions: Applications in Material Science and Organic Synthesis. *Curr. Org. Chem.* 2006, *10*, 1791–1815.

57. Fleming, D.A.; Thode, C.J.; Williams, M.E. Triazole Cycloaddition as a General Route for Functionalization of Au Nanoparticles. *Chem. Mater.* 2006, *18*, 2327–2334.

58. Nakanishi, K.; Sakiyama, T.; Imamura, K. On the adsorption of proteins on solid surfaces, a common but very complicated phenomenon. *J. Biosci. Bioeng.* 2001, *91*, 233–244.

59. Shang, W.; Nuffer, J.H.; Dordick, J.S.; Siegel, R.W. Unfolding of Ribonuclease A on Silica Nanoparticle Surfaces. *Nano Lett.* 2007, *7*, 1991–1995.

60. Mandal, H.S.; Kraatz, H.-B. Effect of the Surface Curvature on the Secondary Structure of Peptides Adsorbed on Nanoparticles. *J. Am. Chem. Soc.* 2007, *129*, 6356–6357.

61. Wu, Z.; Zhang, B.; Yan, B. Regulation of Enzyme Activity through Interactions with Nanoparticles. *Int. J. Mol. Sci* 2009, *10*, 4198–4209.

62. Aubin-Tam, M.-E.; Hamad-Schifferli, K. Gold Nanoparticle−Cytochrome c Complexes: The Effect of Nanoparticle Ligand Charge on Protein Structure.

Langmuir 2005, *21*, 12080–12084.

63. Jakhmola, A.; Anton, N.; Vandamme, T.F. Inorganic Nanoparticles Based Contrast Agents for X-ray Computed Tomography. *Adv. Healthc. Mater.* 2012, *1*, 413–431.

64. Caracciolo, G.; Cardarelli, F.; Pozzi, D.; Salomone, F.; Maccari, G.; Bardi, G.; Capriotti, A.L.; Cavaliere, C.; Papi, M.; Laganà, A. Selective Targeting Capability Acquired with a Protein Corona Adsorbed on the Surface of 1,2-Dioleoyl-3-trimethylammonium Propane/DNA Nanoparticles. *ACS Appl. Mater. Interfaces* 2013, *5*, 13171–13179.

65. Cagliani, R.; Gatto, F.; Bardi, G. Protein adsorption: A feasible method for nanoparticle functionalization? *Materials (Basel).* 2019, *12*.

66. Milani, S.; Baldelli Bombelli, F.; Pitek, A.S.; Dawson, K.A.; Rädler, J. Reversible *versus* Irreversible Binding of Transferrin to Polystyrene Nanoparticles: Soft and Hard Corona. *ACS Nano* 2012, *6*, 2532–2541.

67. Lee, Y.K.; Choi, E.-J.; Webster, T.J.; Kim, S.-H.; Khang, D. effect of the protein corona on nanoparticles for modulating cytotoxicity and immunotoxicity. *Int. J. Nanomedicine Dovepress* 2015, 10–97.

68. Rodriguez, P.L.; Harada, T.; Christian, D.A.; Pantano, D.A.; Tsai, R.K.; Discher, D.E. Minimal "Self" Peptides That Inhibit Phagocytic Clearance and Enhance Delivery of Nanoparticles. *Science (80-.).* 2013, *339*, 971–975.

69. Schöttler, S.; Becker, G.; Winzen, S.; Steinbach, T.; Mohr, K.; Landfester, K.; Mailänder, V.; Wurm, F.R. Protein adsorption is required for stealth effect of poly(ethylene glycol)- and poly(phosphoester)-coated nanocarriers. *Nat. Nanotechnol.* 2016, *11*, 372–377.

70. Pareek, V.; Bhargava, A.; Bhanot, V.; Gupta, R.; Jain, N.; Panwar, J. Formation and Characterization of Protein Corona Around Nanoparticles: A Review. *J. Nanosci. Nanotechnol.* 2018, *18*, 6653–6670.

71. Mukhopadhyay, A.; Basu, S.; Singha, S.; Patra, H.K. Inner-View of Nanomaterial Incited Protein Conformational Changes: Insights into Designable Interaction. *Research* 2018, *2018*, 1–15.

72. Tonigold, M.; Simon, J.; Estupiñán, D.; Kokkinopoulou, M.; Reinholz, J.; Kintzel, U.; Kaltbeitzel, A.; Renz, P.; Domogalla, M.P.; Steinbrink, K.; et al. Pre-adsorption of antibodies enables targeting of nanocarriers despite a biomolecular corona. *Nat. Nanotechnol.* 2018, *13*, 862–869.

73. Pederzoli, F.; Tosi, G.; Vandelli, M.A.; Belletti, D.; Forni, F.; Ruozi, B. Protein corona and nanoparticles: how can we investigate on? *Wiley Interdiscip. Rev. Nanomedicine Nanobiotechnology* 2017, *9*.

74. Shannahan, J.H.; Lai, X.; Ke, P.C.; Podila, R.; Brown, J.M. Silver Nanoparticle Protein Corona Composition in Cell Culture Media. *PLoS One* 2013, *8*, 74001.

75. Keselowsky, B.G.; Collard, D.M.; García, A.J. Surface chemistry modulates fibronectin conformation and directs integrin binding and specificity to control cell adhesion. *J. Biomed. Mater. Res. Part A* 2003, *66A*, 247–259.

76. Veronese, F.M.; Pasut, G. PEGylation, successful approach to drug delivery. *Drug Discov. Today* 2005, *10*, 1451–1458.

77. Owens Iii, D.E.; Peppas, N.A. Opsonization, biodistribution, and pharmacokinetics of polymeric nanoparticles. *Int. J. Pharm.* 2006, *307*, 93–102.

78. Aoyama, M.; Hata, K.; Higashisaka, K.; Nagano, K.; Yoshioka, Y.; Tsutsumi, Y. Clusterin in the protein corona plays a key role in the stealth effect of nanoparticles against phagocytes. *Biochem. Biophys. Res. Commun.* 2016, *480*, 690–695.

79. Malvindi, M.A.; Brunetti, V.; Vecchio, G.; Galeone, A.; Cingolani, R.; Pompa, P.P. SiO 2 nanoparticles biocompatibility and their potential for gene delivery and silencing. *Nanoscale* 2012, *4*, 486–495.

80. Klabunde, K.J.; Stark, J.; Koper, O.; Mohs, C.; Park, D.G.; Decker, S.; Jiang, Y.; Lagadic, I.; Zhang, D. Nanocrystals as Stoichiometric Reagents with Unique Surface Chemistry. *J. Phys. Chem.* 1996, *100*, 12142–12153.

81. Stober, W.; Fink, A.; Ernst Bohn, D. *Controlled Growth of Monodisperse Silica Spheres in the Micron Size Range 1*; JOURNAL OF COLLOID AND INTERFACE SCIENCE 26, 62--69 (1968)

82. Rahman, I.A.; Padavettan, V. Synthesis of Silica Nanoparticles by Sol-Gel: Size-Dependent Properties, Surface Modification, and Applications in Silica-Polymer

Nanocomposites-A Review. *J. Nanomater.* 2012, *2012*, 15.

83. Vansant, E.F.; Van Der Voort, P.; Vrancken, K.C. Part II. Chemical Modification of the Silica Surface. In *Characterization and chemical modification of the silica surface*; Elsevier, 1995; p. 556 ISBN 9780080528953.

84. Sugimoto, H.; Nakanishi, E.; Daimatsu, K.; Takatsu, R.; Yasumura, T.; Inomata, K. Preparation and properties of urethane acrylate-epoxy interpenetrating polymer networks containing silica nanoparticles. *Polym. Bull.* 2006, *57*, 975–982.

85. Lu, Y.; McLellan, J.; Xia, Y. Synthesis and Crystallization of Hybrid Spherical Colloids Composed of Polystyrene Cores and Silica Shells. *Langmuir* 2004, *20*, 3464–3470.

86. Montalti, M.; Prodi, L.; Rampazzo, E.; Zaccheroni, N. Dye-doped silica nanoparticles as luminescent organized systems for nanomedicine. *Chem. Soc. Rev.* 2014, *43*, 4243–4268.

87. Morelli, C.; Maris, P.; Sisci, D.; Perrotta, E.; Brunelli, E.; Perrotta, I.; Panno, M.L.; Tagarelli, A.; Versace, C.; Casula, M.F.; et al. PEG-templated mesoporous silica nanoparticles exclusively target cancer cells. *Nanoscale* 2011, *3*, 3198–3207.

88. Cai, L.; Chen, Z.Z.; Chen, M.Y.; Tang, H.W.; Pang, D.W. MUC-1 aptamer-conjugated dye-doped silica nanoparticles for MCF-7 cells detection. *Biomaterials* 2013, *34*, 371–381.

89. Gamucci, O.; Bertero, A.; Gagliardi, M.; Bardi, G. Biomedical nanoparticles: Overview of their surface immune-compatibility. *Coatings* 2014, *4*, 139–159.

90. Verma, A.; Stellacci, F. Effect of Surface Properties on Nanoparticleâ€“ Cell Interactions. Small 2010, 6, 12–21.

91. Gomes, M.C.; Cunha, A.; Trindade, T.; C Tom, J.P. The role of surface functionalization of silica nanoparticles for bioimaging. *J. Innov. Opt. Health Sci.* 2016, *9*, 1630005.

92. Korzeniowska, B.; Nooney, R.; Wencel, D.; McDonagh, C. Silica nanoparticles for cell imaging and intracellular sensing. *Nanotechnology* 2013, *24*.

93. Baggiolini, M.; Loetscher, P.; Moser, B. Interleukin-8 and the chemokine family. *Int. J. Immunopharmacol.* 1995, *17*, 103–108.

94. Miller, M.C.; Mayo, K.H. Molecular Sciences Chemokines from a Structural Perspective, Int J Mol Sci. 2017 Oct 2;18(10)

95. Ritzman, A.M.; Hughes-Hanks, J.M.; Blaho, V.A.; Wax, L.E.; Mitchell, W.J.; Brown, C.R. The Chemokine Receptor CXCR2 Ligand KC (CXCL1) Mediates Neutrophil Recruitment and Is Critical for Development of Experimental Lyme Arthritis and Carditis. *Infect. Immun.* 2010, *78*, 4593–4600.

96. Walz, A.; Burgener, R.; Car, B.; Baggiolini, M.; Kunkel, S.L.; Strieter~, R.M. *Structure and Neutrophi!-activating Properties of a Novel Inflammatory Peptide (ENA-78) with Homology to Interleukin 8*; J Exp Med. 1991 Dec 1;174(6):1355-62.

97. Xia, J.; Xu, X.; Huang, P.; He, M.; Wang, X. Expert Opinion on Therapeutic Targets The potential of CXCL5 as a target for liver cancer-what do we know so far? 2014.

98. Sepuru, K.M.; Poluri, K.M.; Rajarathnam, K. Solution Structure of CXCL5-A Novel Chemokine and Adipokine Implicated in Inflammation and Obesity, PLoS One. 2014 Apr 2;9(4):e93228.

99. Cheng, Y.; Ma, X. lei; Wei, Y. quan; Wei, X.W. Potential roles and targeted therapy of the CXCLs/CXCR2 axis in cancer and inflammatory diseases, Biochim. Biophys. Acta - Rev. Cancer 2019 Apr;1871(2):289-312

100. Bardi, G.; Lipp, M.; Baggiolini, M.; Loetscher, P. The T cell chemokine receptor CCR7 is internalized on stimulation with ELC, but not with SLC. *Eur. J. Immunol.* 2001, *31*, 3291–3297.

101. Bardi, G.; Niggli, V.; Loetscher, P. Rho kinase is required for CCR7-mediated polarization and chemotaxis of T lymphocytes. *FEBS Lett.* 2003, *542*, 79–83.

102. Bardi, G.; Sengupta, R.; Khan, M.Z.; Patel, J.P.; Meucci, O. Human immunodeficiency virus gp120-induced apoptosis of human neuroblastoma cells in the absence of CXCR4 internalization, J Neurovirol. 2006 Jun;12(3):211-8.

103. Bardi, G.; Malvindi, M.A.; Gherardini, L.; Costa, M.; Pompa, P.P.; Cingolani, R.; Pizzorusso, T. The biocompatibility of amino functionalized CdSe/ZnS quantum-dot-Doped SiO2 nanoparticles with primary neural cells and their gene carrying performance. *Biomaterials* 2010, *31*, 6555–6566.

104. Gamucci, O.; Bertero, A.; Malvindi, M.A.; Sabella, S.; Pompa, P.P.; Mazzolai, B.; Bardi, G. Detection of Fluorescent Nanoparticle Interactions with Primary Immune Cell Subpopulations by Flow Cytometry. *J. Vis. Exp* 2014, 51345.

105. Mercier #1, F.E.; #1, C.R.; Scadden, D.T. The bone marrow at the crossroads of blood and immunity. *Nat Rev Immunol* 2012, *12*, 49–60.

106. Kurth, I.; Willimann, K.; Schaerli, P.; Hunziker, T.; Clark-Lewis, I.; Moser, B. *The Rockefeller University Press • 0022-1007*; 2001; Vol. 194;.

107. Uguccioni, M.; Mackay, C.R.; Ochensberger, B.; Loetscher, P.; Rhis, S.; LaRosa, G.J.; Rao, P.; Ponath, P.D.; Baggiolini, M.; Dahinden, C.A. *Basophil Activation via CCR3 High Expression of the Chemokine Receptor CCR3 in Human Blood Basophils Role in Activation by Eotaxin, MCP-4, and Other Chemokines*; 1997; Vol. 100;.

108. Marone, G.; Triggiani, M.; De Paulis, A. Mast cells and basophils: Friends as well as foes in bronchial asthma? *Trends Immunol.* 2005, *26*, 25–31.

109. Randolph, G.J.; Ochando, J.; Partida-Sánchez, S. Migration of Dendritic Cell Subsets and their Precursors. *Annu. Rev. Immunol.* 2008, *26*, 293–316.

110. Gerszten, R.E.; Garcia-Zepeda, E.A.; Lim, Y.C.; Yoshida, M.; Ding, H.A.; Gimbrone, M.A.; Luster, A.D.; Luscinskas, F.W.; Rosenzwelg, A. MCP-1 and IL-8 trigger firm adhesion of monocytes to vascular endothelium under flow conditions. *Nature* 1999, *398*, 718–725.

111. Sokol, C.L.; Luster, A.D. The Chemokine System in Innate Immunity, Cold Spring Harb Perspect Biol. 2015 Jan 29;7(5).

112. Savarin-Vuaillat, C.; Ransohoff, R.M. *Chemokines and Chemokine Receptors in Neurological Disease: Raise, Retain, or Reduce?*; Neurotherapeutics. 2007 Oct;4(4):590-601.

113. Allen, S.J.; Crown, S.E.; Handel, T.M. Chemokine:Receptor Structure, Interactions, and Antagonism. *Annu. Rev. Immunol.* 2007, *25*, 787–820.

114. Baugher, P.J.; Richmond, A. The Carboxyl-terminal PDZ Ligand Motif of Chemokine Receptor CXCR2 Modulates Post-endocytic Sorting and Cellular Chemotaxis *. *J. Biol. Chem.* 2008, *283*, 30868–30878.

115. Neel, N.F.; Schutyser, E.; Sai, J.; Fan, G.-H.; Richmond, A. Chemokine receptor internalization and intracellular trafficking, Cytokine Growth Factor Rev. 2005 Dec;16(6):637-58.

116. Marchese, A. Endocytic trafficking of chemokine receptors, Curr Opin Cell Biol. 2014 Apr;27:72-7.

117. Veenstra, M.; Ransohoff, R.M. Chemokine receptor CXCR2: physiology regulator and neuroinflammation controller? J Neuroimmunol. 2012 May 15;246(1-2):1-9.

118. Mori, Y.; Nagaoka, S.; Takiuchi, H.; Kikuchi, T.; Noguchi, N.; Tanzawa, G.; Noishiki, Y. A new antithrombogenic material with long polyethyleneoxide chains. *Trans. Am. Soc. Artif. Intern. Organs* 1982, *28*, 459–463.

119. Dalsin, J.L.; Messersmith, P.B. Bioinspired antifouling polymers. *Mater. Today* 2005, *8*, 38–46.

120. Ballou, B.; Lagerholm, B.C.; Ernst, L.A.; Bruchez, M.P.; Waggoner, A.S. Noninvasive Imaging of Quantum Dots in Mice. *Bioconjug. Chem.* 2004, *15*, 79–86.

121. Perrault, S.D.; Walkey, C.; Jennings, T.; Fischer, H.C.; Chan, W.C.W. Mediating Tumor Targeting Efficiency of Nanoparticles Through Design. *Nano Lett.* 2009, *9*, 1909–1915.

122. Dai, Q.; Walkey, C.; Chan, W.C.W. Polyethylene Glycol Backfilling Mitigates the Negative Impact of the Protein Corona on Nanoparticle Cell Targeting. *Angew. Chemie Int. Ed.* 2014, n/a-n/a.

123. Waku, T.; Matsusaki, M.; Kaneko, T.; Akashi, M. PEG Brush Peptide Nanospheres with Stealth Properties and Chemical Functionality. *Macromolecules* 2007, *40*, 6385–6392.

124. Malvindi, M.A.; De Matteis, V.; Galeone, A.; Brunetti, V.; Anyfantis, G.C.; Athanassiou, A.; Cingolani, R.; Pompa, P.P. Toxicity Assessment of Silica Coated Iron Oxide Nanoparticles and Biocompatibility Improvement by Surface Engineering, PLoS One. 2014 Jan 21;9(1):e85835.

125. Nallathamby, P.D.; Hopf, J.; Irimata, L.E.; McGinnity, T.L.; Roeder, R.K. Preparation of fluorescent Au-SiO2 core-shell nanoparticles and nanorods with

tunable silica shell thickness and surface modification for immunotargeting. *J. Mater. Chem. B* 2016, *4*, 5418–5428.

126. Winey, M.; Meehl, J.B.; O'toole, E.T.; Giddings, T.H. Conventional transmission electron microscopy. 2014, *25*.

127. Phelps, C.F. Dynamic light scattering, with application to chemistry, biology and physics. *Biochem. Educ.* 1977, *5*, 22.

128. Tackling nanobubble characterization challenges Available online: https://www.slideshare.net/Malvern_Instruments/charcnanobubbles-ultra-fine-bubbles (accessed on Dec 7, 2019).

129. electrokinetic potential, ζ. In *IUPAC Compendium of Chemical Terminology*; IUPAC, 2008.

130. Hanaor, D.A.H.; Michelazzi, M.; Leonelli, C.; Sorrell, C.C.; Hanaor, D.A.H.; Michelazzi, M.; Leonelli, C.; Sorrell, C.C. *The Effects of Carboxylic Acids on the Aqueous Dispersion and Electrophoretic Deposition of ZrO 2*; Journal of the European Ceramic Society, Volume 32, Issue 1, 2012, Pages 235-244

131. Cagliani, R.; Gatto, F.; Cibecchini, G.; Marotta, R.; Catalano, F.; Sanchez-Moreno, P.; Pompa, P.P.; Bardi, G. CXCL5 Modified Nanoparticle Surface Improves CXCR2+ Cell Selective Internalization. *Cells* 2019, *9*, 56.

132. Friedman, M. Applications of the Ninhydrin Reaction for Analysis of Amino Acids, Peptides, and Proteins to Agricultural and Biomedical Sciences. *J. Agric. Food Chem.* 2004, *52*, 385–406.

133. Goldstein, J.I.; Newbury, D.E.; Echlin, P.; Joy, D.C.; Lyman, C.E.; Lifshin, E.; Sawyer, L.; Michael, J.R. Introduction. In *Scanning Electron Microscopy and X-ray Microanalysis*; Springer US: Boston, MA, 2003; pp. 1–20.

134. Ranjbar, B.; Gill, P. Circular Dichroism Techniques: Biomolecular and Nanostructural Analyses- A Review. *Chem. Biol. Drug Des.* 2009, *74*, 101–120.

135. ISA - The AU-CD beam line on ASTRID2 Available online: http://www.isa.au.dk/facilities/astrid2/beamlines/AU-cd/AU-CD_3.asp (accessed on Dec 7, 2019).

136. Errante, P.R.; Ebbing, P.C.C.; Rodrigues, F.S.M.; Ferraz, R.R.N.; Da Silva, N.P.

Flow cytometry: a literature review. *Rev. Ciências Médicas e Biológicas* 2016, *14*, 221.

137. Flow Cytometry Guide - Creative Diagnostics Available online: https://www.creative-diagnostics.com/flow-cytometry-guide.htm (accessed on Dec 7, 2019).

138. Das Murtey, M. Immunogold Techniques in Electron Microscopy, Methods Mol Biol. 2016;1474:309-25.

139. Vogiatzi, K.; Apostolakis, S.; Vlata, Z.; Krabovitis, E.; Spandidos, D.A. Opposite effect of angiotensin receptor blockade on CXCL8 production and CXCR1/2 expression of angiotensin II-treated THP-1 monocytes. *Exp. Ther. Med.* 2013, *5*, 987–991.

140. Walana, W.; Wang, J.J.; Yabasin, I.B.; Ntim, M.; Kampo, S.; Al-Azab, M.; Elkhider, A.; Dogkotenge Kuugbee, E.; Cheng, J. wei; Gordon, J.R.; et al. IL-8 analogue CXCL8 (3-72) K11R/G31P, modulates LPS-induced inflammation via AKT1-NF-kβ and ERK1/2-AP-1 pathways in THP-1 monocytes. *Hum. Immunol.* 2018, *79*, 809–816.

141. Xie, Y.; Wang, Y.; Li, J.; Hang, Y.; Oupický, D. Promise of chemokine network-targeted nanoparticles in combination nucleic acid therapies of metastatic cancer. *Wiley Interdiscip. Rev. Nanomedicine Nanobiotechnology* 2019, *11*.

142. Defea, K.A. Arrestins in actin reorganization and cell migration. In *Progress in Molecular Biology and Translational Science*; Elsevier B.V., 2013; Vol. 118, pp. 205–222 ISBN 9780123944405.

143. Jonkman, J.; Brown, C.M. Any Way You Slice It-A Comparison of Confocal Microscopy Techniques, J Biomol Tech. 2015 Jul;26(2):54-65.

144. Santi, M.; Maccari, G.; Mereghetti, P.; Voliani, V.; Rocchiccioli, S.; Ucciferri, N.; Luin, S.; Signore, G. Rational Design of a Transferrin-Binding Peptide Sequence Tailored to Targeted Nanoparticle Internalization. *Bioconjug. Chem.* 2017, *28*, 471–480.

145. Moglianetti, M.; Solla-Gullón, J.; Donati, P.; Pedone, D.; Debellis, D.; Sibillano, T.; Brescia, R.; Giannini, C.; Montiel, V.; Feliu, J.M.; et al. Citrate-Coated, Size-Tunable Octahedral Platinum Nanocrystals: A Novel Route for Advanced

Electrocatalysts. *ACS Appl. Mater. Interfaces* 2018, *10*, 41608–41617.

146. Morry, J.; Ngamcherdtrakul, W.; Yantasee, W. Oxidative stress in cancer and fibrosis: Opportunity for therapeutic intervention with antioxidant compounds, enzymes, and nanoparticles. *Redox Biol.* 2017, *11*, 240–253.

147. Oberdörster, G.; Oberdörster, E.; Oberdörster, J. Nanotoxicology: An emerging discipline evolving from studies of ultrafine particles. *Environ. Health Perspect.* 2005, *113*, 823–839.

148. Neagu, M.; Piperigkou, Z.; Konstantina Karamanou, ·; Ayse, ·; Engin, B.; Anca, ·; Docea, O.; Constantin, C.; Negrei, C.; Nikitovic, D.; et al. Protein bio-corona: critical issue in immune nanotoxicology. *Arch Toxicol* 2017, *3*, 1031–1048.

149. Moglianetti, M.; De Luca, E.; Pedone, D.; Marotta, R.; Catelani, T.; Sartori, B.; Amenitsch, H.; Retta, S.F.; Pompa, P.P. Platinum nanozymes recover cellular ROS homeostasis in an oxidative stress-mediated disease model. *Nanoscale* 2016, *8*, 3739–3752.

150. Abbas, A.K.; Lichtman, A.H.H.; Pillai, S. *Cellular and Molecular Immunology, Eighth Edition*; 2014; ISBN 9780323316149.

151. Birnie, G.D. *The HL60 cell line: A model system for studying human myeloid cell differentiation*; Br J Cancer Suppl. 1988 Vol 58, Dec;9:41-5.

152. Meyer, P.A.; Kleinschnitz, C.; Gieseler, F. Dimethylsulfoxide and Retinoic Acid-Induced Differentiation and Commitment in HL-60 Cells. In *Leukemias*; Springer Berlin Heidelberg, 1993; pp. 33–39.

153. Gatto, F.; Cagliani, R.; Catelani, T.; Guarnieri, D.; Moglianetti, M.; Pompa, P.P.; Bardi, G. PMA-induced THP-1 macrophage differentiation is not impaired by citrate-coated platinum nanoparticles. *Nanomaterials* 2017, *7*.

154. Ilinskaya, A.N.; Dobrovolskaia, M.A. Understanding the immunogenicity and antigenicity of nanomaterials: Past, present and future, Toxicol Appl Pharmacol. 2016 May 15;299:70-7

155. Zolnik, B.S.; González-Fernández, Á.; Sadrieh, N.; Dobrovolskaia, M.A. Minireview: Nanoparticles and the immune system. *Endocrinology* 2010, *151*, 458–465.

156. Rehman, M.U.; Yoshihisa, Y.; Miyamoto, Y.; Shimizu, T. The anti-inflammatory effects of platinum nanoparticles on the lipopolysaccharide-induced inflammatory response in RAW 264.7 macrophages. *Inflamm. Res.* 2012, *61*, 1177–1185.

157. Vermes, I.; Haanen, C.; Steffens-Nakken, H.; Reutellingsperger, C. A novel assay for apoptosis Flow cytometric detection of phosphatidylserine expression on early apoptotic cells using fluorescein labelled Annexin V. *J. Immunol. Methods* 1995, *184*, 39–51.

158. Fried, J.; Perez, A.G.; Clarkson, B.D. FLOW CYTOFLUOROMETRIC ANALYSIS OF CELL CYCLE DISTRIBUTIONS USING PROPIDIUM IODIDE Properties of the Method and Mathematical Analysis of the Data. *J. Cell Biol.* 1976, *71*, 172–181.

159. Rieger, A.M.; Nelson, K.L.; Konowalchuk, J.D.; Barreda, D.R. Modified Annexin V/Propidium Iodide Apoptosis Assay For Accurate Assessment of Cell Death. *J. Vis. Exp* 2011, 2597.

160. Harris, P.; Ralph, P. Human Leukemic Models of Myelomonocytic Development: A Review of the HL-60 and U937 Cell Lines. *J. Leukoc. Biol.* 1985, *37*, 407–422.

161. Guarnieri, D.; Melone, P.; Moglianetti, M.; Marotta, R.; Netti, P.A.; Pompa, P.P. Particle size affects the cytosolic delivery of membranotropic peptide-functionalized platinum nanozymes. *Nanoscale* 2017, *9*, 11288–11296.

162. Pedone, D.; Moglianetti, M.; De Luca, E.; Bardi, G.; Pompa, P.P. Platinum nanoparticles in nanobiomedicine. *Chem. Soc. Rev.* 2017, *46*, 4951–4975.